The effects of mixed promoters on gas hydrate formation

Jean-Sébastien Renault-Crispo

Department of Chemical Engineering
McGill University, Montréal
August 2017

A thesis submitted to McGill University in partial fulfillment of the requirements of the degree of Doctor of Philosophy

Abstract

Gas hydrates are studied for a wide variety of industrial applications extending from exploitation of natural gas to gas storage, transportation and separation. A stronger understanding of the kinetics of various hydrate promoters is necessary to pursue the large-scale implementation of such technologies. This thesis investigates gas hydrate growth and dissolution of different combinations of known kinetic and thermodynamic promoters. A novel method of analyzing kinetics for carbon dioxide gas hydrates is developed due to the high variability in gas consumption rates. A first-order response between gas consumption and induction time is shown for carbon dioxide gas hydrates. This is attributed to the different quantities of dissolved gas at nucleation owing to the different induction times. This behaviour is not observed for methane hydrates due to longer average induction times and lower methane solubility in water than carbon dioxide. This new method is used to inspect the carbon dioxide hydrate kinetics of adding multi-walled carbon nanotubes (MWCNTs) to a tetrabutylammonium bromide (TBAB) solution. The addition of MWCNTs does not result in a change in the actual hydrate growth rate but only in the dissolution rate, hinting that hydrate growth is not limited by carbon dioxide transfer at the gas-liquid interface. In another study, the kinetic promoter, sodium dodecyl sulfate (SDS), is added to the thermodynamic promoter TBAB in a methane hydrate system over a range of different concentrations of both promoters. The growth rates of pure TBAB systems decrease monotonically with increasing TBAB concentration. The addition of SDS to a dilute TBAB solution initially inhibits hydrate growth rate until a threshold SDS concentration is reached at which the system enters a promotion regime. This effect is also observed at high TBAB concentrations whereby the thermodynamic equilibrium is changed. This study highlights the importance of considering the effect of mixtures of hydrate additives on the process of hydrate nucleation and growth.

Résumé

Les hydrates de gaz sont étudiés pour une grande variété d'applications industrielles notamment l’exploitation du gaz naturel, le stockage, le transport et la séparation des gaz. Une meilleure compréhension de la cinétique de divers promoteurs d'hydrates est nécessaire pour poursuivre le développement de ces technologies. Cette thèse étudie la croissance et la dissolution des hydrates de gaz sous différentes combinaisons de promoteurs cinétiques et thermodynamiques connus. Une nouvelle méthode d'analyse de la cinétique des hydrates de dioxyde de carbone est développée dû à une grande variabilité des vitesses de consommation de gaz. Une fonction du premier ordre entre la consommation de gaz et le temps d'induction est démontrée pour les hydrates de dioxyde de carbone et est attribuée à la différente quantité de gaz dissous à la nucléation à différents temps d'induction. Ce comportement n'est pas observé pour les hydrates de méthane en raison de temps d'induction plus élevés et d'une solubilité plus faible que celle du dioxyde de carbone. Ce nouveau procédé est utilisé pour inspecter la cinétique de l'hydrate de dioxyde de carbone en ajoutant des nanotubes de carbone multi-parois (MWCNTs) à une solution de tetrabutylammonium bromide (TBAB). L'addition de MWCNTs n'entraîne pas de changement de la vitesse de croissance de l'hydrate mais seulement de la vitesse de dissolution, ce qui suggère que la croissance de l'hydrate n'est pas limitée par le transfert de dioxyde de carbone à l'interface gaz-liquide. Ensuite, le promoteur cinétique du sodium dodecyl sulfate (SDS) est ajouté au promoteur thermodynamique TBAB dans un système d'hydrate de méthane à une gamme de concentrations différentes. Les systèmes TBAB purs ont une vitesse de croissance monotone décroissante avec une augmentation de la concentration de TBAB. L'addition de SDS à une solution de TBAB à faible concentration inhibe initialement la vitesse de croissance d'hydrates jusqu'à ce qu'une concentration seuil de SDS soit atteinte pour obtenir un régime de promotion. Cet effet est également observé à une concentration de TBAB plus élevée où l'équilibre thermodynamique est modifié.

Cette étude souligne l'importance de considérer les divers effets des mélanges d'additifs hydrates sur le processus de nucléation et de croissance.

Acknowledgements

First I would like to thank my supervisor Dr. Phillip Servio for the opportunity to pursue graduate studies. Phil, your positive attitude and constant encouragements have pushed me to believe that I can achieve anything if I put my mind to it. Our almost daily conversations on research and non-research topics were great. The friendship we have developed goes far beyond this thesis. I would also want to thank my co-supervisor Dr. Sylvain Coulombe for the invaluable feedback despite my project's direction changing several times.

Next, I would like to recognize the importance of the HydrateTech group during my Ph.D. Special thanks to the two lab members that I consider as mentors, Jon and Jason. Jon, my office and travel mate, thanks for the advice, criticism and great discussions. Forgetting our conference posters in the Shanghai airport was definitely a hilarious experience! Jason, my proof-reader by excellence and fellow homebrewer, thanks for the help, positive support and enjoyable conversations. The rest of my current and former colleagues can't go without notice; Oleg, Francis, James, Edwin, Faraz, Thomas, François, thank you for the help and pleasant diversions over the years.

I would also like to acknowledge the aid of Frank Caporuscio. Over the years, I don't think there was one problem in the laboratory that you could not solve. Thanks to the supporting staff in the Chemical Engineering department, Ranjan Roy, Gerald Lepkyj, Roberto Tariello, Lisa Volpato, Louise Aspin and Jo-Ann Gadsby for your precious time and assistance over the years.

Last but certainly not least, I would like to thank my friends and family. You were a vital part to my success. To my gang of friends, the positive spirit in our group of friends is a great source of motivation. Thank you for the awesome memories that helped distract me from the lab. To my family, thanks for the unconditional encouragement and trust throughout my life. Jess, tu m'as toujours inspiré avec ta motivation et dévouement à vivre ses rêves. J'ai hâte de venir te rejoindre à l'autre bout du monde!

Table of Contents

List of Figures

List of Tables

Contribution of Authors

The following is a manuscript-based thesis containing two published peer-reviewed articles, and one article that has been submitted for consideration in a peer-reviewed journal. The author of this dissertation is the primary author for all works contained herein. The author is responsible for the literature search, the experimental work, developing models in MATLAB®, data analysis, as well as the writing and preparation of each article. Co-authors Servio and Coulombe provided guidance as supervisors of this doctoral research project.

1. Renault-Crispo, J.-S. and Servio, P. "Role of induction time on carbon dioxide and methane gas hydrate kinetics." *Journal of Natural Gas Science and Engineering* 43: 81-89. 2017.

2. Renault-Crispo, J.-S., Coulombe, S. and Servio, P. "Kinetics of Carbon Dioxide Gas Hydrates with Tetrabutylammonium Bromide and Functionalized Multi-Walled Carbon Nanotubes" *Energy* 128: 414-420. 2017.

3. Renault-Crispo, J.-S. and Servio, P. "Methane Gas Hydrate Kinetics with Mixtures of Dodecyl Sulfate and Tetrabutylammonium Bromide." *Fuel*. Submitted 2017.

Original Contributions

The following is a list of original contributions to knowledge provided by this work:

- Demonstrated the variability in gas consumption rate values for carbon dioxide (CO_2) gas hydrates at a fixed experimental condition.

- Investigated the first-order response of growth rate with induction time for CO_2 gas hydrates.

- Investigated the effect of multi-walled carbon nanotubes (MWCNTs) on a tetrabutylammonium bromide (TBAB)-water-CO_2 semi-clathrate system.

- Established that the addition of aluminum oxide nanoparticles to a SDS methane hydrate system does not affect growth rates.

- Established that the increase in carbon dioxide gas consumption rate in a TBAB system is due to the MWCNTs enhancement of gas dissolution and that added MWCNTs had no effect on actual hydrate growth rate.

- Measured the effect of sodium dodecyl sulfate (SDS) on methane hydrate systems with low to high concentration of TBAB.

- Demonstrated that SDS does not affect carbon dioxide growth kinetics in a 40 wt % TBAB solution.

Chapter 1

1 Introduction

Gas hydrates are solid inclusion compounds formed from the combination of water and gas molecules at high pressures and low temperatures. The solid phase consists of a host lattice of hydrogen-bonded water molecules that encage guest gas molecules such as methane and carbon dioxide. Naturally occurring methane hydrates in ocean beds and permafrost regions are thought to contain the majority of all recoverable carbon on earth. Recognizing this immense energy resource, the Methane Hydrate Research and Development Act was enacted by the United States Congress, an initiative which was followed by other countries such as Japan, India and China (Tabuchi, 2013; Letcher, 2014; Yamamoto et al., 2014; Collett et al., 2015).

Furthermore, commercial development of technologies using gas hydrates has recently gained interest. These applications include the storage and transportation of natural gas and hydrogen in hydrate form. With global warming and climate change becoming an issue of worldwide concern, the proposed use of clathrate hydrates to capture and store carbon dioxide is becoming conceivable. Lastly, gas hydrate technologies could provide a means to purify water, addressing the lack of access to clean water and basic sanitation due to human population growth. At the present time, the relatively severe conditions required for formation, the slow hydrate growth kinetics and the lack of scalability studies stand as the most significant barriers to the large-scale development of the described technologies. The focus of this work is to provide a further understanding on gas hydrate kinetics and to investigate the effect of combining different known promoters on the formation process to ultimately facilitate the development of different applications.

The present thesis begins with a literature background in Chapter 2 to provide the reader with a perspective on the field of hydrate research as well as previous research in hydrate kinetics. Chapter 3 investigates the kinetic behaviour of pure carbon dioxide and methane gas hydrates with respect to different induction times. Chapter 4 expands on this first study by applying this knowledge to the carbon dioxide hydrate system of tetrabutylammonium bromide (TBAB) with and without the addition of multi-walled carbon nanotubes (MWCNTs). Chapter 5 builds on Chapter 4 by considering the addition of Al_2O_3 nanoparticles to a methane-sodium dodecyl sulfate (SDS)-water hydrate system. Chapter 6 focuses on methane hydrate growth with the combination of two well-known hydrate promoters, TBAB and SDS. The final study found in Chapter 7 consists of an analysis of the combination of TBAB and SDS with a carbon dioxide hydrate system. Chapter 8 offers a comprehensive conclusion to the thesis and recommends potential future work.

Chapter 2

2 Background

2.1 Historical Perspective and Applications

A clathrate consists of the inclusion of a guest molecule within the cavities of the crystal lattice of another host molecule. In a subgroup of clathrates known as hydrates, the host molecule consists of hydrogen-bonded water molecules as the crystal lattice. Gas hydrates are nonstoichiometric crystalline compounds that arise when a gas or volatile liquid is encapsulated within the cavities of water molecules. Without the presence of this gas or volatile liquid, the water molecules would not be thermodynamically stable in the solid hydrate phase. The size of the guest molecules must be of a specific size to fit inside and stabilize the crystal lattice via weak Van der Waals forces with the host water molecules (Sloan et al., 2008). Pure gas hydrates generally form at moderate temperatures (0-10 °C) and high pressures (above 1 MPa). There are over 180 different molecules that form gas hydrates, notably methane and carbon dioxide, which are of particular interest for research and industrial applications (Englezos, 1993).

Gas hydrates were first documented in 1810 by Sir Humphrey Davy with the discovery that chlorine gas dissolved in water would freeze at temperatures of up to 9.0 °C (Sloan et al., 2008). Until the 1930s, the clathrate research consisted mainly of identifying the different compounds that produced hydrates and the ratio of gas to water of each type. In 1934, Hammerschmidt showed that gas hydrates were causing blockages in natural gas transmission lines (Hammerschmidt, 1934). This discovery lead to a growing interest in gas hydrate prevention, also called flow assurance, for the petroleum industry. Academic interest in the field increased significantly and focused primarily on predicting and inhibiting hydrate formation. Recently, complications with the BP oil spills in the Gulf of Mexico were due to a large volume of hydrates that formed inside a pipe the containment dome (CBCNews, 2010). Increasing the temperature and adding inhibitors are the current methods of preventing gas hydrate formation in pipelines. Researchers in industry and academia are constantly working on finding ideal additives to prevent hydrate formation.

The next turning point in hydrate research was the discovery of *in situ* natural gas hydrates in Siberian permafrost during the 1960s by Makogon (Makogon, 1965). Furthermore, it was determined that gas hydrates occurred very frequently in the earth's crust (Englezos, 1993). Following this discovery, gas hydrates also became relevant as a potential energy resource. Geophysical properties and gas recovery became new additions to the field of study (Dallimore et al., 1998; Sloan et al., 2008). Of particular interest are methane hydrates that occur in both permafrost areas and marine sediments where equilibrium conditions are found (Pellenbarg et al., 2000). Current conservative estimates suggest that the amount of energy stored in natural gas hydrate deposits, which predominantly consist of methane gas, is double the amount of all the other fossil fuels combined (Sloan et al., 2008). Recognizing this immense energy resource potential, the Methane Hydrate Research and Development Act was enacted by the United States Congress in 2000 to evaluate the feasibility of their extraction and use (Collett et al., 2015). On-shore hydrate deposits have already been successfully extracted and Japan has recently started testing deep sea reserves (Tabuchi, 2013; Yamamoto et al., 2014). India and China have also invested in methane hydrate research and development programs for the possible recovery of natural deposits (Letcher, 2014; CNN, 2017). The enormous quantities of methane stored as metastable hydrates also pose an environmental issue as methane is a strong greenhouse gas (Suess et al., 1999).

A few other prospective gas hydrate applications are a main part of present-day hydrate research. The use of gas hydrate pellets could be used for natural gas and hydrogen storage and transportation (Gudmundsson et al., 1995; Sugahara et al., 2009). Remote natural gas recovery projects, where production is too expensive for a pipeline or liquefied natural gas plant, would be a case where hydrates could be more economically viable (Gudmundsson et al., 2000). Gas hydrate pellet technology is near commercialization in Japan with current reports now focusing on the optimization of production efficiency at the pilot-plant scale (Watanabe et al., 2008). The main advantage lies in the fact that hydrates can be stored at moderate temperatures and pressures that are safer and less costly compared to liquefied natural gas (-162 °C) and compressed gas (200 atm) (Thomas, 2003). Another exciting novel application is the use of gas hydrates in separation processes, such as flue gases, where carbon dioxide can be preferentially captured while excluding nitrogen and other benign molecules (Kang et al., 2000b; Chatti et al., 2005; Eslamimanesh et al., 2012; Babu et al., 2013; Babu et al., 2015; Ma et al., 2016). Carbon dioxide recovery and sequestration in the petroleum industry using gas hydrates could be an economic alternative to current processes that exhibit a high energy costs and require large quantities of chemicals (ZareNezhad et al., 2016). Collectively, each of these applications is made possible by using the high storage capacity of gas hydrates in which one cubic meter of methane hydrate can release up to 160 cubic meters of methane gas at standard conditions (Taylor et al., 2003).

At the present time, the relatively severe conditions required for formation, the slow hydrate growth kinetics and the lack of scalability studies stand as the most significant barriers to the large-scale development of the described technologies (Yin et al., 2016).

2.2 Clathrate Structure

Gas hydrates consist of a host water molecule and a guest compound. The host molecule forms a crystal lattice that accommodates the guest molecule: a gas or volatile liquid. The crystal lattice is held together not only through hydrogen bonding between water molecules but also by the weak Van der Waals forces between guest molecules and water. In fact, the water structure is not thermodynamically stable and would collapse in the absence of the encapsulated molecule. The diameter of the guest molecule must be smaller than that of the cavity; furthermore, the guest molecule must not interfere with the hydrogen bonding in the crystal lattice.

Hydrates form in different configurations based on the thermodynamic conditions and guest molecule sizes. The three most common pure hydrate structures are: structure I (sI), structure II (sII), and structure H (sH) (Sloan et al., 2008).

The various structures are made up of multiple polyhedron sub-cages. A cage common to all three structures is named the small cage. The naming convention that describes the cavities as a polyhedron was provided by Jeffrey as follows (Jeffrey, 1984): the number of edges n_i with face type i and m_i faces with n_i edges is written as $n_i^{m_i}$. For instance, the small cage found in all structures is denoted by a 5^{12} polyhedron because it has 12 pentagonal faces.

Structure I consists of a small and a large cavity. The small cage is a 5^{12} polyhedron with an average radius of 0.395 nm while the large cage is a $5^{12}6^{2}$ polyhedron with an average radius of 0.433 nm (Gabitto et al., 2010). The unit cell is body-centered cubic with 2 small and 6 large cavities, which amounts to 46 water molecules. Structure I usually accommodates molecules whose diameters are between 0.41 nm and 0.58 nm, such as methane and carbon dioxide (Englezos, 1993). Structure I hydrates occur naturally because they form with naturally occurring gases such as methane, ethane and carbon dioxide.

Structure II consists of the same small cage 5^{12} and a large cage of $5^{12}6^{4}$ (Mak et al., 1965). The small cage and large cage have an average radius of 0.391 nm and 0.473 nm, respectively (Gabitto et al., 2010). Notice that the radius of the small cage is smaller than that of a structure I hydrate even though their shapes are the same. The unit cell is a face-centered cubic with 16 small cavities and 8 large cavities. The unit cell contains 136 water molecules. The guest molecules for Structure II typically have an average radius below 0.41 nm or above 0.55 nm and include molecules such as propane, tetrahydrofuran (THF), and nitrogen (Englezos, 1993). It is the structure commonly found in pipeline for natural gas hydrates.

The last structure discovered by Ripmeester et al. (Ripmeester et al., 1987) is called structure H, and is characterized by the need for two distinct guest molecules to occupy its cages. Once again, the small cage 5^{12} is found with an average radius of 0.391 nm. Structure H has a medium $4^{3}5^{6}6^{3}$ cage of 0.406 nm radius and a large $5^{12}6^{8}$ cage of 0.571 nm radius (Gabitto et al., 2010). The unit cell is hexagonal and contains 34 water molecules. The large cavity is estimated to fit guests up to 0.9 nm in diameter. Structure H is found in nature as well as man-made environments (Sloan et al., 1998). Figure 2.1

displays the different unit cells with the associated cavity types for the three different structures.

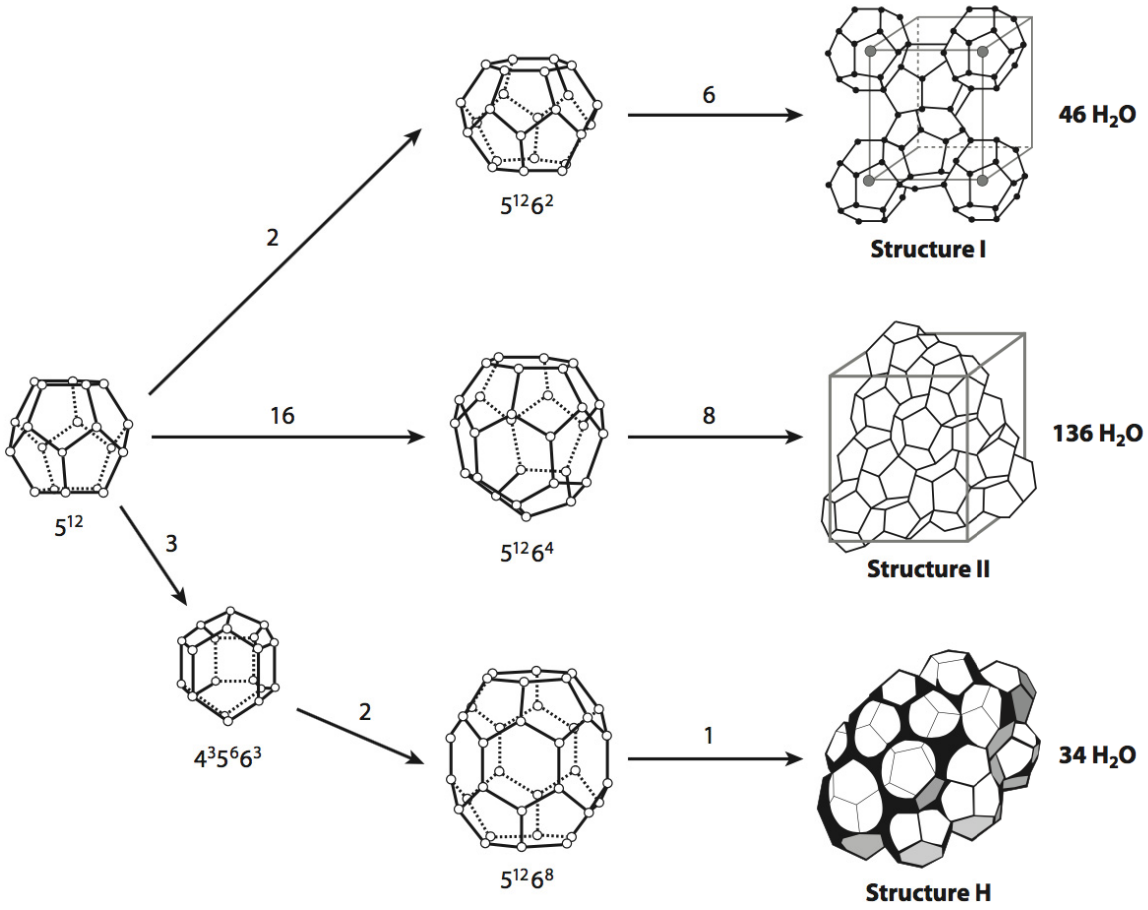

Figure 2.1: Structure I, II, and H unit cells and polyhedrons that form them. Adapted from (Koh et al., 2011).

An important difference between structures is that structure H requires two molecules of different sizes to stabilize the crystal. Structure I and II, on the other hand, only need one component to occupy the cavities to make it thermodynamically stable. For example, methane gas hydrates form with one gas where methane can enter both the small and large cage to stabilize the structure I crystal lattice. It is also possible to only have one cavity filled and the other one empty to form the hydrate, as is the case with ethane and structure I (ethane is too large for the small cage). Structure H is unique in that a large molecule is not enough to stabilize the lattice and requires a smaller molecule to fill the smaller cages.

Another important aspect of hydrate structure is cage occupancy. The cages are seldom 100 % occupied by guest molecules. Methane hydrates forming structure I are estimated to fill 50 % and 95 % of the small and large cages, respectively (Sloan et al., 1998). This is the reason why clathrate hydrates are referred to as non-stoichiometric compounds.

2.3 Phase Equilibria

Phase equilibria of gas hydrates are one of the most significant research areas fuelling practical applications. It is crucial for the oil and gas sector to identify the pressure and temperature conditions at which the gas hydrates will form or dissociate. Additionally, it is useful to establish the conditions at which specific gas hydrate systems will form in the laboratory. Phase equilibrium provides information about the fractions of different components in each phase and the cage occupancy. Gas hydrate equilibrium depends on temperature, pressure, gas composition, and the composition of the condensed phase (including liquid hydrocarbon phase and chemical inhibitor concentration) (Koh et al., 2011). Vapour, liquid, and gas hydrate solid are usually the co-existing phases present, but other phases such as ice and liquefied hydrate former can also be present (Mullin, 2001). An example of a carbon dioxide gas hydrate equilibrium phase diagram can be seen in Figure 2.2.

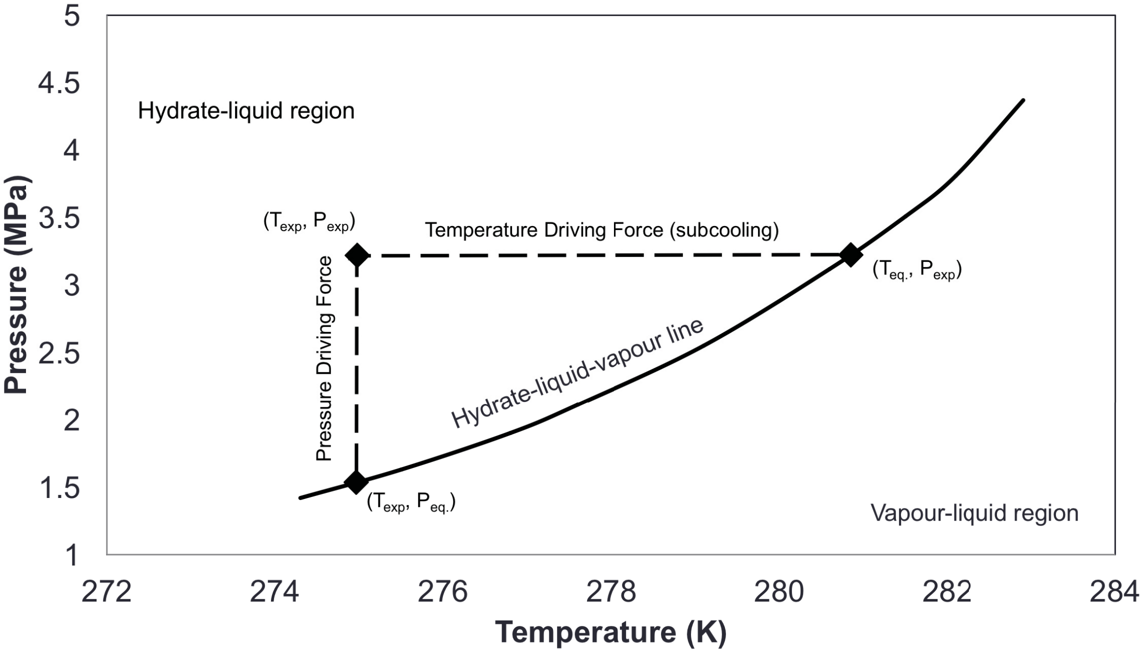

Figure 2.2: Phase diagram for the carbon dioxide hydrate system.

Since there is a very large number of hydrate-forming multi-component mixtures in industrial processes, it is uneconomical and impossible to obtain the equilibrium data for all these mixtures. A thermodynamic modeling approach to predicting hydrate properties has been developed and is widely used today to conduct these estimates. The vapour-liquid region is well characterized both experimentally and with models using equations of state such as the Peng-Robinson (Peng et al., 1976) and Trebble-Bishnoi (Trebble et al., 1987; 1988) to accurately describe the thermodynamic properties of these phases. Liquid models have also been developed to focus on the complexity of this phase, such as the non-random two liquid model (NRTL) (Renon et al., 1968) and the statistical associating fluid theory (SAFT) (Chapman et al., 1989), for example. The solid phase modeling of gas hydrates uses a successful application of statistical thermodynamics called the van der Waals and Platteeuw model (van der Waals et al., 1959). This model calculates the fugacity of water in the hydrate phase and makes it possible to solve for two-phase (hydrate-liquid or hydrate-vapour) or three-phase (hydrate-vapour-liquid) equilibria. Due to the lengthy and complex experimental determination of liquid mole fractions, accurate prediction of these values are essential to identify the thermodynamics of hydrate formation and kinetic models of different systems (Renault-Crispo et al., 2014).

2.4 Kinetics

To study hydrate kinetics, a vapour-liquid system must be placed in a hydrate-liquid region subject to a pressure or temperature driving force as depicted in Figure 2.2. Given the thermodynamically favourable conditions, hydrates will eventually nucleate and grow until the system reaches the three-phase equilibrium line or all the water has been consumed. Experimentally, the system must be kept at constant pressure and temperature throughout a kinetic run to ensure a constant driving force. Hydrate growth rates are typically studied in chilled high-pressure crystallizers that vary based on experimental needs. These can range from small to large reactors, stirred or quiescent systems, and can include a large variety of sensors for measuring parameters ranging from temperature to crystal size (Linga et al., 2017). In this work, a stirred semi-batch crystallizer is used. The temperature is kept constant by submerging the reactor in a glycol bath, while the pressure is maintained using a control valve. The amount of gas supplied by this control valve is used to calculate the gas consumption over time.

A typical gas consumption curve over time is shown in Figure 2.3. The hydrate formation curve can be separated into three distinctive stages: dissolution, induction, and growth.

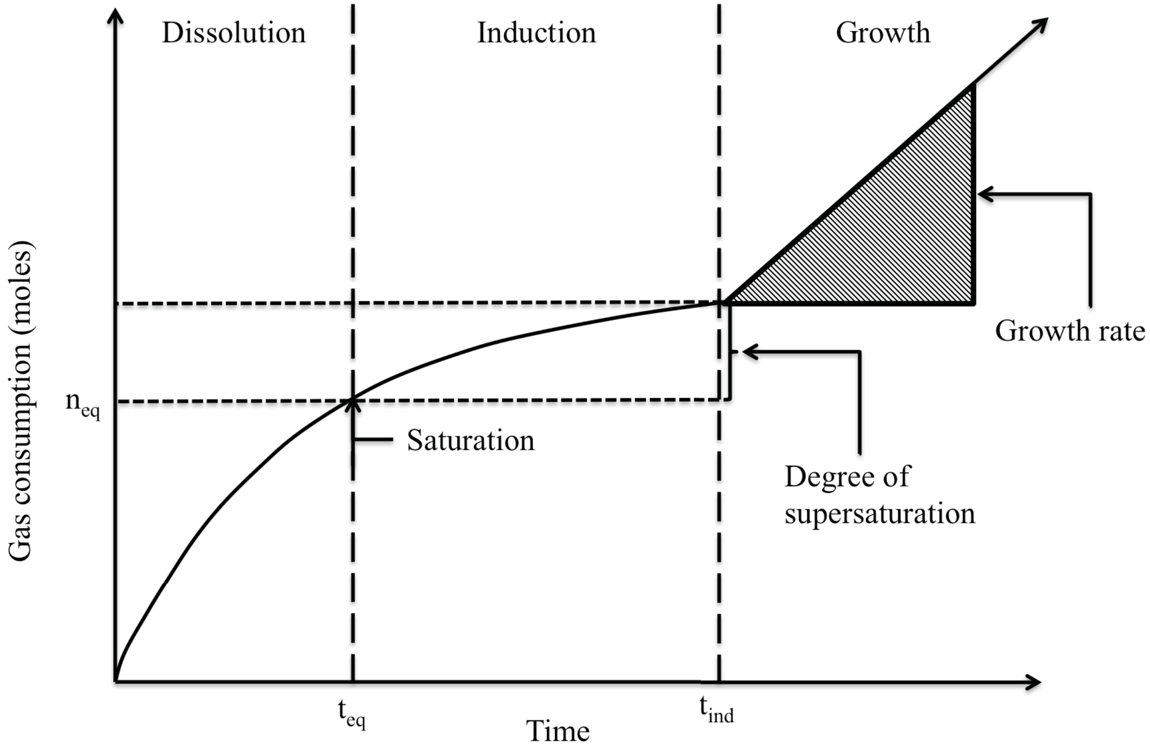

Figure 2.3: Typical gas consumption curve measured during a hydrate formation experiment.

2.4.1 Dissolution and Induction

The dissolution or saturation phase is the period during which the guest molecules dissolve in the liquid water through the gas-liquid interface without the presence of a solid phase. At a given time the system will reach the point of saturation denoted as n_{eq} at time t_{eq} in Figure 2.3. This occurs when the liquid becomes fully saturated with the gas and the liquid mole fraction is at the hydrate-liquid equilibrium value. After the saturation point is reached, the gas will continue dissolving into the liquid due to the driving force, allowing for supersaturation in a stage called the induction phase, or nucleation phase.

In the induction stage, small clusters of hydrate nuclei continuously form and dissociate as a result of local concentration gradients until a critical cluster radius is achieved, whereby the nucleus has reached energetic stability (Mullin, 2001; Sloan et al., 2008). The turbidity point is achieved when the first nucleus reaches the critical size, triggering the onset of hydrate growth. The induction time, t_{ind}, is defined as the time taken for nucleation. Two types of nucleation are commonly found: homogeneous and heterogeneous (Mullin, 2001). Homogeneous nucleation occurs when the crystal clusters of the new hydrate phase are only in contact with the liquid phase and occurs in the bulk of this liquid phase (Kashchiev, 2000). Heterogeneous nucleation takes place when supersatured liquid phase is in contact with other phases or molecular species. Heterogeneous nucleation is almost exclusively found in gas hydrate systems because of the presence of foreign molecules, microscopic particles, bubbles, and the contact with other solid phases, such as the reactor wall. The heterogeneous contact reduces the energy barrier required for crystal formation by diminishing the surface area of the new interface (Callister et al., 2010). The induction time for nucleation is stochastic in nature but is influenced by different factors such as the driving force (Bishnoi et al., 1996), secondary nucleation sites (Natarajan et al., 1994), size of guest molecule (Sloan et al., 2008), mixing (Englezos et al., 1987) and history of the water (Vysniauskas et al., 1983). A temperature spike characterizes this turbidity point, which is a result of the enthalpy of solidification.

The gas dissolution section of the hydrate formation process can be modeled using a mass balance across the gas-liquid interface and a mass transfer coefficient. Assuming the system is well mixed, the system is described using the equation Eq. 2.1.

$$\frac{dn}{\mathrm{dt}} = \frac{\mathrm{A\,k(n_s - n)}}{\mathrm{V}} \qquad \text{Eq. 2.1}$$

The number of moles dissolved is represented by n, t represents the time, A is the gas-liquid interfacial area, k is the mass transfer coefficient, V is the volume, and n_s is the hypothetical number of moles dissolved at time infinity. A time constant τ is defined as $\frac{A\,k}{V}$ and integrating Eq. 2.1 yields Eq. 2.2.

$$\mathrm{n} = \mathrm{n_s}\left(1 - e^{-\frac{t}{\tau}}\right) \qquad \text{Eq. 2.2}$$

Thus, the dissolution and induction processes behave as a first order response according to this model. The time constant τ corresponds to the time required to dissolve 63.2 % of n_s. Dissolution data of moles dissolved over time can be used to determine both τ and $\mathrm{n_s}$ through regression, and these can be used to compare different systems.

It is important to distinguish two types of dissolution experiments based on the thermodynamic conditions. If the temperature and pressure conditions matches or is below the three-phase equilibrium line, mass transfer will terminate at n_s. However, if the system is above this equilibrium line, providing a driving force for nucleation, it will enter the induction phase and hydrate can stochastically nucleate at any given time. In these experiments, only the gas dissolution before hydrate nucleation can be modeled according to Eq. 2.2.

2.4.2 Growth

Following hydrate nucleation, the consumption of hydrate former gas increases linearly until the limits of the system are approached (e.g. all water converts to hydrate phase) (Mullin, 2001). This linear consumption of gas is referred to as the hydrate growth rate. The growth period is an exothermic process where the supersaturated gas and water form a solid hydrate phase. Numerous studies have attempted to analyze and ultimately predict a model for this growth rate. The pioneering model was proposed by Glew and Hagget and was based on the temperature difference between the reactor and cooling bath (Glew et al., 1968a; 1968b). More recently, an assortment of kinetic models has been developed where the main difference is the driving force employed. Different driving forces include temperature (Vysniauskas et al., 1983; 1985), pressure, chemical potential, fugacity (Englezos et al., 1987) and concentration (Skovborg et al., 1994). To address the difficulty in characterizing mass transfer across the vapour-liquid interface in these models, Bergeron and Servio measured the bulk liquid mole fraction of the hydrate former and developed a model using this as the driving force represented in Eq. 2.3 (Bergeron et al., 2008a; 2008b).

$$\frac{\mathrm{dn}_i}{\mathrm{dt}} = \frac{\mathrm{V_L}\,\rho_\mathrm{w}(\mathrm{x}_i^L - \mathrm{x}_i^{HL})}{\mathrm{MW_w}\ 1/(\pi\mu_2\mathrm{k_r})} \qquad \text{Eq. 2.3}$$

The model relates the gas consumption ($\frac{\mathrm{dn}_i}{\mathrm{dt}}$) to a driving force determined by the difference between the hydrate former bulk liquid mole fraction (x_i^L) and the hydrate former solubility under hydrate-liquid equilibrium at experimental temperature and pressure (x_i^{HL}). This driving force eliminates the need to calculate the mass transfer effects at the vapour-liquid interface. The equation includes terms for the liquid volume (V_L), mass density of water (ρ_w) and molecule weight of water (MW_w). The second moment of particle size distribution (μ_2) is a representation of the hydrate crystal size. The last variable is the intrinsic reaction rate constant (k_r). The rate constant is fit to experimental data to be used to later predict the kinetics of the system. This model has been successfully applied to pure gas hydrate systems of CO_2 (Bergeron et al., 2008a) and CH_4 (Bergeron et al., 2010).

2.5 Hydrate Additives

Many different compounds can be added to water in order to promote or inhibit hydrate formation and growth. This work focuses primarily on improving the slow growth kinetics of gas hydrate growth by the addition of various promoters. The use of chemical promoters to increase the rate of hydrate formation has been investigated extensively and is still the topic of many publications in the field. Promoters can be separated into two broad categories: kinetic promoters and thermodynamic promoters.

2.5.1 Kinetic Promoters

Kinetic promoters refer to substances that have been shown to significantly increase hydrate formation rates without affecting the thermodynamic conditions of the system. In other words, the hydrates will form at the same temperature and pressure but exhibit enhanced growth rates compared to a system without the promoting compound. They are normally used at very low concentrations, thus not affecting the thermodynamic equilibrium (Sloan et al., 2008).

2.5.1.1 Surfactants

An example of these kinetic promoters is surfactant molecules, the most notable of which is sodium dodecyl sulphate (SDS) (Zhong et al., 2000; Ricaurte et al., 2012; Verrett et al., 2012b; Verrett et al., 2012a; Kumar et al., 2013). The use of 242 ppmw

SDS increased hydrate growth rates up to 700 times compared to pure water in a quiescent system (Zhong et al., 2000). SDS and other surfactants also increased gas storage capacity by converting more of the available water into solid hydrate (Sun et al., 2003). In stirred systems, SDS increased the growth rate by a factor of nearly 5 compared to a pure water system (Verrett et al., 2012a). A sigmoidal trend is observed between SDS concentration and growth rate, with a maximum plateau reached around 575 ppmw SDS (Verrett et al., 2012a). In a review on the use of surfactants for gas hydrate promotion, Kumar et al. reported that systems with added surfactants show reduced induction times, increased hydrate growth rates, and increased conversion of water to hydrate (Kumar et al., 2015).

It was initially thought that the surfactants molecules were grouping together as micelles at gas hydrate-forming conditions (Zhong et al., 2000). Micelles are spherical aggregates on the order of 100 molecules that consist of a hydrophobic hydrocarbon chain at one end (pointing inwards) and a hydrophilic anionic head group (pointing outwards) to provide dissolution in water (Young et al., 2011). It was thought that theses micelles would contain hydrate guest gas molecules, further increasing solubility and ultimately providing a gas-rich nucleation and growth site for hydrates (Zhong et al., 2000). Micelles form only above a certain concentration of surfactant called the critical micelle concentration (CMC) and above a critical temperature called Krafft temperature (Atkins et al., 2009). Their formation is usually attributed to a positive change in entropy in order for the Gibbs energy of the formation process to be negative and thermodynamically favour the formation. This positive change in entropy is counter-intuitive because of the ordering of the surfactant particles but it is attributed to the solvent molecules no longer solvating as many surfactants molecules and hence becoming less ordered (Atkins et al., 2009). Higher temperatures should display a lower CMC as can be deduced from the Gibbs free energy equation, where entropy is multiplied by temperature (Smith et al., 2005). In recent years, it has been suggested that the promotion mechanism is not directly linked to micelle formation, as the concentrations used are usually significantly below the critical micelle concentration of 2278 ppmw measured at 25 °C (Mata et al., 2004; Di Profio et al., 2005). Rather, it is believed that the presence of surfactants reduces the vapour-liquid surface tension which ultimately enhances the mass transfer across the vapour-liquid interface. A second reason that is given is a change in hydrate morphology, facilitating the transfer of gas to the hydrate phase (Kumar et al., 2015).

2.5.1.2 Nanoparticles

More recently, dissolved nanomaterials have been used in hydrate systems to study their effect, which revealed their kinetic promoting capabilities (Li et al., 2006a; Yulong et al., 2008; Park et al., 2010; Pasieka et al., 2013a; 2014; Pasieka et al., 2015). These so-called nanofluids have been studied for the potential to increase heat and mass transfer during hydrate growth as well as secondary nucleation sites for hydrate formation. Oxygen-functionalized multi-walled carbon nanotubes (MWCNT)-hydrate experiments were first reported in 2010 by Park et al. (Park et al., 2010). They used 40 ppmw MWCNT in water and observed an increase in methane consumption and hydrate growth rate (Park et al., 2010; Park et al., 2012). Pasieka et al. reported a slight enhancement in hydrate growth and increased dissolution rates using 1 to 10 ppmw MWCNT (Pasieka et al., 2013a; 2014). Additionally, many groups reported a significant decrease in induction time with the presence of nanoparticles (Arjang et al., 2013; Zhou et al., 2014; Nesterov et al., 2015).

2.5.2 Thermodynamic Promoters

Thermodynamic promotion involves the addition of a molecule that renders hydrate formation more energetically favourable. These compounds are used in much larger concentrations than kinetic promoters, sometimes at or above of 50 wt %. This means that the equilibrium condition shifts to either lower the pressure or correspondingly increase the temperature at which hydrates will form. Commonly studied thermodynamic promoters include tetrahydrofuran (THF) and cyclopentane, which generally integrate into larger cages of the hydrate structure and thus facilitate the storage of smaller gas molecules into the empty small cages (Torré et al., 2012; Lirio et al., 2013; Zhong et al., 2013).

2.5.2.1 Semi-Clathrate Salts

Semi-clathrates are a special type of thermodynamic promoters where the compound partly integrates into the crystal structure, thereby stabilizing the lattice and allowing hydrate formation at more moderate conditions (Arjmandi et al., 2007). Studies have focused on using a variety of halide salts as semi-clathrates, the most notable being tetra-n-butyl ammonium bromide (TBAB) (Mayoufi et al., 2010; Sun et al., 2010). The cation part of TBAB (TBA^+) acts as a guest in the large cage while its anion (Br^-) is integrated into the crystal lattice as shown in Figure 2.4 (Arjmandi et al., 2007; Sun et al., 2010). TBAB owes its popularity to its commercial availability and to the fact that it can form semi-clathrates at temperatures of up to 12.4 °C at atmospheric pressure (Aladko et al., 2002; Shimada et al., 2005). Research in the field of semi-clathrates has generally focused on the thermodynamics of TBAB hydrates, specifically the equilibrium temperatures, pressures, and TBAB liquid concentrations with single and multiple guest gases (Arjmandi et al., 2007; Sun et al., 2010; Bouchemoua et al., 2011; Verrett et al., 2015). Li et al. investigated the use of gas hydrates for separation of carbon dioxide from flue gases using TBAB hydrates (Li et al., 2010). They demonstrated the capability of separating out CO_2, and that TBAB accelerated gas hydrate growth rates. Another study showed that a 40 wt % TBAB solution may be a promising cold storage material for air conditioning systems due to its high phase change temperature and its improved overall conversion of liquid to gas hydrate (Mahmoudi et al., 2016).

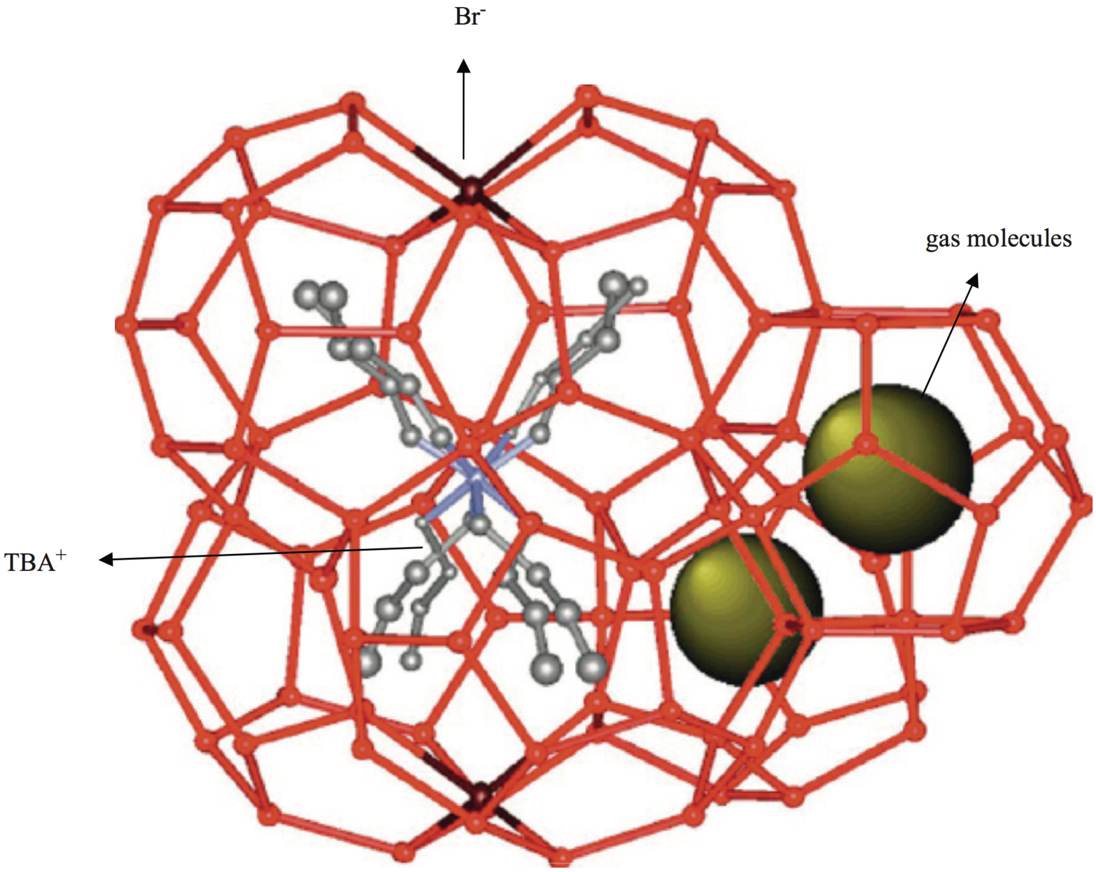

Figure 2.4: Semi-clathrate structure with TBAB. Adapted from (Shimada et al., 2005).

2.5.3 Combination of Promoters

The idea of combining thermodynamic and kinetic additives has sparked renewed interest for gas hydrate promotion in hopes of vastly improving induction times and growth rates. Ganji et al. added xanthan to a SDS solution and observed a lower hydrate dissociation rate, which is valuable for storage and transportation applications (Ganji et al., 2007). Another report from Kakati et al. described that combining a thermodynamic promoter, THF, with a kinetic promoter, SDS, results in a gas consumption rate increase with increasing SDS concentration (Kakati et al., 2016a). The growth kinetics of methane hydrate systems containing either THF or TBAB along with SDS was investigated (Mech et al., 2016a). The THF-SDS system showed a drastic increase in methane consumption rate compared to the TBAB-SDS system. They also observed a behaviour where gas consumption decreased over time after the initial hydrate formation (Mech et al., 2016a). This was attributed to the possible absorption of SDS micelles around the TBAB molecules.

Nanoparticles combined with other additives were also studied to enhance hydrate promotion. It is important to note that in some cases the additives were used to stabilize the nanoparticles in solution. Li et al. were the first to report nanoparticles and surfactants experiments in 2006 (Li et al., 2006a). They noticed a decreased hydrate formation time in HCFC141b hydrates with the addition of copper nanoparticles and surfactant SDBS. The group followed up with a study on HFC134a hydrates with copper nanoparticles and LAS surfactant that showed a decrease in hydrate formation time due to an increase in heat and mass transfer rates (Li et al., 2006b). It was shown that a mixture of water, copper oxide nanoparticles, and SDS increased the methane solubility at hydrate formation conditions (Moraveji et al., 2013). THF hydrates were shown to form at lower sub-cooling and reject more heat in the presence of MWCNTs (Pasieka et al., 2013b). In 2013, Mohammadi et al. demonstrated that MWCNTs and SDS mixtures can significantly increase methane solubility at relevant temperatures and pressures (Mohammadi et al., 2013a). They also concluded that the addition of cyclodextrin to the previous mixture further increased methane solubility (Mohammadi et al., 2013b). The same group measured an increase in carbon dioxide gas consumption in hydrates with silver nanoparticles and SDS (Mohammadi et al., 2014). Another study used MWCNTs and THF to study methane hydrate formation (Lim et al., 2014). They observed an augmentation in hydrate growth rate when both additives were combined compared to when they are used individually. They saw an increase in methane consumption with increasing MWCNTs up to 0.0003 wt %, after which the consumption started decreasing (Lim et al., 2014). Choi et al. found an optimum ratio of Al_2O_3, SDS, and THF that increased the growth rate of CO_2 hydrates (Choi et al., 2014). Natural gas hydrates exhibited enhanced gas consumption rates and total gas consumed by adding Al_2O_3 or ZnO to a SDS solution (Kakati et al., 2016b). Another group conducted experiments with nano-graphene particles dispersed using SDS on natural gas hydrates (Hosseini et al., 2015). They concluded that the nano-graphene particles increased the total gas consumption and decreased the induction time. Furthermore, experiments were completed that observed increased methane hydrate growth rate with CuO and SDS

(Najibi et al., 2015). A CuO and SDS mixture was also shown to decrease induction time by 92.7 % and increase storage capacity of gas hydrates by 34 % compared to pure water hydrates (Aliabadi et al., 2015).

Chapter 3

3 Role of Induction Time on Carbon Dioxide and Methane Gas Hydrate Kinetics[1]

3.1 Preface

As discussed in Chapter 2, the understanding of formation kinetics is essential to the development of hydrate-based applications. Properly comparing different gas hydrate systems using a standard method is necessary. This study was instigated from the variability in the results for hydrate growth rate discovered for carbon dioxide gas hydrates during experiments. The objective of this study was to assess the effect of induction time on gas hydrate kinetics. Carbon dioxide and methane hydrate were used as the model system. The effect of induction time was studied at different driving forces and mixing rates. An analysis of liquid mole fraction before nucleation is also performed to better understand the kinetic behaviour of these systems.

---

[1] Reproduced with permission from “Renault-Crispo, J.-S. and Servio, P. Role of induction time on carbon dioxide and methane gas hydrate kinetics." *Journal of Natural Gas Science and Engineering* 43: 81-89. 2017.”

3.2 Abstract

This study showed a significant variability in gas consumption rate values during gas hydrate growth at a same experimental condition for a specific experimental setup. This is important since many studies report a singular gas consumption rate or no associated statistics. Carbon dioxide hydrate gas consumption rates had of coefficient of variation of 2.7% for 204 kPa, 9.7% for 317 kPa and 9.6% for 435 kPa driving forces. The gas consumption rates decreased with increasing induction time following a first-order response. A high induction time resulted in a higher bulk liquid temperature increase meaning a greater amount of initial carbon dioxide hydrates formed. Methane hydrates did not exhibit the same behaviour of gas consumption rate with induction time. Variations in methane gas consumption rates were 4.8% for 698 kPa and 2.4% for 1564 kPa driving forces. A regression of metastable dissolution during these kinetic experiments demonstrated that the liquid mole fraction limit increased with increasing driving force. The dissolution time constant decreased with increasing mixing rate. Finally, the maximum experimental liquid mole fraction supersaturation achieved during all experiments was 75 times smaller than the thermodynamically predicted spinodal limit.

3.3 Introduction

Gas hydrates are non-stoichiometric crystalline compounds that form when a gas molecule is encapsulated by water molecules at relatively low temperatures and high pressures. Suitable guest molecules are mostly determined by size and stabilize the crystal lattice of hydrogen-bonded water molecules through weak van der Waals forces (Sloan et al., 2008). There are over 180 different molecules that form hydrates, with the most notable being methane and carbon dioxide (Englezos, 1993). Until the 1930's, hydrates remained mainly of academic interest until industrial research was spurred by the discovery of hydrates blocking natural gas transmission lines (Hammerschmidt, 1934). To this day, this problem of blockages remains quite significant and costly, as can be seen in the complications with the BP oil spills in the Gulf of Mexico that were due to a large volume of hydrates formed (CBCNews, 2010). Another turning point in the field was the discovery of *in situ* natural gas hydrates in the Siberian permafrost (Makogon, 1965). Recently, various applications using hydrates have been proposed such as gas transportation, storage and separation (Thomas, 2003; Eslamimanesh et al., 2012; Xia et al., 2016). Carbon dioxide sequestration in hydrate form has been studied as a mean to mitigate global warming (Chatti et al., 2005; Duc et al., 2007). Dashti et al. provided a comprehensive study on the recent advances in gas hydrate-based CO_2 capture (Dashti et al., 2015). Slow and unpredictable formation kinetics and the lack of scalability studies have prevented larger scale development of these proposed technologies (Eslamimanesh et al., 2012; Ma et al., 2016).

Numerous studies have been performed to investigate the kinetics of gas hydrate formation in stirred tank crystallizers. These studies make use of the gas consumption rate to model the system and calculate the reaction rate constant. The pioneering publication by Vysniauskas and Bishnoi (Vysniauskas et al., 1983; 1985) discussed the kinetics of methane and ethane hydrate formation. They assumed an Arrhenius-type function of temperature for the reaction rate kinetics. More recently, Bergeron and Servio (Bergeron et al., 2008a; 2008b; Bergeron et al., 2009; Bergeron et al., 2010) developed a model, shown in Eq. 3.1, for hydrate growth in stirred tank reactors that focuses on the liquid phase, eliminating the need to calculate the mass transfer at the gas-liquid interface.

$$\frac{\mathrm{dn}}{\mathrm{dt}} = \frac{\mathrm{V_L}\,\rho_\mathrm{w}(\mathrm{x^L} - \mathrm{x^{HL}})}{\mathrm{MW_w}\ 1/(\pi\mu_2 \mathrm{k_r})} \qquad \text{Eq. 3.1}$$

where $\frac{dn}{dt}$ is the amount of moles consumed over time after the onset of growth, also called the gas consumption rate, V_L is the liquid volume in the reactor, ρ_w and MW_w are respectively the mass density and molecular weight of the liquid water at reactor conditions. The driving force for growth is the difference between the mole fraction of the hydrate-forming gas in the bulk liquid (x^L) and its solubility under hydrate-liquid equilibrium (x^{HL}). The second moment, μ_2, is a representation of the hydrate particle size. The last variable and what these models aim to predict is the intrinsic reaction rate constant k_r. In literature, the intrinsic reaction rate predictions vary by a few orders of magnitude for similar systems (Lederhos et al., 1996; Bergeron et al., 2008a; Bergeron et al., 2010). This discrepancy can be attributed to different reactor geometries, mixing rates, as well as error in measuring particle size, liquid mole fraction or gas consumption rates. Some reports used the initial gas consumption rate (e.g. first 15 minutes of growth) (Bergeron et al., 2008a; 2008b; Bergeron et al., 2010) while others utilized the gas consumption rate after up to 10 hours of growth (Lederhos et al., 1996). Hence, the gas consumption rate can be significantly different for each experimental setup depending on the geometry of the reactor vessel, the speed of mixing, the amount of liquid present and the method of selecting the rate.

A molar gas consumption curve of hydrate formation and growth for a stirred reactor is presented in Figure 3.1. The process can be divided into three steps. The first step involves the dissolution of the hydrate-forming gas into the liquid phase until the liquid mole fraction reaches the point of three-phase equilibrium at the experimental temperature. As seen Figure 3.1, this occurs at time t_{eq} where n_{eq} moles have been dissolved. The next step is the induction step, and is characterized by the liquid phase being supersaturated with the hydrate-forming gas. This occurs because the pressure is above the three-phase equilibrium pressure, enabling the formation of a new phase. Due to the stochastic nature of nucleation, gas hydrates can form at any time during this metastable induction period (Sloan et al., 2008). Small hydrate nuclei continuously form and dissociate until a critical radius size is reached where hydrate growth is energetically favourable (Sloan et al., 2008). This is denoted by the induction time t_{ind} and marks the start of the hydrate growth step (Söhnel et al., 1988). A bulk liquid temperature spike, ΔT, from exothermic solidification, and an increase in opacity of the liquid are two indicators of the nucleation of hydrates in the reactor. Hydrate former gas consumption generally increases linearly over time at the early stage of growth.

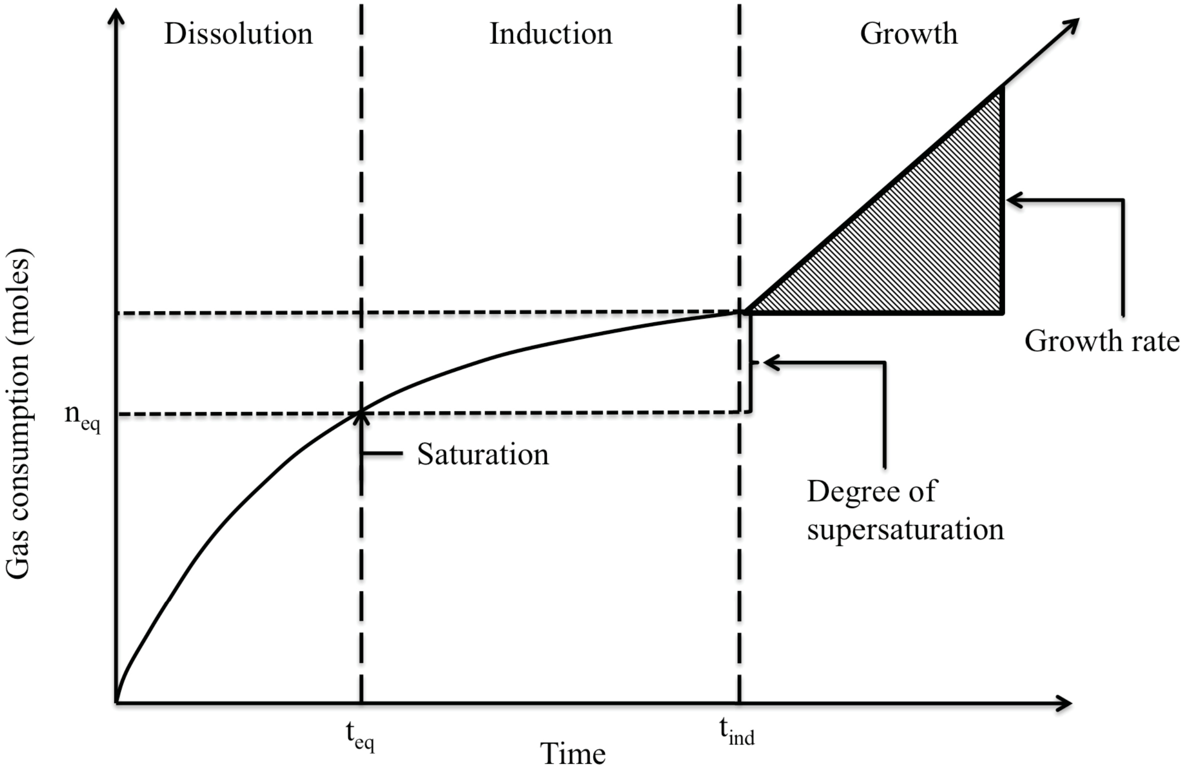

Figure 3.1: Simplified hydrate growth curve of gas consumption over time.

The dissolution and induction phases can be modeled together by applying dissolution kinetics. A first-order kinetic rate model is usually used to fit the data (Zhu et al., 2008; Pasieka et al., 2014) and can be seen in Eq. 3.2.

$$n = n_{liq}\left(1 - e^{-\frac{t}{\tau}}\right) \qquad \text{Eq. 3.2}$$

where n_{liq} is the hypothetical maximum liquid moles dissolved if hydrates would not form and τ is the time constant used to designate the point in time where 63.2% of the n_{liq} is reached. A reduction of τ would thus indicate an increase in rate of dissolution. With a metastable system, the dissolution can only be fitted up to the growth phase since the presence of hydrates changes the gas consumption dynamics completely. It follows that the mole fraction of the hydrate forming gas in the liquid phase can also contribute to the understanding of kinetics. Bergeron and Servio (Bergeron et al., 2009) demonstrated that the mole fraction of the gas hydrate former in the bulk liquid phase during growth remained greater than its two-phase hydrate-liquid equilibrium value.

Although many studies have considered modeling and quantifying gas hydrate growth kinetics, the effect of induction time on the gas consumption rates has not been reported or even mentioned to the knowledge of the authors. It is critical to accurately determine the gas consumption rate in order to properly compare kinetic performances of different additives, especially when these gas consumption rates are compared directly or used to calculate the intrinsic kinetic rate. This study could also contribute to various industrial applications where time is a factor; hence rapid dissolution and short induction time are essential to reducing cost and improving efficiency. The liquid mole fractions of the gas hydrate former during dissolution are also investigated to provided further insights on the complete kinetic process.

3.4 Experiments

3.4.1 Experimental Setup

A detailed description of the experimental setup and procedure can be found in a previous report (Bruusgaard et al., 2010). A simplified diagram of the experimental setup is shown in Figure 3.2. It consists of a 600 mL reactor made of 316 stainless steel with a pressure rating of 20 MPa submerged in a temperature controlled 20% ethylene glycol-water bath. The reactor is equipped with a MM-D06 magnetic stirrer from Pressure Products Industries with a standard magnetic stir bar with spinning ring from Cole Parmer. The reactor is connected to a reservoir gas tank through a Baumann 51000 control valve that keeps the pressure constant during kinetic experiments. For increase in accuracy, the control valve is regulated with the difference in pressure between the reactor bias gas tank and the reactor. The absolute pressures are monitored using Rosemount pressure transducers configured to a span of 0-14 MPa while the differential pressure transducers are configured to a span of 0-2 MPa, both with an accuracy of 0.065% of the given span. The system temperatures are recorded with RTD probes from Omega with accuracy of 0.1 K. All pressure and temperature readings are sent to a computer through a National Instrument data acquisition system. Liquid samples are removed from the reactor through a sampling port. A digital gasometer from Chandler

Engineering is used to measure the amount of gas evolved from the liquid when the sample is left to equilibrate at room temperature and atmospheric pressure. All gases used were obtained from MEGS Inc., and included ultra-high purity methane gas (99.99%) and carbon dioxide gas (99.995%). The water was treated in-house by reverse-osmosis with a 0.22 µm filter having a conductivity of 10 µS and total organic content < 10 ppmw.

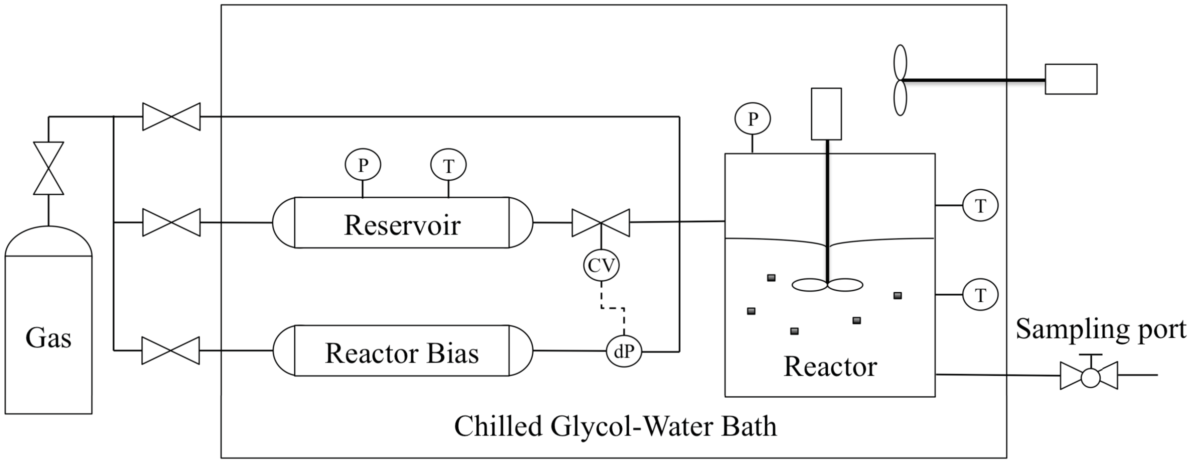

Figure 3.2: Schematic of the experimental setup used in all experiments.

3.4.2 Kinetic Experiments

Initially, the reactor was rinsed three times with 360 mL of water. Then, it was loaded with 240 mL of RO water. All kinetic experiments were performed with the same 240 mL of water to ensure the hydrodynamics were consistent across all experiments. The temperature of the bath was set to 2 °C for all experiments. The temperature was always kept at 2 °C and it was the pressure that was varied to provide the driving force for hydrate formation. Following water injection, the reactor gas was purged three times by pressurizing to 1100 kPa and then de-pressurizing to 110 kPa. Once thermal equilibrium was reached in the liquid, the reactor was pressurized to the desired pressure for the run based on the driving force. This driving force can be interpreted as either a temperature subcooling or a pressure driving force when compared to the three-phase equilibrium line. The reservoir and reactor bias gas tanks were pressurized to 1000 kPa above the reactor value to provide a differential pressure for gas transfer during the run. When the temperature stabilizes, the data acquisition system and control valve were turned on, and the stirrer was started. Once nucleated, the hydrates were allowed to grow for at least 300 seconds before the data acquisition system and control valve were turned off. 300 seconds was chosen to calculate the gas consumption rate as it was considered sufficient time to fit a linear slope but not too long so that the hydrodynamics would be changed by the presence of solids in the reactor. The system was subsequently brought down to 110 kPa for the hydrates to dissociate. Once all hydrates were dissociated, the reactor pressure was set to the initial pressure and the experiment was repeated. The moles consumed were calculated from the temperature and pressure data of the reservoir using the Trebble-Bishnoi equation of state (Trebble et al., 1987; 1988). The gas consumption rate was calculated from the slope of moles consumed over time for the first 300 seconds of hydrate growth. The temperature spike ΔT was calculated from the difference between the highest temperature after nucleation and the average temperature before nucleation. The liquid mole fraction was calculated from the amount of moles consumed before hydrate formation accounting for the gas dissolved at the start of the run when reactor was at 110 kPa. The pressure slightly above atmospheric was to prevent gases from the atmosphere to enter the system.

3.4.3 Mole Fraction Experiments

An analytical flash technique, similar to the one used by Gaudette and Servio (Gaudette et al., 2007), was employed to calculate the mole fraction of methane in the bulk liquid during the dissolution and growth steps. The reactor was loaded with 360 mL to allow for multiple removals of liquid samples. Three sample vessels were evacuated and cooled to the experimental temperature prior to sample extraction. They were also weighed before and after the sample was collected. Prior to the removal of a sample, the stirrer was turned off to avoid having hydrates or air bubbles enter the sample vessel. The liquid from the reactor was extracted into the three sample vessels. Through the use of a gasometer, the content of the sample vessel was brought to atmospheric pressure and room temperature. The mole fraction was determined from the volume of gas released when exposed to atmospheric conditions, as shown in Bergeron et al. (Bergeron et al., 2010).

3.5 Results and Discussion

3.5.1 Carbon Dioxide Hydrate Kinetics

3.5.1.1 Effect of Driving Force

For the carbon dioxide-water gas hydrate system, experiments were completed at three different driving force presented in Table 3.1. Mixing speed and temperature in these experiments were kept constant at 560 rpm and 2 °C respectively.

Table 3.1: Three different driving force conditions for CO_2 hydrate kinetic experiments.

Temperature (°C)	Pressure (kPa)	Temperature subcooling (°C)	Pressure driving force (kPa)	Mixer speed (rpm)
2	1778	1	204	560
2	1891	1.5	317	560
2	2009	2	435	560

The dependency of gas consumption rate on induction time can be observed in Figure 3.3. Average induction times are 1077 seconds for 435 kPa driving force, 1692 seconds for 317 kPa driving force and 3635 seconds for 204 kPa driving force. As expected, average induction time decreases with increasing driving force (Natarajan et al., 1994). More significantly, shorter induction times relate to higher gas consumption rates at a given temperature. Looking at the 317 kPa driving force runs, as induction time increases, the gas consumption rate eventually decreases to what is expected to be a plateau. Unfortunately, since induction time is stochastic, not many experimental points were collected in this plateau region of long induction times. At 204 kPa driving force, the coefficient of variance is 2.7% (average of 5.13E-5 mol/s with standard deviation of 1.4E-6 mol/s) compared to 9.7% (average of 6.28E-5 mol/s with standard deviation of 6.1E-6 mol/s) for 317 kPa driving force and 9.6% (5.13E-5 average of mol/s and standard deviation of 4.9E-6 mol/s) for 435 kPa driving force. For the two highest driving forces, there is a significant variation considering the experiments were conducted at the same conditions, namely 2 °C and 1891 kPa. According to Eq. 3.1 and assuming other parameters are constant, this means that the predicted intrinsic reaction rate constant would also vary by the same amount as the gas consumption rate, which leads to error in its calculation since the intrinsic reaction rate is only a function of temperature in the system investigated. This result highlights the issue of solely reporting the gas consumption rate or intrinsic kinetic rate for systems where this trend is present since there could be a large variability in the results. Hence, the need for replicates and adequate statistical analysis are extremely important when reporting hydrate kinetics.

However, the gas consumption rate is not significantly affected by the induction time at the lowest driving force. This can be explained by the fact that it has longer periods for dissolution into the liquid and liquid mole fraction limit is lower due to the smaller pressure. At long induction times, the dissolution process is nearly completed and the liquid is close to its liquid mole fraction limit at a specific condition. In this case, it is possible to decouple the growth and dissolution phase and define our gas consumption rate as the actual hydrate growth rate, meaning that all the gas going into the liquid is for hydrate growth. At long induction times, the 317 and 435 kPa driving forces would probably also exhibit reproducible gas consumption rates. However, long induction times are difficult to achieve because of the elevated pressure conditions and overall driving forces for nucleation. This is a consistent statement with Herri et al. (Herri et al., 1999) who observed an inversely proportional trend between induction time and driving force. At short induction time, it was impossible to decouple dissolution kinetics and hydrate growth rates and this is the reason gas consumption rates are used throughout the paper. The presence of hydrates significantly affects the dissolution dynamics making it unreasonable to use the dissolution model from before hydrate formation to represent the dissolution during growth.

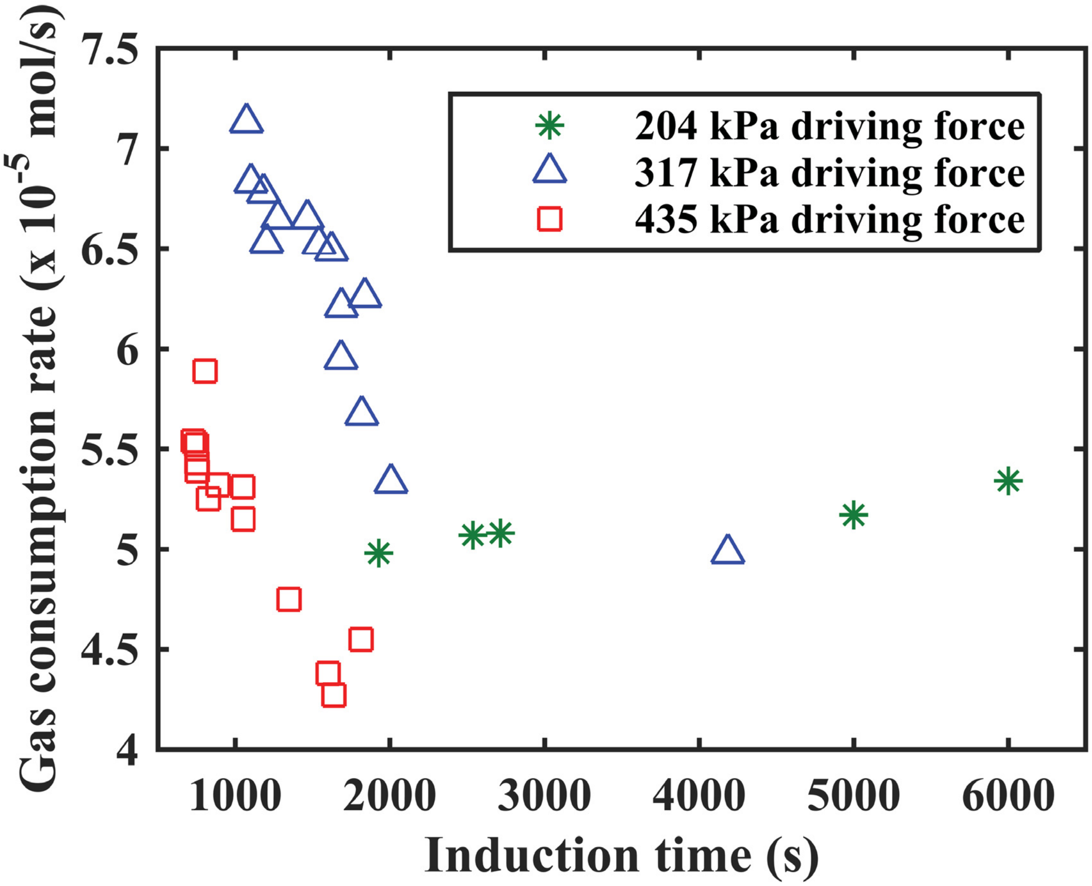

Figure 3.3: Gas consumption rate versus induction time for 3 different driving forces in a CO_2-water gas hydrate system: * 204 kPa, △ 317 kPa, □ 435 kPa.

As shown by Figure 3.3, the precise moment in the induction phase when the gas hydrates nucleate can be very important for characterizing the ensuing gas consumption rate. Figure 3.4 shows the change in temperature of the bulk liquid at hydrate formation for different induction times. The dissolution phase of the hydrate formation process is extremely reproducible for a given driving force at a fixed temperature. The dissolution section of the curves only varies when the experimental conditions do. In other words, the total amount of gas consumed at a specific induction time will always be the same before hydrate nucleation if the experimental conditions are consistent. This total gas consumed is directly related to the initial amount of gas hydrates formed at the induction time. The initial amount of gas hydrates formed at nucleation can also be linked to a bulk temperature spike because this process is exothermic. Hence, the more initial hydrates formed, the greater the temperature spike.

This explains the increasing trend with induction time that is evident in Figure 3.4. Furthermore, this trend is present as a first-order response as it seems to follow dissolution kinetics. Greater driving forces show higher temperature spikes because of the enhanced dissolution rates and greater levels of liquid mole fraction limit.

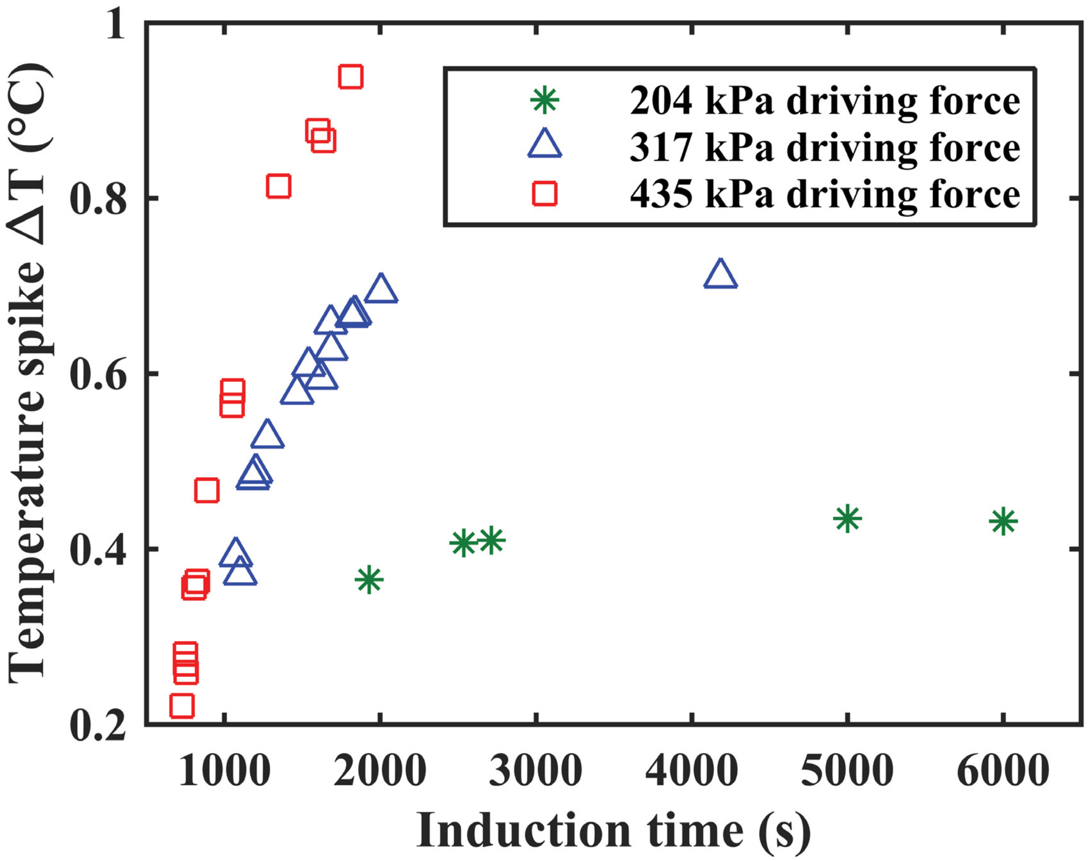

Figure 3.4: Temperature spike versus induction time for 3 different driving forces in a CO_2-water gas hydrate system: * 204 kPa, △ 317 kPa, □ 435 kPa.

This temperature spike dependency can help explain why gas consumption rates decreases with increasing induction times as observed in Figure 3.3. The presence of a greater initial amount of gas hydrates changes the hydrodynamics of the system. The mixing could be less efficient with the presence of more initial hydrates in the reactor and this also affects the gas-liquid mass transfer of the system. Additionally, having a greater temperature increase of the bulk liquid lowers the driving force for hydrate growth and slows down the kinetics. These two arguments are a suitable explanation to the reason why the gas consumption rate decreases with increasing induction time.

To further investigate this effect, one specific experiment was selected and the instantaneous gas consumption rates and bulk liquid temperature were compared over time during hydrate growth to see their relationship. The results can be observed in Figure 3.5. The instantaneous gas consumption rate is the slope of gas consumed over a duration of 10 seconds to eliminate the effect of noise in the growth rate calculation. The instantaneous gas consumption rate decreases slowly over time, following a similar decreasing trend than the bulk liquid temperature over time. This growth rate goes below the average gas consumption rate reported throughout this paper after approximately 600 seconds for this experimental run. The decrease can be mainly attributed to the bulk liquid temperature decrease but also to change in hydrodynamics (e.g. change in viscosity of the liquid). This is the reason why the initial growth rate of the first 300 seconds was selected in this report to decouple it from the other effects on the growth rate. It is important to keep in mind that the bulk liquid temperature is not simply a linear function of consumption rate as can be concluded from the higher temperature spikes of the 2 °C driving force compared to 1.5 °C but the lower gas consumption rates as seen in Figure 3.3 and Figure 3.4.

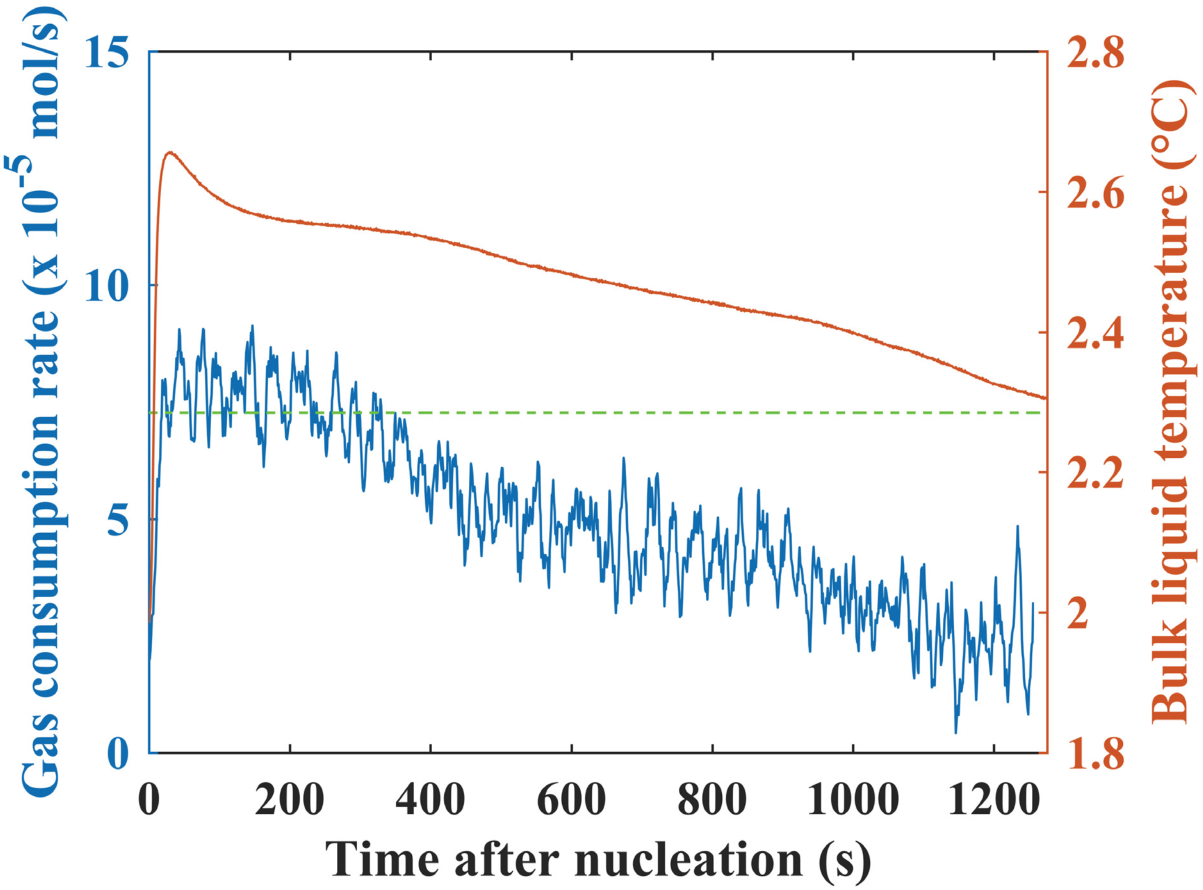

Figure 3.5: Instantaneous gas consumption rate (slope over a 10 second period) versus time after hydrate nucleation on the left y-axis. Dotted green line represents the 300 second average gas consumption rate. The right y-axis represents the bulk liquid temperature over time during the hydrate growth.

3.5.1.2 Effect of Mixing Rate

For the carbon dioxide-water gas hydrate system, the second set of experiments was completed at three different mixing rates namely 525 rpm, 560 rpm and 595 rpm. The driving force in all experiments was kept constant at 317 kPa. This driving force was selected since it had a significant variability at a mixing rate of 560 rpm as seen in Figure 3.3. The maximum mixing rate was set at 595 rpm since mixing rates above this speed would create gas bubbles in the liquid that would drastically change the hydrodynamics of the system. When bubbles were present in the liquid, gas consumption rates were unreliable for the experimental setup used in this study. At mixing rates lower than 525 rpm, the hydrates had very long induction times and would usually form a layer at the gas-liquid interface at nucleation as described in other reports (Taylor et al., 2007; Davies et al., 2010; Daniel-David et al., 2015). This layer significantly reduced the gas consumption rate since the gas needs to traverse a solid hydrate phase before accessing the water molecules beneath for further growth.

Gas consumption rate increases with increasing mixing rate as shown in Figure 3.6. Once again, the same trend where gas consumption rate decreases with increasing induction time is observed at all three mixing rates. The coefficients of variation are 3.0% (average of 3.64E-5 mol/s and standard deviation of 1.1E-6 mol/s) for 525 rpm, 9.7% (average of 6.28E-5 mol/s and standard deviation of 6.1E-6 mol/s) for 560 rpm, and 0.7% (average of 7.67E-5 mol/s and standard deviation of 5.4E-7 mol/s) for 595 rpm. A higher mixing rate seems ideal for minimizing the variability in the calculated gas consumption rates since lower mixing rates have longer induction times and more frequent hydrate layer formation. As shown by these results, the mass transfer of the gas cannot be neglected at the two lowest mixing speed because of the different average consumption rates at the highest mixing speed. It was impossible to increase the stirrer speed even higher because of low quantity of liquid used and bubble formation therefore it cannot be shown that the mass transport limitations were completely eliminated at 595 rpm. However, it is possible that the effect of induction time on gas consumption rate previously observed is not present when the mass transport limitations can be neglected.

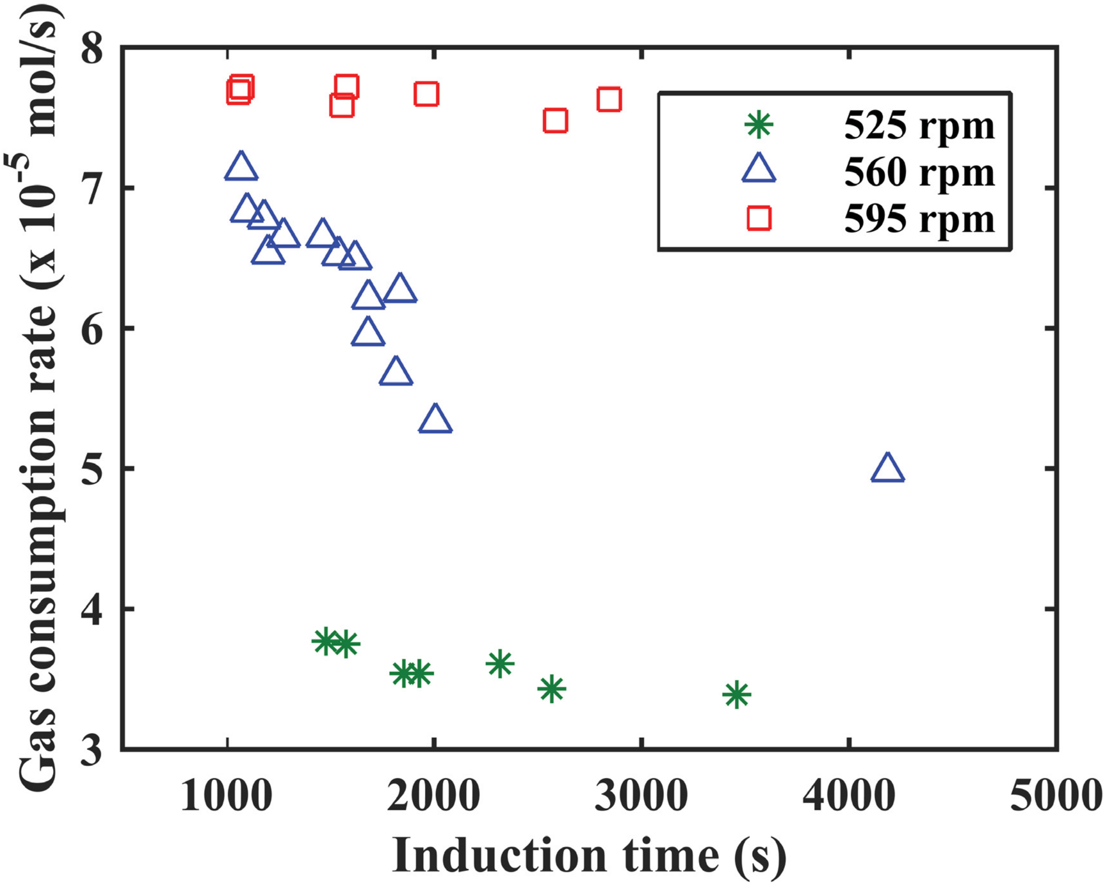

Figure 3.6: Gas consumption rate versus induction time for 3 different mixing rates in a CO2-water gas hydrate system: * 525 rpm, △ 560 rpm, □ 595 rpm.

To explain the different variability in the gas consumption rates with different mixing rates, the temperature difference of the bulk liquid with induction time is analyzed. Figure 3.7 illustrates the dependence of the temperature spike on induction time at different mixing rates. A first-order response characterizes the relation between the variables, similarly to Figure 3.4. Once again, this is expected since it follows dissolution kinetics. The lowest mixing rate of 525 rpm has smaller temperature spikes than the two higher mixing rates at a similar induction time. At the lowest mixing rate, it takes longer for the same amount of gas to dissolve in the liquid than at a higher mixing rate. Mixing rates of 560 rpm and 595 rpm are not significantly different from each other with respect to their temperature spikes changes with induction time. This means that the initial amount of gas hydrates formed at nucleation for both cases are very similar. The lowest variability in gas consumption rate at 595 rpm compared to 560 rpm can be explained by the more efficient mixing since in both cases, the same amount of hydrates is present at nucleation. Gas transfer to the liquid phase in the presence of solid particles is enhanced at the highest mixing rate. This could be due to the increasing heat transfer coefficient and contact area as described in Herri et al. (Herri et al., 1999).

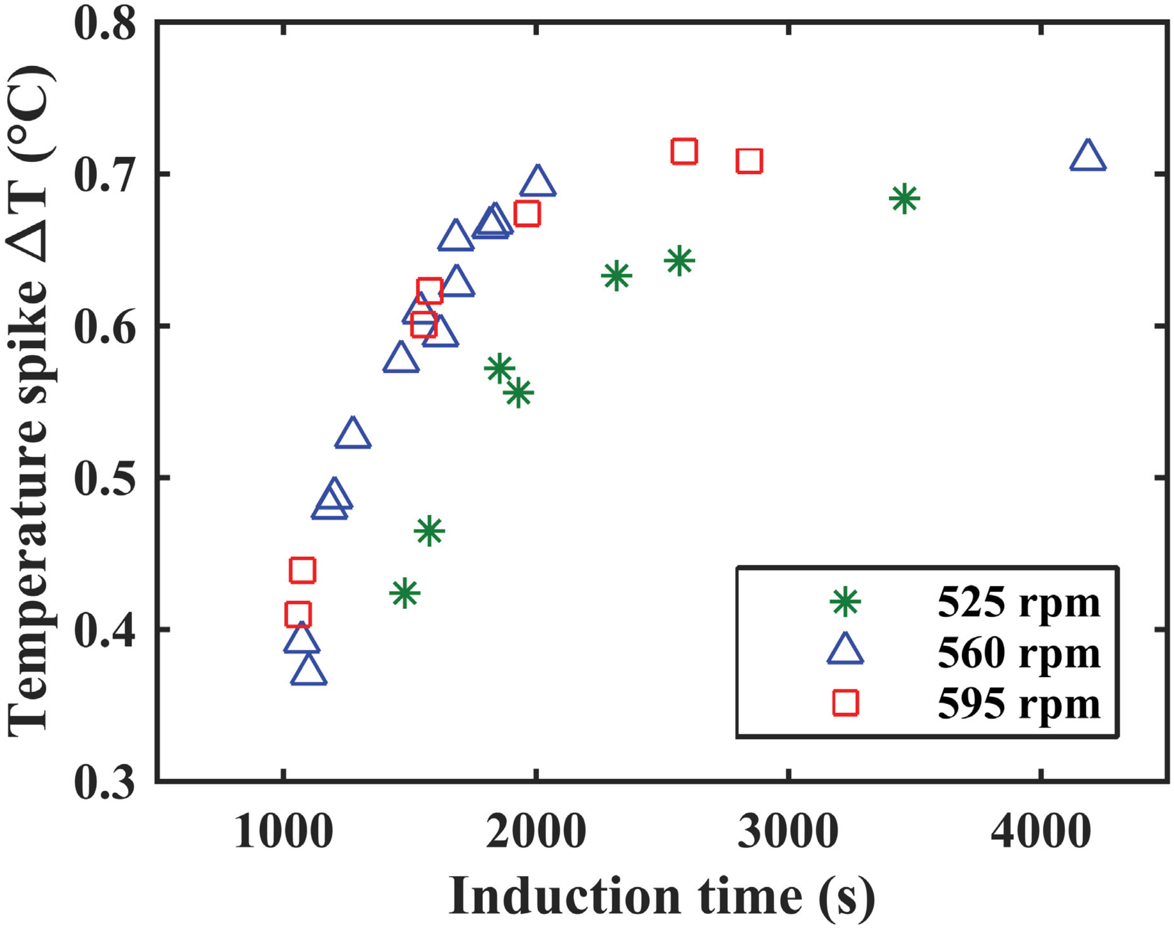

Figure 3.7: Temperature spike versus induction time for 3 different mixing rates in a CO2-water gas hydrate system: * 525 rpm, △ 560 rpm, □ 595 rpm.

3.5.1.3 Analysis of Liquid Mole Fraction Before Nucleation

Focusing on the moles consumed before hydrate nucleation during a kinetic run, it is possible to extract information from the gas dissolution kinetics. The model presented in Eq. 3.2 is used to regress the hypothetical maximum amount of liquid moles dissolved n_{liq} and the time constant τ, used to designate the point in time where 63.2% of the n_{liq} is reached. The data regressed was using the CO_2 hydrate experimental runs from the previous two sections. Only the gas consumption data before hydrate formation is used for the regression. This differs from traditional dissolution results that are taken at the three-phase equilibrium conditions because the moles consumed used in the regression are taken at hydrate-forming conditions where the system is metastable. Results are presented in Table 3.2 with the 95% confidence intervals on each parameter. The dissolution at the same mixing rate but different driving forces has the same time constant with 95% confidence. Therefore, there is no significant difference in the amount of time to dissolve n_{liq} moles for different driving force. However, the liquid mole fraction limits are higher with greater driving force. This explains the faster nucleation and the presence of a greater initial amount of gas hydrate for the highest driving forces. Even though the time constant is the same, the mole fraction limit is greater for higher driving forces, resulting in more moles dissolved in the same amount of time. For different mixing rates, opposite trends are observed. With 95% confidence, the time constant decreases with increasing mixing rate. On the other hand, the hypothetical liquid mole fraction is not affected by the mixing rate. This means that gas dissolves faster for a higher mixing rate at the same conditions and driving forces. The mole saturation values are directly related to the driving force and do not seem to be influenced by the mixing rate, at least for the range investigated in this work. These values were compared to the number of moles dissolved at nucleation for all the carbon dioxide experiments. With 95% confidence, the values of mole saturation and mole dissolved at nucleation were the same. This means that the excess gas in the liquid can be calculated by subtracting the amount of equilibrium three-phase moles in the experimental quantity of liquid (300 mL) to n_{liq}. To use intensive properties, the mole fractions were used instead of quantity of moles for the supersaturation discussion.

Table 3.2: Metastable dissolution modeling parameters of all experimental conditions for CO2 hydrates.

Pressure driving force (kPa)	Mixing speed (rpm)	τ (s)	$\tau_{95\%,\text{lower}}$ (s)	$\tau_{95\%,\text{upper}}$ (s)	n_{liq} (mol)	$n_{\text{liq},95\%,\text{lower}}$ (mol)	$n_{\text{liq},95\%,\text{upper}}$ (mol)
204	560	326	314	338	0.237	0.233	0.242
317	560	314	310	318	0.248	0.245	0.250
435	560	304	299	310	0.256	0.252	0.260
317	525	405	386	423	0.244	0.238	0.249
317	595	278	272	284	0.248	0.243	0.252

Figure 3.8 plots the liquid mole fraction supersaturation percent against the temperature difference in the bulk liquid for all the carbon dioxide experiments at all driving forces and mixing rates. Liquid mole fraction supersaturation is defined in Eq. 3.3.

$$\text{Liquid mole fraction supersaturation } \% = 100\% \left(\frac{x^{L} - x^{HLV}}{x^{HLV}}\right) \qquad \text{Eq. 3.3}$$

Where x^{L} is the calculated liquid mole fraction just before nucleation and x^{HLV} is the liquid mole fraction at three-phase equilibrium at the same temperature as the experimental condition. The baseline of 0% liquid mole fraction supersaturation corresponds to the mole fraction value from the three-phase equilibrium of carbon dioxide hydrates at 2 °C and 1574 kPa. At these conditions, the three-phase equilibrium liquid mole fraction of carbon dioxide was predicted to be 0.0161 using the model by Hashemi et al. (Hashemi et al., 2006) based on the thermodynamic equilibrium of gas hydrates (van der Waals et al., 1959; Parrish et al., 1972) and the Trebble-Bishnoi equation of state (Trebble et al., 1987; 1988). The linear fit and 95% confidence intervals show that the temperature spike increases linearly with liquid supersaturation independently of the driving force and mixing rate of the system. This validates the fact that the more the system is supersaturated, the greater initial formation of gas hydrates at nucleation. Additionally, of the 46 carbon dioxide hydrate experiments, no system ever goes above 30% liquid mole fraction supersaturation. This could indicate that there is an actual experimental limit of liquid mole fraction before nucleation occurs. Contrary to spontaneous nucleation at the spinodal point (Englezos et al., 1988), this experimental limit is significantly lower. For example, the spinodal limit of methane hydrates at 0.85 °C and 3290 kPa is 3.266E-2 while the equilibrium point is 1.40E-3 (Englezos et al., 1988). This results in a liquid mole fraction supersaturation that is at least 75 times greater than the thermodynamically prediction spinodal values seen in this study. Obviously, increasing the driving force will allow the potential supersaturation percent to go up, however, this would also decrease the induction time and the hydrates would form before the liquid mole fraction gets above this experimental limit. These results are characteristic of the hydrodynamics of the present experimental setup. However, it is believed that the same trend than in Figure 3.8 can be realized in any experimental setup. Unstirred systems would be more suitable to achieve greater liquid mole fraction supersaturation values and study this experimental supersaturation limit.

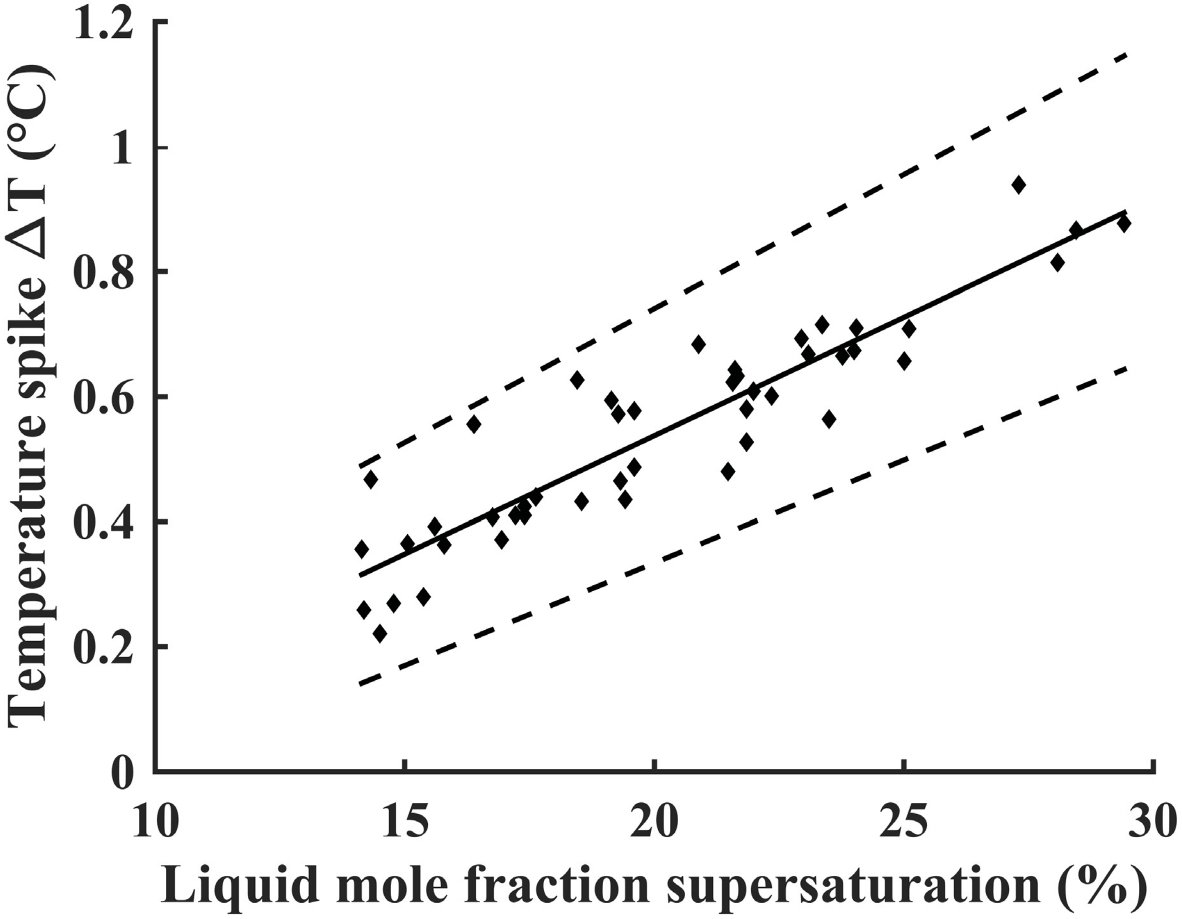

Figure 3.8: Temperature spike versus liquid mole fraction supersaturation of CO2 hydrates for all experimental conditions. Data was fit with a linear trend shown by the solid line and the 95% confidence intervals shown in dotted lines.

3.5.2 Methane Hydrate Kinetics

3.5.2.1 Effect of Driving Force

The effect of induction time on methane gas hydrates is studied below. Experiments were conducted at two different driving forces, 698 kPa and 1564 kPa and the same mixing rate of 560 rpm. The conditions are displayed in Table 3.3. The 698 kPa driving force was selected to compare with the same temperature driving force (subcooling) as the CO_2 hydrate system while the 1564 kPa driving force was chosen because it is the same as a driving force used in previous reports (Bergeron et al., 2010; Verrett et al., 2012a; Pasieka et al., 2013a).

Table 3.3: Two different driving force conditions for CH_4 hydrate kinetic experiments.

Temperature (°C)	Pressure (kPa)	Temperature subcooling (°C)	Pressure driving force (kPa)	Mixer speed (rpm)
2	3869	2	698	560
2	4735	4	1564	560

In Figure 3.9, the gas consumption rate is plotted against induction time. The decreasing trend that is evident with carbon dioxide hydrate growth is not present with methane hydrates. The coefficient of variation for 698 kPa driving force is 4.8% (average of 7.27E-6 mol/s and standard deviation of 3.5E-7 mol/s). For 1564 kPa driving force, the difference is 2.4% (average of 1.27E-5 mol/s and standard deviation of 3E-7 mol/s). Once again, it was observed that with higher driving forces came shorter induction times. This is even more apparent with methane hydrates because the induction times of different driving forces are further apart than the carbon dioxide experiments and they do not even overlap.

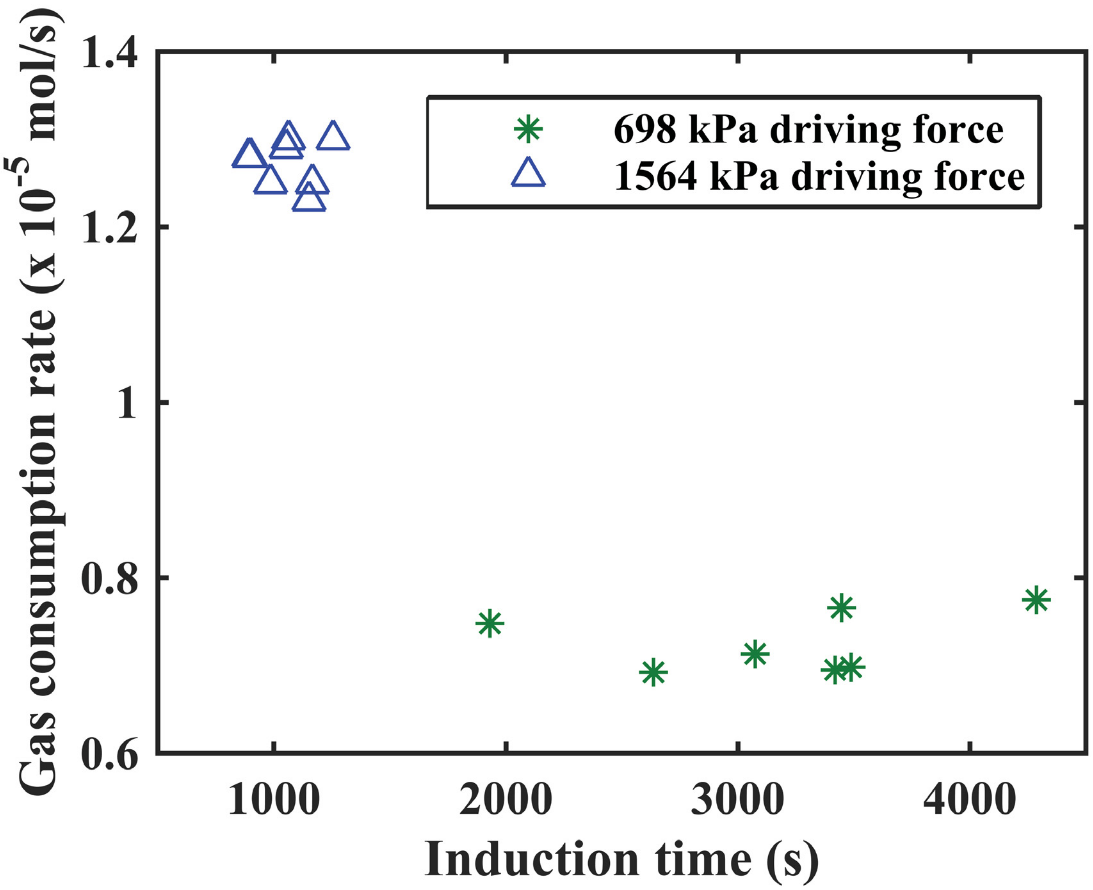

Figure 3.9: Gas consumption rate versus induction time for 2 different driving forces in a CH_4-water gas hydrate system: * 698 kPa, △ 1564 kPa.

Figure 3.10 demonstrates the dissolution kinetics of the methane hydrate system by comparing the temperature difference in the bulk liquid change with induction time. In all experiments at the 298 kPa driving force, the liquid phase had enough time to reach near its complete supersaturation state. This can be comprehended from the temperature spike measurements that are very similar. For the 1564 kPa driving force, the temperature spikes vary quite significantly but with no clear trend with the induction time. This indicates that, to the contrary of carbon dioxide gas hydrates, methane gas hydrates do not have a clear trend between the supersaturation liquid mole fraction and the temperature difference in the bulk liquid. One reason for this can be the limitation of the precision of the temperature probes being achieved. It can also be due to the fact that methane is about ten times less soluble in water than carbon dioxide. This can help explain why the supersaturation dissolution kinetics are much less important in the case of methane hydrate formation. Incidentally, the temperature spike, or initial amount of hydrates formed at nucleation, is also about ten times smaller in methane than carbon dioxide when comparing both 698 kPa driving force experiments. In sum, at these experimental conditions, it is not as crucial to study the change of gas consumption rate with induction time in the case of methane hydrates as it is with carbon dioxide hydrates. However, the trend could become apparent if the driving force and mixing rate are different, so it should remain an important consideration.

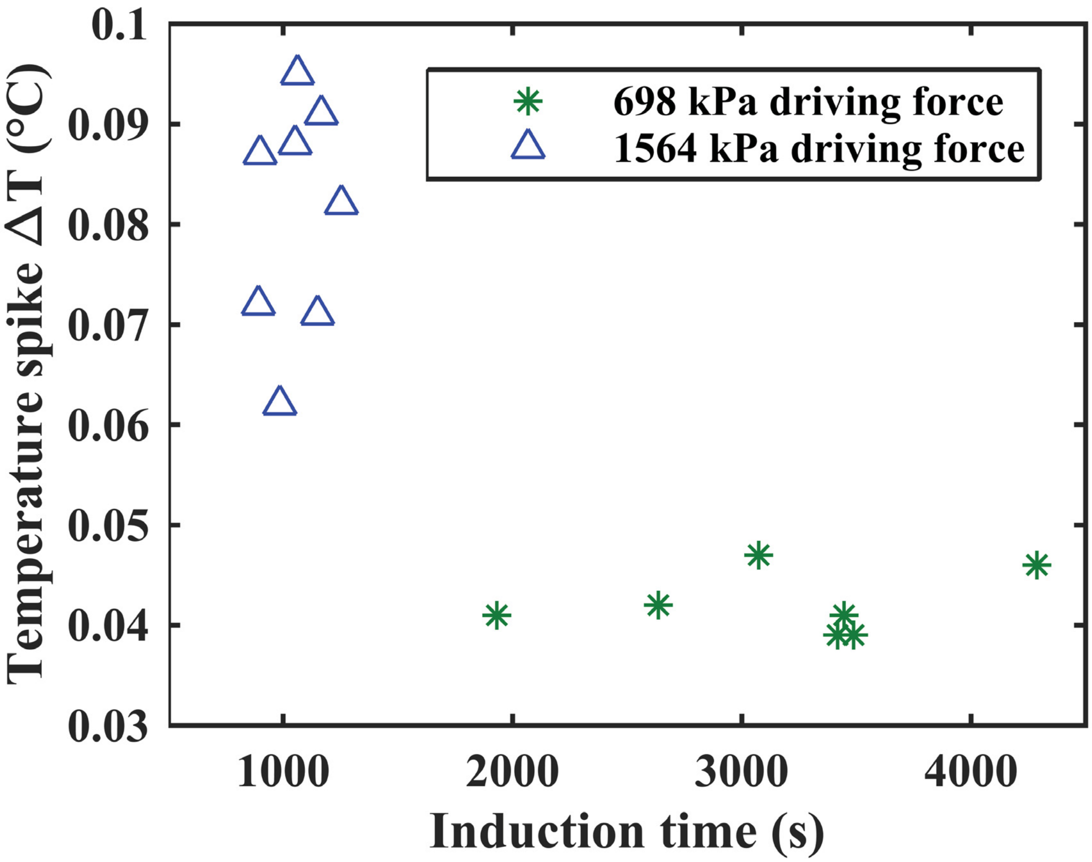

Figure 3.10: Temperature spike versus induction time for 2 different driving forces in CH4-water gas hydrate system: ∗ 698 kPa, △ 1564 kPa.

3.5.2.2 Discussion on Mole Fraction

The last part of this study investigates the liquid mole fraction during dissolution of a supersaturated methane gas hydrate system. Pure system mole fraction has been studied at the three-phase equilibrium and during the hydrate growth phase (Servio et al., 2002; Bergeron et al., 2009) but not during the dissolution phase of a supersaturated system to the knowledge of the authors. An experimental run where the gas hydrate formation took a very long time was used. The mole fraction was measured when no more detectable amount of methane gas would dissolve into the liquid phase; hence it had reached complete supersaturation for the specific conditions and the gas consumption had reached a plateau. For these results, the dissolution mole fraction measurement was taken at 7450 seconds and the gas hydrates nucleated at 10 795 seconds. Shortly after nucleation, the growth phase liquid mole fraction sample was collected for comparison. It is assumed that the thermodynamically dependent mole fraction measurements are not affected by the decrease in volume in the reactor. Pressure and temperature in the system were kept constant throughout the whole experiments, including during sample extraction. The results are shown in Table 3.4. The three-phase equilibrium value was predicted using the model by Hashemi et al. (Hashemi et al., 2006) based on the thermodynamic equilibrium of gas hydrates (van der Waals et al., 1959; Parrish et al., 1972) and the Trebble-Bishnoi equation of state (Trebble et al., 1987; 1988). The predicted three-phase equilibrium value is within the confidence interval of the hydrate growth liquid mole fraction measurement. As shown in Hashemi et al. (Hashemi et al., 2009), the liquid mole fraction at nucleation should be equal to its equilibrium value. They showed that the liquid mole fraction increases with time until eventually decreases towards its equilibrium with time. Verrett et al. (Verrett et al., 2012a) also observed the increasing trend of liquid mole fraction upon nucleation experimentally. The liquid mole fraction measurement during the dissolution phase is greater than the growth phase mole fraction with 95% confidence. Since the liquid mole fraction drops down to the three-phase equilibrium mole fraction upon hydrate nucleation, the system depends on the gas transfer to the liquid phase to start the hydrate growth. According to this explanation, for the system used in this study, the growth process would be mass-transfer limited at the gas-liquid at initial nucleation. This is a similar conclusion to the work by Skovborg et al. (Skovborg et al., 1994). Eventually, as the hydrates grow and the liquid mole fraction increases, growth becomes a reaction-limited system as shown by Bishnoi and coworkers (Vysniauskas et al., 1983; 1985). These results provide additional insight on the work by Bergeron et al. (Bergeron et al., 2009) and the behaviour of the liquid mole fraction before and after gas hydrate nucleation at supersaturated conditions for a stirred tank reactor.

Table 3.4: Mole fraction of CH4 at 2 °C and three different conditions: three-phase equilibrium at 3160 kPa, full supersaturation before hydrate formation at 3780 kPa and during hydrate growth at 3780 kPa.

	Temperature (°C)	Pressure (kPa)	x_{CH4}	$x_{CH4,95\%,lower}$	$x_{CH4,95\%,upper}$
3-phase equilibrium	2	3160	1.15E-03	-	-
Full supersaturation before hydrates	2	3780	1.25E-03	1.18E-03	1.31E-03
During hydrate growth	2	3780	1.12E-03	1.07E-03	1.16E-03

3.6 Conclusion

Kinetic experiments with carbon dioxide-water gas hydrates showed that the gas consumption rate decreases with increasing induction time. This is a significant finding for carbon dioxide gas hydrate studies that report a singular gas consumption rate or use this value to calculate the intrinsic kinetic rate. In all experiments, a higher driving force resulted in a shorter average induction time. The coefficients of variation on the carbon dioxide gas hydrate gas consumption rates were 2.7% for 204 kPa driving force, 9.7% for 317 kPa driving force and 9.6% for 435 kPa driving force. A high mixing rate that does not cause gas bubble formation was optimum for a smaller deviation in gas consumption rate at the same experimental conditions. For carbon dioxide hydrates, a longer induction time for these hydrates also resulted in a higher bulk liquid temperature increase at hydrate nucleation meaning a greater amount of initial hydrates formed. Methane hydrates did not exhibit the same behaviour of gas consumption rate with induction time that was observed with carbon dioxide hydrates. Coefficients of variation in gas consumption rates for methane hydrates were 4.8% for 698 kPa driving force and 2.4% for 1564 kPa driving force. Nevertheless, it was recommended to consider the trend of gas consumption rate with induction time regardless of the hydrate gas former, driving force and mixing rate. A regression of metastable dissolution during these kinetic experiments showed that the dissolution time constant decreased with increasing mixing rate. An increased driving force resulted in a greater the liquid mole fraction limit. Lastly, the maximum experimental liquid mole fraction supersaturation seen in all experiments was still 75 times smaller than the thermodynamically predicted spinodal limit.

3.7 Acknowledgments

The authors are grateful to the Natural Sciences and Engineering Research Council of Canada (NSERC) (grant number: 206269), les Fonds Québécois de la Recherche sur La Nature et les Technologies (FRQNT), McGill University and the McGill Engineering Doctoral Award (MEDA) for financial funding and support.

Chapter 4

4 Kinetics of Carbon Dioxide Gas Hydrates with Tetrabutylammonium Bromide and Functionalized Multi-Walled Carbon Nanotubes[1]

4.1 Preface

Chapter 3 observed the effect of induction time on pure gas hydrate systems. In this chapter, the analysis method of using the relationship between induction time and gas consumption rate for carbon dioxide systems is used on a system that combines two hydrate promoters. The thermodynamic promoter tetrabutylammonium bromide, TBAB, and the kinetic promoter multi-walled carbon nanotubes, MWCNTs, are studied in a carbon dioxide semi-clathrate system. The new method developed in Chapter 3 will allow for the successful kinetic evaluation on the effect of adding MWCNTs to a TBAB-carbon dioxide hydrate system. This system is relevant for potential industrial applications where higher temperatures can be used due to the presence of TBAB.

---

[1] Reproduced with permission from "Renault-Crispo, J.-S. and Servio, P. "Kinetics of Carbon Dioxide Gas Hydrates with Tetrabutylammonium Bromide and Functionalized Multi-Walled Carbon Nanotubes." *Energy* 128: 414-420. 2017."

4.2 Abstract

The effects of oxygen-functionalized multi-walled carbon nanotubes (MWCNTs) on tetrabutylammonium bromide (TBAB)-water-carbon dioxide semi-clathrate system was investigated. A system comprised of 9.5 ppmw MWCNTs and 40 wt % TBAB was chosen and the average gas consumption rate was calculated for different conditions. At 14 °C, the average gas consumption rate during growth decreased to a plateau with increasing induction time at 3.0 °C subcooling for systems with and without MWCNTs. The addition of MWCNTs increased the gas consumption rate during growth for induction times less than one hour but did not affect it at longer induction times. The maximum gas consumption enhancement from the added MWCNTs was 15 %. Dissolution runs at equilibrium conditions indicated that the presence of MWCNTs improved the dissolution rate of carbon dioxide gas into the liquid by lowering the time constant τ by 5 %. This suggests that the gas-liquid interfacial resistance of carbon dioxide gas mass transfer is not the limiting factor for hydrate growth in this TBAB semi-clathrate system with and without nanoparticles. At a lower subcooling of 1.5 °C, there was no significant difference in the gas consumption rates with the addition of MWCNTs, due to prolonged induction times.

4.3 Introduction

Global warming and climate change have become major topics of worldwide concern. Due to its high stability and concentration in the atmosphere, carbon dioxide gas is the largest contributor to the greenhouse effect. Reducing carbon dioxide emissions is an international priority as nations strive to meet the increasingly stringent commitments made at forums such as the 2015 United Nations Climate Change Conference in Paris (2015). A multifaceted approach is needed to achieve this, and developing effective carbon dioxide removal methods is a viable solution. According to the U.S. Department of Energy, novel gas hydrate technologies are promising methods for capturing and storing carbon dioxide gas (Elwell et al., 2006). Carbon dioxide recovery from flue gas using gas hydrate technology has been shown to be thermodynamically possible (Kang et al., 2000a; Linga et al., 2007; Babu et al., 2013; Zheng et al., 2016a). Gas hydrates are nonstoichiometric crystalline compounds that arise when a gas or volatile liquid is encapsulated inside cavities formed by water molecules. The guest molecule must be of correct size to fit inside and stabilize the crystal lattice via weak van der Waals forces with the host water molecules (Sloan et al., 2008). There are over 180 different molecules that form gas hydrates; the most relevant for research and industrial applications being methane, ethane and carbon dioxide (Englezos, 1993). Transportation and storage of natural gas, methane or carbon dioxide have been discussed as feasible alternatives to current technologies because gas hydrates have high gas storage capacities. One single cubic meter of methane hydrate can release up to 160 cubic meters of methane gas (Taylor et al., 2003). In addition, separation of gases using gas hydrate technologies has been extensively discussed in literature and offers a promising opportunity for carbon dioxide capture (Chatti et al., 2005; Eslamimanesh et al., 2012; Babu et al., 2015; Ma et al., 2016). The lack of scalability studies as well as slow and unpredictable hydrate formation kinetics have prevented large scale development of the proposed technologies (Yin et al., 2016).

One limitation of a hydrate-based technology is the high pressure and low temperature conditions needed for hydrate formation. This can be addressed using thermodynamic promoters that shift the gas hydrate equilibrium to more energetically favourable conditions. One category of thermodynamic promoter chemicals is called semi-clathrates since the molecule incorporates itself inside the water lattice, consequently stabilizing the structure and significantly lowering the hydrate energetics. These semi-clathrate forming compounds are typically ionic molecules that have their cationic part occupying cages like guests and their anionic part involved in the cage formation alongside water. The tetrabutylammonium bromide (TBAB) salt is the most commonly used semi-clathrate forming promoter. At atmospheric pressure, TBAB hydrates can form at temperatures up to 12.4 °C (Aladko et al., 2002). Previous studies have generally focused on the thermodynamics of TBAB hydrates, namely the equilibrium temperature, pressure and TBAB liquid concentration with single and multiple guest gases (Arjmandi et al., 2007; Sun et al., 2010; Bouchemoua et al., 2011; Verrett et al., 2015). Multiple groups have demonstrated the possibility of separating carbon dioxide from flue gases using TBAB hydrates (Li et al., 2010; Babu et al., 2014b).

Li et al. showed that TBAB shortens induction time and accelerates hydrate kinetic formation rates (Li et al., 2010). In another report, it was shown that a 40-45 wt % TBAB solution may be a promising cold storage material for air conditioning systems due to its high phase change temperature and its improved hydrate conversion (Mahmoudi et al., 2016). Recently, the kinetic behaviour of TBAB and carbon dioxide gas hydrates was thoroughly investigated at temperatures ranging from 13.85 °C to 15.85 °C (Verrett et al., 2016). Other semi-clathrate forming salts, such as tetrabutylammonium nitrate ($TBANO_3$) and tetrabutylammonium fluoride (TBAF) have also been studied and proven feasible for use in hydrate based gas separation applications (Babu et al., 2014a; Babu et al., 2014c; Zheng et al., 2016b).

Carbon nanotubes (CNTs) show great potential for a wide range of products and applications, including the use as kinetic promoters in the field of gas hydrates. CNTs are self-assembling rolled sheets of graphene that exhibit excellent mechanical strength in addition to high thermal and electrical conductivity (Hordy et al., 2013b). Many different synthesis strategies and applications exist to produce various types of carbon nanostructured materials (Reddy et al., 2008; Reddy et al., 2009; Reddy et al., 2010; Khan et al., 2016). Carbon nanotubes have a very high aspect ratio, which makes them attractive for use as a kinetic gas hydrate promoter (Dresselhaus et al., 2001). The nanotubes are dispersed in a base fluid to create a “nanofluid” that can be used as the hydrate-forming liquid phase (Choi et al., 1995). Oxygen-functionalized multi-walled carbon nanotubes (MWCNTs)-hydrate experiments were first reported in 2010 by Park et al. (Park et al., 2010). They used 40 ppmw MWCNT in water and observed an increase in methane consumption and hydrate growth rate (Park et al., 2010; Park et al., 2012). Pasieka et al. reported a slight hydrate growth enhancement and increased dissolution rates using 1 to 10 ppmw MWCNT (Pasieka et al., 2013a; 2014). Additionally, many groups reported a significant decrease in induction time with the presence of nanoparticles (Arjang et al., 2013; Zhou et al., 2014; Nesterov et al., 2015). At this point, few publications have investigated the effect of combining a thermodynamic promoter such as TBAB with a kinetic promoter such as MWCNT. The addition of 200 to 500 ppmw silver nanoparticles, 0.1 wt % SDS and 0.5 to 1.0 wt % cyclodextrin to a gas hydrate system resulted in an increase in carbon dioxide gas consumption and apparent kinetic growth rate constant (Mohammadi et al., 2014).

Furthermore, the combination of 10 to 60 ppmw MWCNTs with 19.1 wt % tetrahydrofuran also improved the kinetic growth rate (Lim et al., 2014). In a system with 20.3 wt % tetrahydrofuran (THF) at atmospheric conditions, it was shown that the addition of MWCNTs decreased the subcooling required for nucleation and enhanced the system's ability to expel the heat of formation via an increase in effective thermal conductivity (Pasieka et al., 2013b).

The goal of this paper is to observe the effect that the addition of MWCNTs has on the hydrate growth rate and dissolution rate (at three-phase equilibrium conditions) in a TBAB-water-carbon dioxide hydrate system. To the best knowledge of the authors, this is the first time that a report discusses the combination of TBAB and MWCNTs in any gas hydrate system. Semi-clathrate kinetic and dissolution analysis with the addition of nanoparticles is novel and provides crucial information for the possible hydrate based applications using these compounds.

4.4 Materials and Methods

4.4.1 Experimental Setup

A simplified diagram of the experimental setup can be found in Figure 4.1. A detailed description of the experimental setup and procedure can be found in a previous report (Bruusgaard et al., 2010). A 612 mL stainless steel reactor is submerged in a temperature-controlled 20 % by volume ethylene glycol-water bath. The inner reactor has dimensions of 4.5 inches height and 3.25 inches diameter. The reactor and temperature-controlled bath are equipped with a MM-D06 magnetic stirrer from Pressure Product Industries with a standard magnetic stir bar with spinning ring from Cole Parmer. The stirrer speed was fixed at 560 rpm. A reservoir gas tank is employed to keep the reactor pressure constant during experiments with a Baumann 51000 control valve. The valve is controlled by the difference in pressure signals between the reactor bias gas tank and the reactor. Pressures are monitored using Rosemount pressure transducers configured to a span of 0-14,000 kPa for absolute pressure measurements and 0-2000 kPa for differential pressure measurements, with an accuracy of 0.065 % of the given span. Resistance temperature detectors (RTD) probes from Omega record temperatures from the reactor liquid, reactor gas and reservoir tank. The reactor liquid RTD being located near the bottom of the reactor is always well below the liquid line, while the reactor gas RTD being located near the top of the reactor is always well above the liquid level line. Carbon dioxide gas with a purity of 99.995 % was obtained in Canada from MEGS Inc. The water was treated in-house by reverse-osmosis with a 0.22 µm filter and it has a conductivity of 10 µS and total organic content less than 10 ppmw. 50 wt % TBAB in liquid water was obtained from Sigma Aldrich United States and used to prepare the 40 wt % TBAB mixture used in this study. The solution of 40 wt % TBAB was selected because this value is near the stoichiometric amount of TBAB required to form hydrates and the thermodynamic equilibrium data was available at this concentration making it possible to fix the driving force (Verrett et al., 2015).

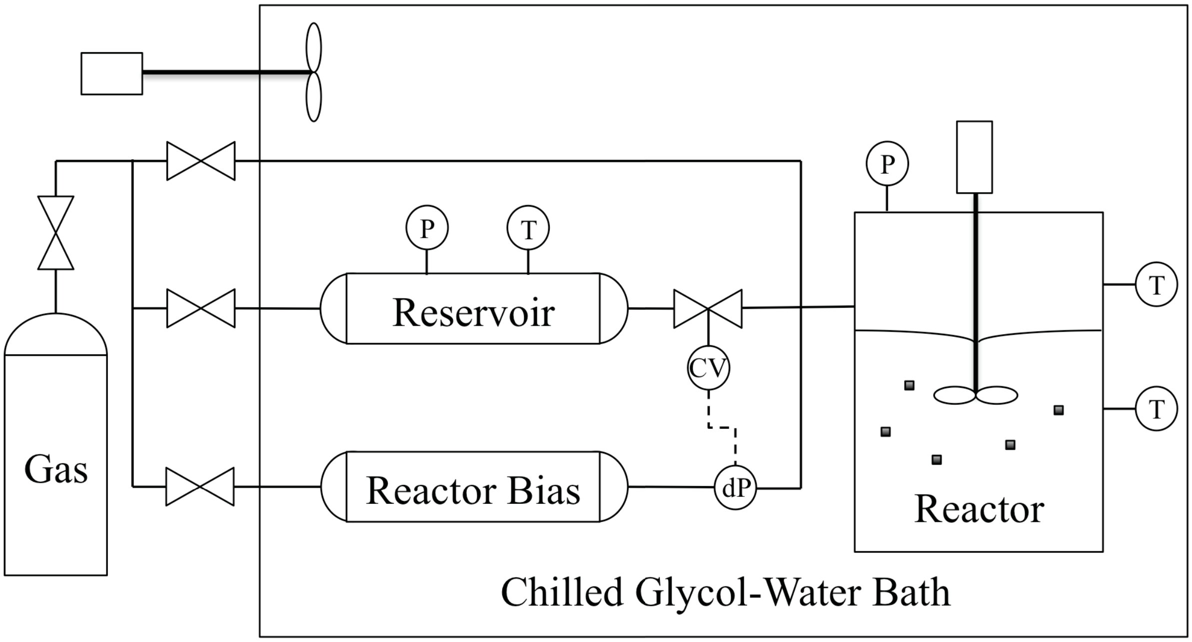

Figure 4.1: Schematic of the experimental setup.

Oxygen functionalized multi-walled carbon nanotubes were produced following the procedure developed by Hordy et al. (Hordy et al., 2013b). A 316 stainless steel mesh acts as a support material and catalyst for MWCNT growth. The stainless steel mesh was placed on a ceramic boat, itself inserted into a quartz tube furnace for MWCNT growth by thermal chemical vapour deposition. The carbon source, acetylene, was flowed for 4 minutes at a furnace temperature of 700 °C, conditions that led to the growth of a dense MWCNT forest on the mesh. The as-produced MWCNT-covered mesh was then exposed to a capacitively-coupled radio-frequency (13.56 MHz) glow discharge plasma in an $Ar/O_2/C_2H_6$ gas mixture (250/5/1 sccm). Exposure to the plasma led to the addition of oxygen-containing functional groups onto the MWCNTs (CO, COOH, OH), thus rendering them superhydrophilic. The MWCNT-covered mesh was then submerged in water and placed in an ultrasonic bath where intense agitation broke off the nanotubes from the mesh and dispersed them into the surrounding liquid. The suspended MWCNTs measure on average 3-5 μm in length and ~30 nm in diameter and are stable in water for extended periods of time (Hordy et al., 2013a). Fourier transform infrared spectroscopy (FTIR) spectroscopy of the produced nanoparticles can be found in the following reference (Vandsburger et al., 2009); however, it was found that X-ray photoelectron spectroscopy (XPS) was more useful in elemental analysis for these MWCNTs (Hordy et al., 2013b; Hordy et al., 2013a; Jorge et al., 2017). The functionalized MWNTs were shown to be superhydrophilic through contact angle measurement using a goniometer (Vandsburger et al., 2009). Images of the dispersion can be found in the following references (Vandsburger et al., 2009; Hordy et al., 2013b; Hordy et al., 2014). The MWCNTs were shown to be stable in different solutions (Hordy et al., 2014) and at pH ranging from 4 to 12 (Jorge et al., 2017). The reader is referred to Baddour et al. (Baddour et al., 2009), Vandsburger et al. (Vandsburger et al., 2009), Hordy et al. (Hordy et al., 2013b; Hordy et al., 2013a; Hordy et al., 2014) and Jorge et al. (Jorge et al., 2017) for more information regarding the production and characteristics of the MWCNTs. Nanofluid made up of 9.5 ppmw of MWCNTs were used in this work because it was the limitation of the production process and it was the highest concentration used in Pasieka et al. (Pasieka et al., 2013a; 2014; Pasieka et al., 2015).

4.4.2 Hydrate Growth Experiments

Initially, the reactor was rinsed three times with 360 mL of water. The reactor was then loaded with 360 mL of the hydrate forming liquid. This liquid was either 40 wt % TBAB or 40 wt % TBAB with 9.5 ppmw MWCNTs. The system temperature was fixed at 14 °C for all experiments using the chiller to regulate the glycol bath. After the liquid sample was loaded, the reactor was purged with carbon dioxide gas three times by pressurizing to 1,100 kPa followed by de-pressurizing to 110 kPa. Once thermal equilibrium was reached, the system was pressurized to the experimental pressure based on the desired driving force. The driving force can be visualized as either a temperature subcooling or a pressure driving force when compared to the three-phase equilibrium line. TBAB equilibrium data for carbon dioxide can be found in the following references (Arjmandi et al., 2007; Deschamps et al., 2009; Verrett et al., 2015). The reservoir and reactor bias gas tanks were pressurized to 1,000 kPa above the reactor value to provide a pressure differential for gas transfer during the kinetic run. When the reactor temperature and pressure stabilized, the data acquisition system and control valve were turned on, and the stirrer inside the reactor was started. Hydrate nucleation was detected by a temperature increase in the bulk liquid and confirmed by visual inspection through the polycarbonate window mounted on the reactor. The time lapse between when the stirrer was turned on and the onset of gas hydrate nucleation was taken as the induction time. Once the hydrates nucleated, they were allowed to grow for at least 600 seconds. After the experiment, the data acquisition system and control valve were turned off and the reactor pressure was subsequently brought down to 110 kPa for the hydrates to dissociate. A pressure slightly above atmospheric was used to prevent entry of atmospheric gases into the reactor. At this point, the experiment could have been repeated at any selected driving force or the reactor liquid could have been changed for subsequent experiments.

Molar gas consumption rates, also referred to as hydrate growth rates, were calculated from the reservoir's pressure and temperature data over time using the Trebble-Bishnoi equation of state (Trebble et al., 1987; 1988). In these experiments, the gas consumption profile did not change for the first 120 seconds after nucleation. This trend is consistent with results reported by Verrett et al. (Verrett et al., 2016). Therefore, a linear regression was performed to fit a straight line after the initial 120 seconds of the growth phase. A fitting period of 300 seconds was selected to calculate gas consumption rates since the slope was constant over time at this point. Hydrate nucleation is indicated by a temperature spike ΔT that can be calculated from the difference between the highest temperature after nucleation and the temperature immediately before nucleation. A typical gas consumption versus time profile is shown in blue in Figure 4.2.

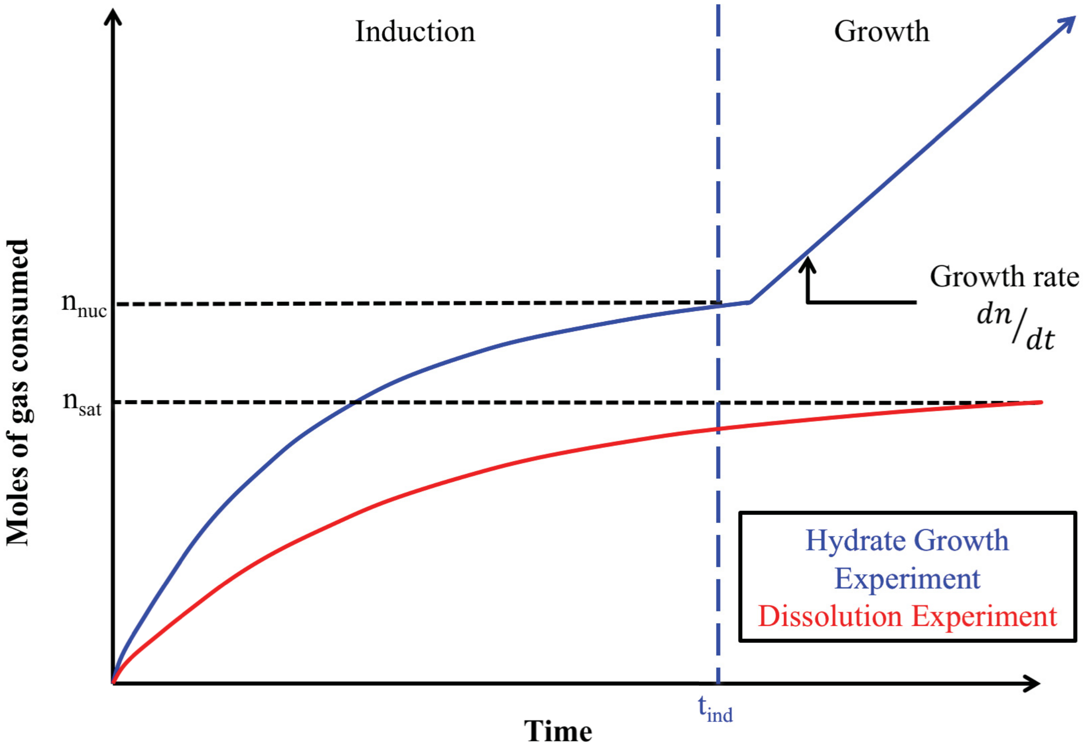

Figure 4.2: Simplified hydrate gas consumption curve. Blue: hydrate growth; Red: dissolution.

4.4.3 Dissolution Experiments

The two-phase dissolution experiments were performed in a similar manner to the three-phase hydrate growth experiments. In these experiments, the experimental pressure was set to the three-phase equilibrium value of 14 °C and 972 kPa (Verrett et al., 2015). This prevented hydrate nucleation and allowed the liquid to reach carbon dioxide saturation. Since it was impossible to enter the induction phase, this process terminated when the liquid phase became saturated at the saturated moles, denoted as n_{sat} in Figure 4.2. This occurred within one hour of the beginning of the experiment from the point where mixing is started, similar to the experiments completed by Pasieka et al. (Pasieka et al., 2015). First-order dissolution kinetics were subsequently fitted to the experimental data to regress for the time constant τ and the moles saturated n_{sat}. The time constant is used to designate the point in time when 63.2 % of the n_{sat} is reached. In Figure 4.2, the red line displays the mole consumption over time of a typical dissolution experiment.

4.5 Results and Discussion

4.5.1 3.0 ˚C Subcooling

The first set of experiments was conducted at 14 °C and 2678 kPa, corresponding to a subcooling of 3.0 °C. An example of kinetic run is shown in Figure 4.3. In this run, the gas hydrates nucleated at 3294 seconds, designated by the leftmost vertical green dotted line. As discussed in Verrett et al. (Verrett et al., 2016), there is a slight time delay at nucleation before gas starts being consumed again. This is because the oversaturated liquid has enough carbon dioxide dissolved to form and grow the hydrates for a short period of time without the need for more gas. This amount of time was estimated to be approximately 120 seconds. The gas consumption rate is obtained from a linear regression of 300 seconds after this time delay, as shown by the bounded green vertical dotted lines in Figure 4.3. Temperature spike or temperature difference from nucleation is calculated from the difference between the temperature immediately before nucleation and the maximum temperature after nucleation in the bulk liquid.

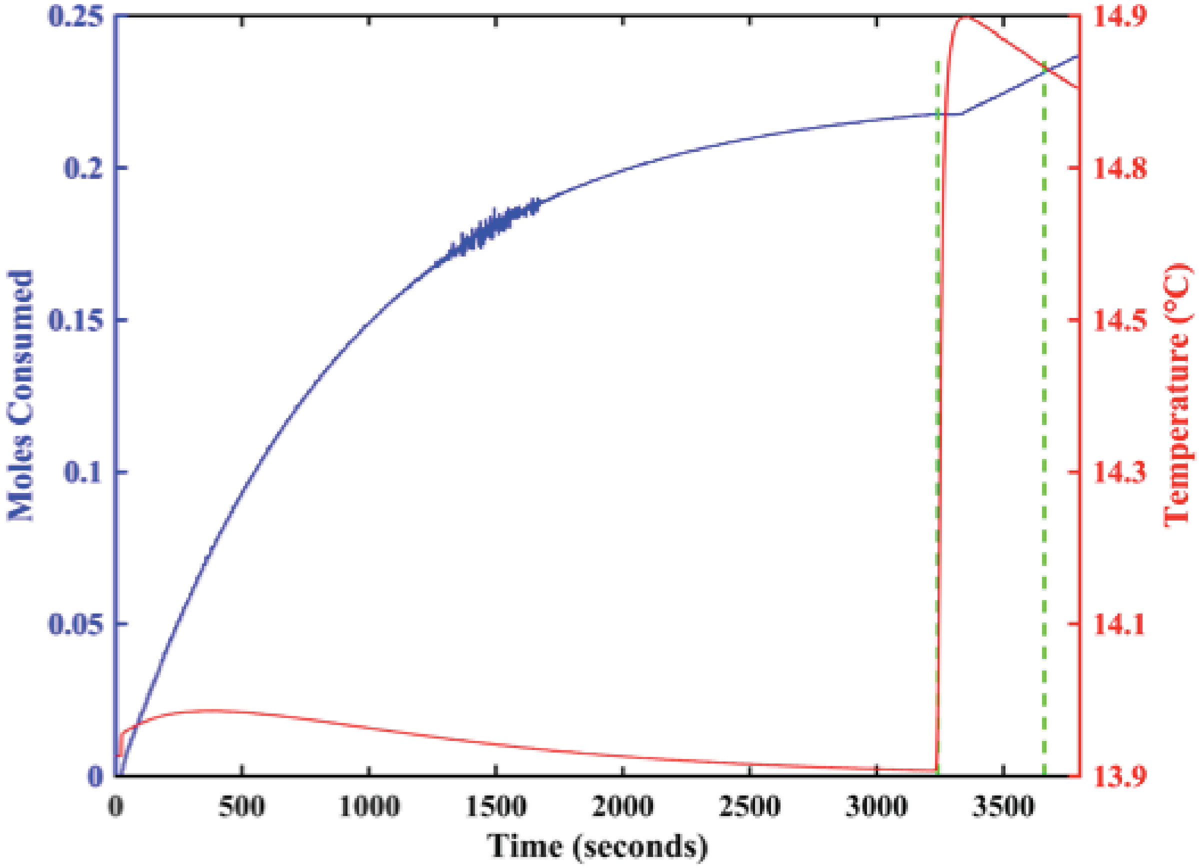

Figure 4.3: Example of a kinetic run during growth for TBAB-MWCNT-water-carbon dioxide gas hydrate system at 14 °C and 2678 kPa. Moles consumption data is shown in blue; reactor liquid temperature is shown in red.

The liquid phase was composed of either 40 wt % TBAB or 40 wt % TBAB + 9.5 ppmw MWCNTs. The average gas consumption rate for TBAB-water at this condition was 5.56E-5 mol/s with a 95% confidence interval (CI) of [4.51E-5, 6.60E-5] mol/s over 9 replicates. The average rate for TBAB-MWCNT-water was 5.28E-5 mol/s with a 95% CI of [4.45E-5, 6.11E-5] mol/s over 13 replicates. Since the confidence intervals of both systems significantly overlap, it cannot be said that the gas consumption rate is statistically different. However, when the rates are plotted against induction time, additional information can be extracted. The trend between gas consumption rate and induction time displays a clear first-order response that can be seen in Figure 4.4. Renault-Crispo et al. recently presented a similar trend with pure water kinetic runs. They showed that the gas consumption rate decreased to what seems like a plateau with increasing induction time, the same behaviour is observed with this semi-clathrate system, as shown in Figure 4.4 (Renault-Crispo et al., 2017). The gas consumption rates in both cases, TBAB and TBAB-MWCNT, decrease to a plateau when the induction time exceeds one hour (3600 seconds). The average induction time of both systems are not statistically different from each other. The 95 % confidence interval on the induction time for TBAB system is [1557, 6425] seconds while it is [1042, 4896] seconds for the TBAB-MWCNT system so it cannot be said that the addition of the nanotubes decreases induction time.

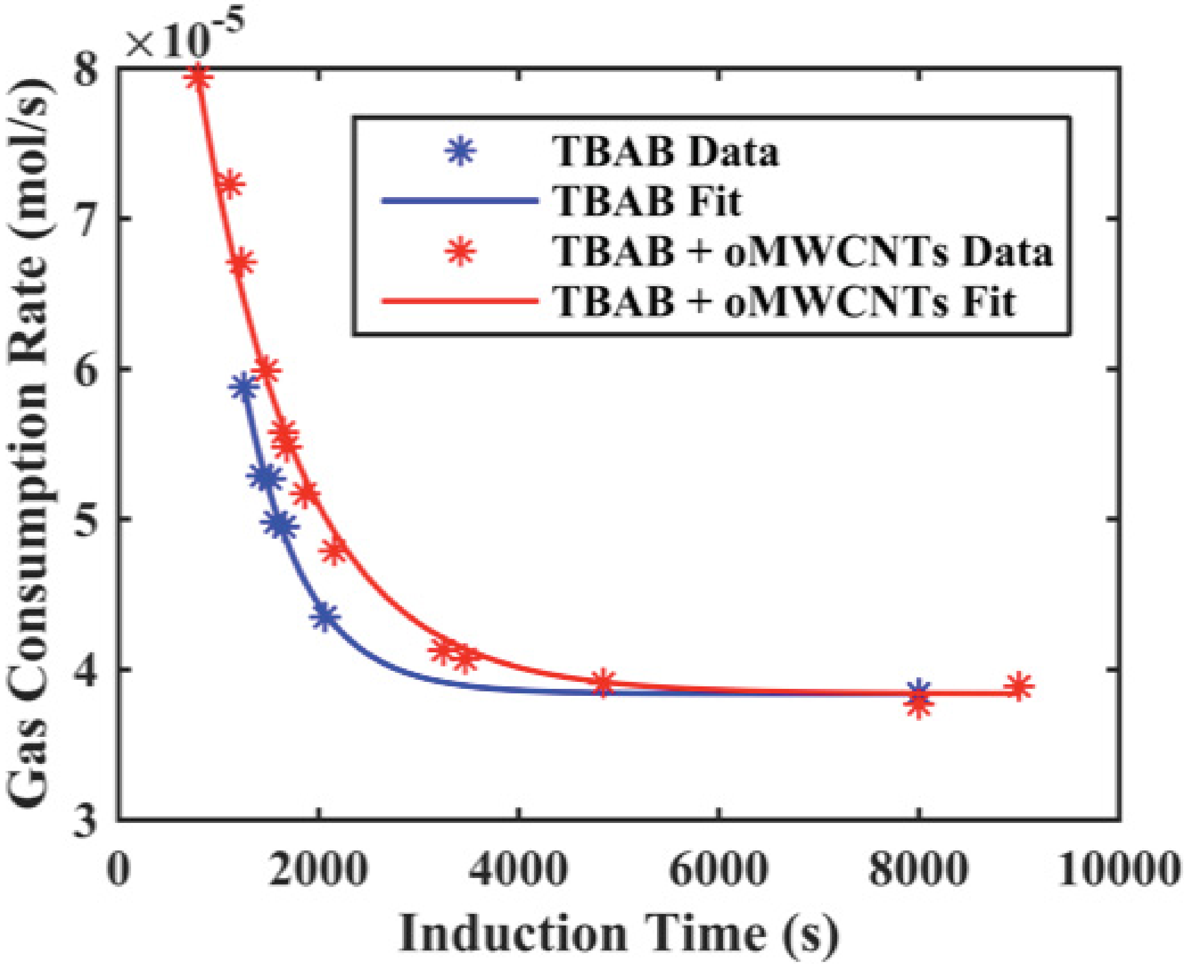

Figure 4.4: Gas consumption rate plotted against induction time for CO_2 hydrates at 14 °C and 3.0 °C subcooling. TBAB results are shown in blue and TBAB + MWCNT results are shown in red.

At shorter induction times, the gas consumption rate of TBAB-water hydrates is lower than the rate of TBAB-MWCNT-water hydrates. This is confirmed by regressing the time constant of a first-order response to the data from Figure 4.4. The 95 % confidence interval on the time constant for the TBAB system is from [533, 677] seconds, while the 95% confidence interval for the TBAB-MWCNT system is from [933, 1098] seconds. The regression of the gas consumption rate plateau value is statistically the same for both systems, a conclusion also visibly noticeable in Figure 4.4. Therefore, the addition of MWCNTs changes the kinetics of the TBAB gas hydrate system at short induction times. The gas consumption rate enhancement is visible in Figure 4.5. The enhancement percent compares gas consumption rates during growth of 40 wt % TBAB + 9.5 ppmw MWCNT hydrates against 40 wt % TBAB hydrates. Initially, the percent enhancement increases up to a maximum of 15 % at an induction time of 1870 seconds, followed by a decrease to 0 % when approaching induction times of about 8000 seconds. Hence, for this system and at these conditions, the maximum achievable gas consumption rate improvement with the addition of MWCNTs is 15 %.

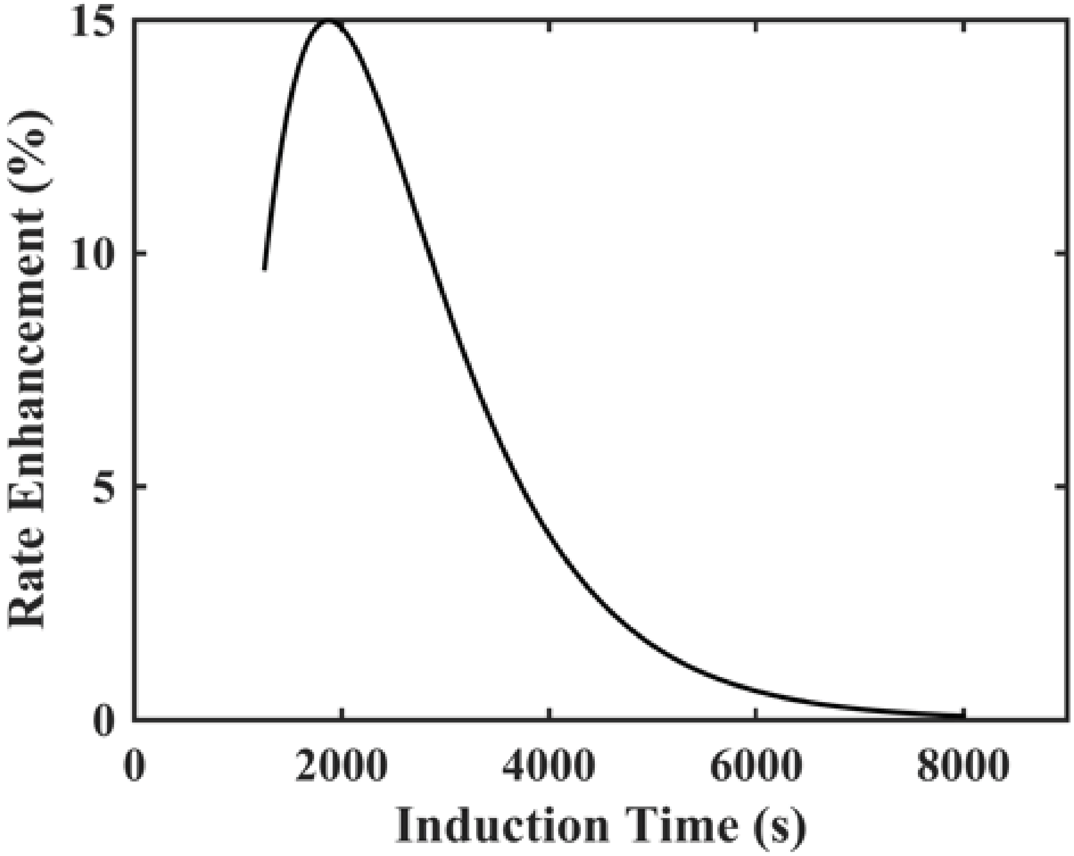

Figure 4.5: Gas consumption rate enhancement during growth of the fit of TBAB + MWCNT data over the fit of TBAB data plotted against induction time for CO2 hydrates at 14 °C and 3.0 °C subcooling.

To further investigate this behaviour, the liquid phase temperature spike from hydrate nucleation versus induction time is plotted in Figure 4.6. The temperature spike or temperature difference at nucleation is directly related to the initial amount of hydrates formed (Renault-Crispo et al., 2017). The addition of MWCNTs shifts the curve to lower temperature spikes. This can be attributed to two different causes. The first could be that the enhanced heat and mass transfer offered by a nanofluid helps dissipate the heat of hydrate formation more efficiently. The second could be that the addition of MWCNTs changes the dissolution kinetics in such a way that a different amount of gas is dissolved in the liquid in a given amount of time, resulting in a different temperature spike. The dissolution phase (induction phase) of the hydrate formation process is extremely reproducible and therefore the total gas consumed at a specific induction time will always be the same before hydrate nucleation. A system with better dissolution kinetics will therefore have more total gas consumed after the same induction time. This total gas consumed is also directly related to the mole fraction in the liquid phase which in turn determines the initial amount of gas hydrates formed at nucleation. The initial amount of gas hydrates formed at nucleation being an exothermic process can also be linked to a bulk temperature spike; the more initial hydrates formed, the greater the temperature spike. Accordingly, the effect of MWCNTs on the carbon dioxide dissolution kinetics at equilibrium are investigated more thoroughly in the next section.

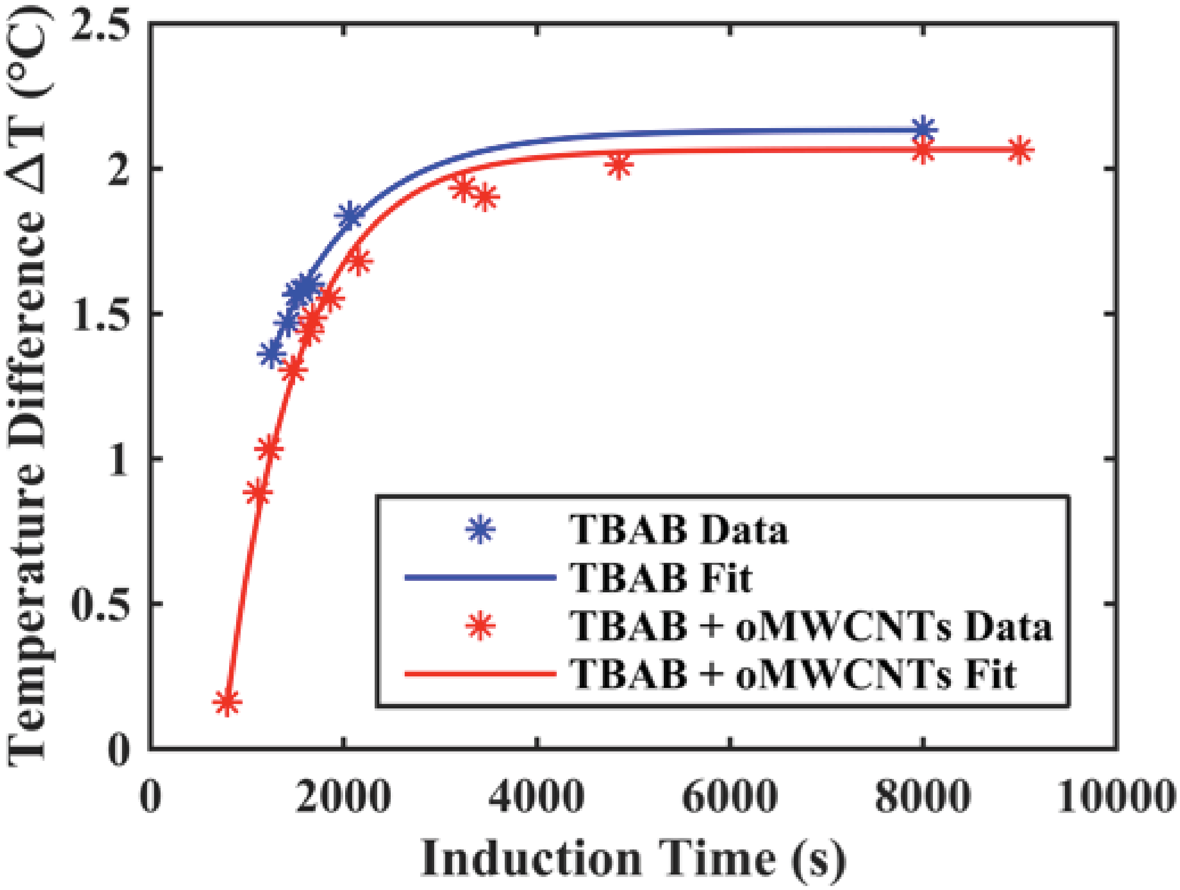

Figure 4.6: Temperature spike plotted against induction time for CO2 hydrates at 14 °C and 3.0 °C subcooling. TBAB results shown in blue and TBAB + MWCNT results shown in red.

4.5.2 Dissolution Experiments

Dissolution experiments for the carbon dioxide gas hydrate systems of TBAB or TBAB + MWCNT were performed at the same temperature as the kinetic experiments, (14 °C), but at the three-phase equilibrium pressure of 972 kPa. Due to the lack of driving force at this condition, hydrates cannot form and the system can be allowed to reach full saturation during the dissolution phase. All experiments were conducted for at least one hour since this was determined to be enough time to reach the mole saturation limit, when there was no more change in moles consumed. The moles consumed with time for each dissolution experiment were fitted to a first-order response (Zhu et al., 2008; Pasieka et al., 2014), where a regression for the time constant and moles saturated was accomplished. The time constant is defined as the time required for the liquid to reach 63.2 % of the saturation value. The lower the value of the time constant, the faster the dissolution of the system. The results for the regression are shown in Table 4.1 with the associated 95 % CIs. Five replicates for each system were completed.

Table 4.1: Dissolution kinetic regression of time constant and moles saturated for TBAB and TBAB + MWCNT systems.

System	**Time Constant (s)**			**Moles Saturated (mol)**		
	Average	Lower 95 % CI	Upper 95 % CI	Average	Lower 95 % CI	Upper 95 % CI
TBAB	906	899	913	0.080	0.077	0.084
TBAB + MWCNT	865	857	873	0.080	0.079	0.081

The time constant is lower for the system with the added MWCNTs. This means that the dissolution is faster in the presence of nanotubes. This helps understand the results in Section 3.1, where the runs with a shorter induction time had enhanced gas consumption. At short induction times, the carbon dioxide is still dissolving into the liquid phase and will continue to do so until the liquid is fully saturated even if the hydrates nucleate beforehand. At longer induction times where the dissolution phase is approximately complete, the gas consumption rate can be equated to the hydrate growth rate and no gas consumption rate enhancement is observed with the addition of

MWCNTs. Hence, the added nanotubes help improve the dissolution rate and therefore gas consumption rate at low induction time but they do not affect the hydrate growth rate. This suggests that the hydrate growth for this semi-clathrate system is not limited by the dissolution of carbon dioxide at the gas-liquid interface but rather by the resistance at the liquid-hydrate interface. It is important to note that this conclusion is made from results in a two-phase system without hydrates and at a lower pressure and not for a three-phase system with hydrates. Furthermore, these very low concentrations of MWCNTs should have negligible impact on the thermodynamics of the system (Pasieka et al., 2015). Pasieka et al. (Pasieka et al., 2014) reported that in a methane-water system, the addition of MWCNTs to water enhances the two-phase dissolution rate up to loadings of 5 ppmw, beyond which it comes back down to nominal values. It was also shown in a carbon dioxide gas hydrate system that the addition of amine-functionalized MWCNTs do not enhance two-phase carbon dioxide dissolution (Pasieka et al., 2015). These gas hydrate systems are notably different from the ones used in this publication. Here, the temperature is roughly 12 °C higher, the pressure is lower and the presence of the salt TBAB affects the liquid dissolution in a different way than with pure water systems. Even though there is a statistical difference between the time constants, it is important to consider that it is only a 5 % improvement in dissolution rates.

4.5.3 1.5 °C Subcooling

The final set of experiments was conducted at 14 °C and 1673 kPa corresponding to a subcooling of 1.5 °C. The purpose was to observe the difference between the addition of MWCNTs at two different driving forces. Gas consumption rates with induction times are shown in Figure 4.7 for TBAB and TBAB + MWCNT systems. The same trend as the 3.0 °C subcooling is present where the gas consumption rates decrease to a plateau with increasing induction time. The average consumption rate for the TBAB system is 1.55E-5 mol/s with a 95% CI of [1.45E-5, 1.65E-5] mol/s with 6 replicates. For the system of TBAB with MWCNTs, the average consumption rate is 1.61E-5 mol/s with a 95% CI of [1.51E-5, 1.71E-5] mol/s with 6 replicates. The variation in the lower subcooling experimental data is significantly lower. Figure 4.7 shows the gas consumption rates against induction time for both systems. There is no significant difference between the TBAB system and TBAB + MWCNT system at a driving force of 1.5 °C, since the 95 % CIs overlap. At this lower subcooling, the enhanced dissolution from the addition of MWCNTs does not significantly affect the gas hydrate kinetics. On average, the induction times are longer with the lower driving force experiments, suggesting that the dissolution phase is always almost completed at hydrate formation for the lower subcooling. In summary, for a TBAB-water-carbon dioxide gas hydrate system, the addition of MWCNTs only influences the dissolution rates and does not modify the hydrate growth rate. This is different than what has been reported for pure water gas hydrate systems where the addition of MWCNTs has been shown to affect the growth rates (Pasieka et al., 2013a; Pasieka et al., 2015). The foremost differences between the systems are the presence of 40 wt % TBAB in the liquid phase and the considerably higher temperature to form the hydrates.

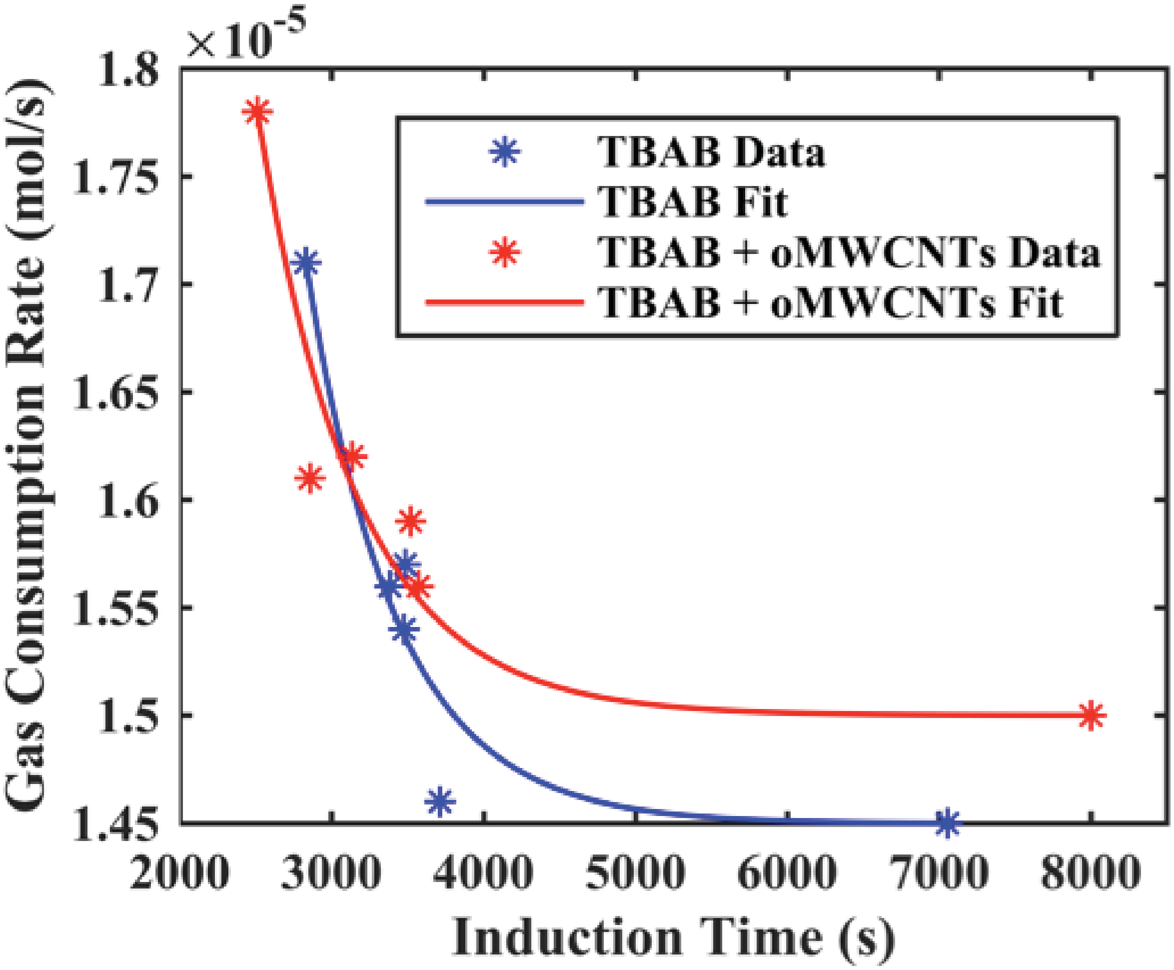

Figure 4.7: Gas consumption rate plotted against induction time for CO2 hydrates at 14 °C and 1.5 °C subcooling. TBAB results shown in blue and TBAB + MWCNT results shown in red.

4.6 Conclusion

The effect on growth and dissolution kinetics with the addition of 9.5 ppmw plasma-oxygenated MWCNTs to a carbon dioxide + TBAB gas hydrate system was investigated. Experiments were performed at 14 °C and at subcooling of 1.5 and 3.0 °C. The gas consumption rate showed a decreasing first-order response with increasing induction time. Furthermore, a regression analysis demonstrated that the addition of MWCNTs increased the gas consumption rate only at induction times less than one hour and did not affect it at longer induction times. Consequently, dissolution kinetics at equilibrium and before hydrate nucleation were examined and it was confirmed that the enhanced consumption rate was due to an improved dissolution caused by the addition of MWCNTs in solution since the dissolution time constants were statistically different. At a the lower subcooling of 1.5 °C, there was no significant difference in gas consumption rates for the systems with and without the MWCNTs. Therefore, as opposed to results on pure water gas hydrates, the addition of MWCNTs to a TBAB-water-carbon dioxide gas hydrate system does not result in a change in the actual gas hydrate formation rate but only in the dissolution rate, hinting that the hydrate growth is not limited by the carbon dioxide transfer at the gas-liquid interface in this system. This study can contribute to the development of various applications that aim to promote the formation of carbon dioxide gas hydrates. Further studies using higher concentration of nanoparticles and different hydrate promoters would help provide a better understanding of the role of nanoparticles in hydrate systems.

4.7 Acknowledgments

The authors are grateful to the Natural Sciences and Engineering Research Council of Canada (NSERC), les Fonds de recherche du Québec – Nature et technologies (FRQNT), the McGill Engineering Doctoral Award (MEDA) program and the Department of Chemical Engineering of McGill University for financial support.

Chapter 5

5 Methane Kinetics with Sodium Dodecyl Sulfate and Aluminum Oxide Nanoparticles

5.1 Preface

This chapter provides a kinetic analysis on different mixtures of sodium dodecyl sulfate and aluminum oxide (Al_2O_3) nanoparticles to a methane hydrate system. Chapter 4 mainly demonstrated that adding nanoparticles promotes the dissolution kinetics of the hydrate forming gas in a TBAB semi-clathrate system. Due to its approximately ten-fold lower solubility in water, methane was found to be suitable for this subsequent analysis. Methane gas hydrates were selected as SDS is known to inhibit carbon dioxide hydrates and would make that gas unsuitable for this kinetic promotion study. Aluminum oxide nanofluid was selected to investigate the effect of considerably greater concentration of nanoparticles than was achievable with MWCNTs produced in house. Experiments were performed for pure nanofluids (10 to 1000 ppmw Al_2O_3) and mixtures of 575 ppmw SDS with aluminum oxide nanoparticles (10 to 1000 ppmw). Methane hydrates did not exhibit any trend with induction time in this study, as was the case in Chapter 3. Hence, gas consumption rates could be compared directly without having to consider the effect of induction times.

5.2 Abstract

Methane hydrate kinetic experiments were completed using different mixtures of aluminum oxide nanofluids with and without the presence of sodium dodecyl sulfate. Concentrations were varied from 10 to 1000 ppmw for Al_2O_3. SDS concentration was set at 575 ppmw. Results showed that the added nanoparticles do not statistically modify gas consumption rates at all concentrations with and without the presence of SDS.

5.3 Introduction

Gas hydrates are non-stoichiometric crystalline compounds that form when a gas molecule is encapsulated by water molecules at relatively low temperatures and high pressures. Suitable guest molecules are determined by size and stabilize the crystal lattice of hydrogen-bonded water molecules through weak van der Waals forces (Sloan et al., 2008). There are over 180 different molecules that form hydrates, with the most notable being methane and carbon dioxide (Englezos, 1993). Until the 1930's, hydrates remained mainly of academic interest until industrial research was spurred by the discovery of hydrates blocking natural gas transmission lines (Hammerschmidt, 1934). To this day, this problem of blockages remains quite significant and costly, as can be seen in the complications with the BP oil spills in the Gulf of Mexico that were due to a large volume of hydrates formed (CBCNews, 2010). Another turning point in the field was the discovery of *in situ* natural gas hydrates in the Siberian permafrost (Makogon, 1965). Recently, various applications using hydrates have been proposed such as gas transportation, storage and separation (Thomas, 2003; Eslamimanesh et al., 2012). Carbon dioxide sequestration in hydrate form has been studied as a means to mitigate global warming (Chatti et al., 2005). Slow and unpredictable formation kinetics and the lack of scalability studies have prevented larger scale development of these proposed technologies (Eslamimanesh et al., 2012; Ma et al., 2016). This study investigates the effect of adding aluminum oxide nanoparticles to a methane hydrate kinetics with and without the presence of sodium dodecyl sulfate. Sodium dodecyl sulfate being a very strong kinetic promoter produces a lot of heat from hydrate formation resulting in a significant bulk temperature increase. The objective of these experiments was to analyze if the presence of nanoparticles could help dissipate this heat and ultimately increase the gas consumption rates.

5.4 Materials and Methods

5.4.1 Experimental Setup

The experimental apparatus consists of a 600 mL stainless steel reactor that is submerged in a temperature-controlled 20 % by volume ethylene glycol-water bath, as displayed in Figure 5.1. Two MM-DO6 magnetic stirrers from Pressure Product Industries are used to evenly mix both the reactor and the temperature-controlled bath. The reservoir gas tank is used to keep the reactor pressure constant during experiments by feeding gas through a Baumann 51000 control valve. The valve receives a signal based on the difference in pressure between the reactor bias gas tank and the reactor. This signal increases when gas is consumed in the reactor and the control valve delivers gas to the reactor in response to this signal in order to maintain constant pressure. Pressures are monitored at three different locations using Rosemount pressure transducers configured to a span of 0 to 14 000 kPa for absolute pressure measurements and 0 to 2000 kPa for differential pressure measurements, with an accuracy of 0.065 % of the given span. Temperatures are recorded with RTD probes from Omega for the reactor liquid, reactor gas, and reservoir tank. Methane obtained from MEGS Inc. has a purity of 99.999 %. The water used is treated by a reverse-osmosis (RO) system with a 0.22 μm filter and has a conductivity of 10 μS and total organic content less than 10 ppmw. SDS is purchased from Fisher Scientific as a solid powder and added to the liquid in measured amounts to obtain 575 ppmw. Aluminum oxide nanoparticles were purchased from Sigma Aldrich as a liquid dispersion of 20 wt % in water. The average particle size was given as 30 to 60 nm.

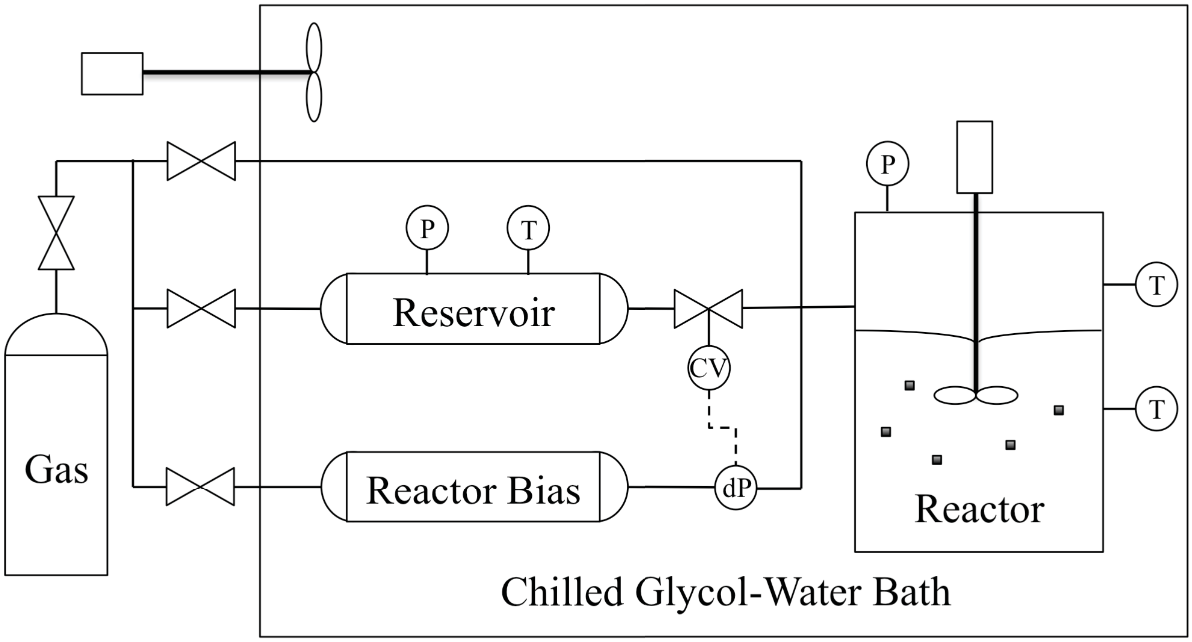

Figure 5.1: Experimental setup.

5.4.2 Experimental Procedure

Before starting experiments, the reactor was rinsed three times with 420 mL of RO water. The reactor was subsequently filled with 360 mL of the hydrate-forming liquid, which varied by experiment. The system temperature was fixed at 2 °C using the chiller to regulate the glycol bath. Once the liquid sample was loaded, the reactor was purged with methane gas three times by pressurizing to 1100 kPa followed by de-pressurizing to 110 kPa. The system was then pressurized to 4646 kPa based on the desired driving force of 1500 kPa. The reservoir and reactor bias gas tanks were filled with methane gas to a pressure 1000 kPa above the reactor value so as to provide a pressure differential for gas transfer during the kinetic runs. Once the reactor pressure and temperature stabilized, the data acquisition system and control valve were activated, and the magnetic stirrer inside the reactor was started. This begins the dissolution phase of a hydrate experiments that continues until the nucleation point, which is detected by a spike in bulk liquid temperature. Hydrate growth was recorded for at least 450 seconds beyond this point. After the run, the data acquisition system and control valve were turned off and the reactor pressure was brought down to 110 kPa to allow the hydrates to dissociate. At this point, the experiment was either repeated to provide replicates or the reactor liquid was changed for experiments using a different mixture. Molar gas consumption rates, or hydrate growth rates, were calculated using the reservoir pressure and temperature data over the first 450 seconds of hydrate growth and converting this data to moles using the Trebble-Bishnoi equation of state (Trebble et al., 1987; 1988).

5.5 Results and Discussion

Experiments were completed at 2 °C and 4646 kPa which is equivalent to a 1500 kPa driving force. The experiments of pure methane hydrate with no SDS at different Al_2O_3 concentrations were the first ones to be completed. The induction times were long compared to previous CO_2 experiments and no trend between gas consumption rates and induction time was observed. This allowed us to decouple dissolution and hydrate growth in this case and look at gas consumption rates as hydrate growth rates. Figure 5.2 shows the results of growth rates at the different Al_2O_3 concentrations with the corresponding 95 % confidence intervals. It is quite evident that the confidence intervals of all 5 Al_2O_3 concentrations overlap consequently the results are not statistically different from each other. This means that adding up to 1000 ppmw Al_2O_3 to a pure methane hydrate system does not enhance the hydrate growth rate.

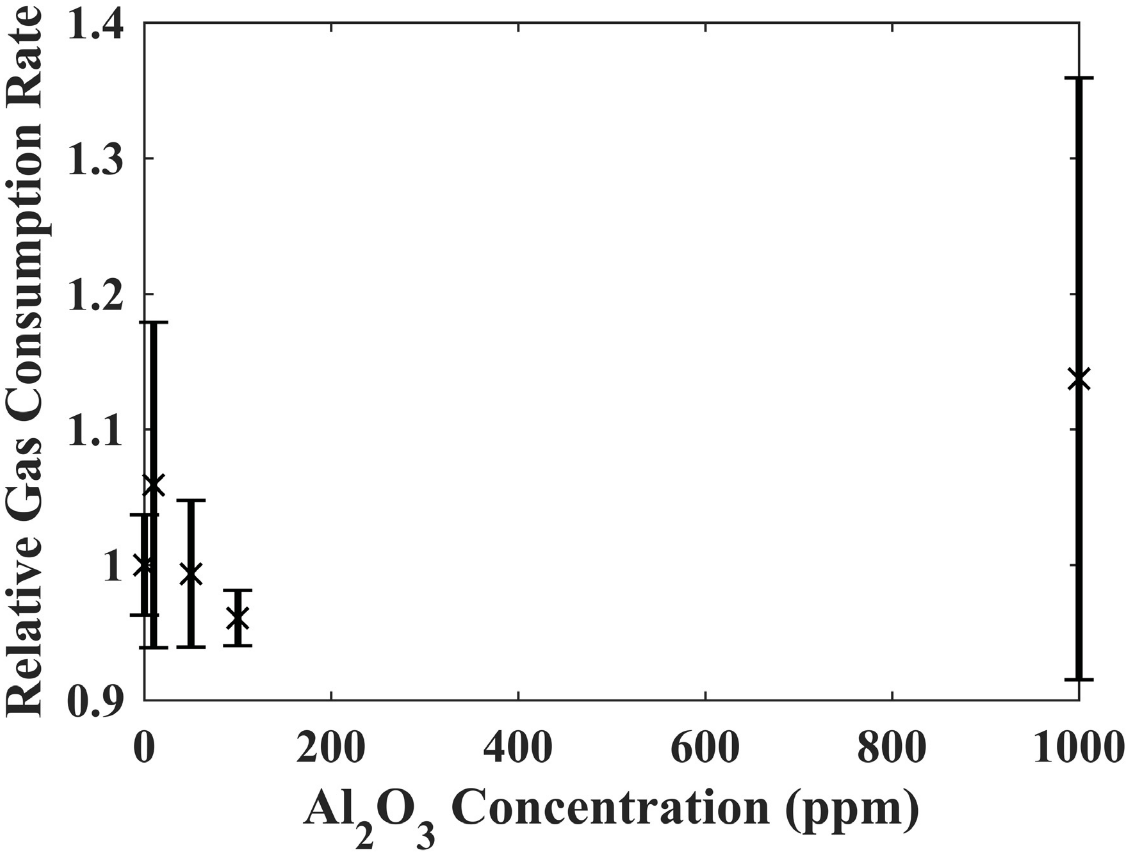

Figure 5.2: Relative methane gas consumption rate compared to pure water as a function of Al_2O_3 concentration. Vertical error bars correspond to 95 % confidence intervals.

The same aluminum oxide concentrations were also tested but with the presence of 575 ppmw of SDS for the methane hydrate. A heat dissipation effect was sought to decrease the bulk liquid temperature spike from hydrate nucleation and thereby increase the growth rate. SDS usually has a large temperature increase resulting from hydrate nucleation associated with its enhanced growth rate. The results can be seen in Figure 5.3 and are very similar to the ones without the presence of SDS. Although the averages are above the baseline for 10 to 1000 ppmw Al_2O_3, the gas consumption rates at all the Al_2O_3 concentrations are not statistically different from each other.

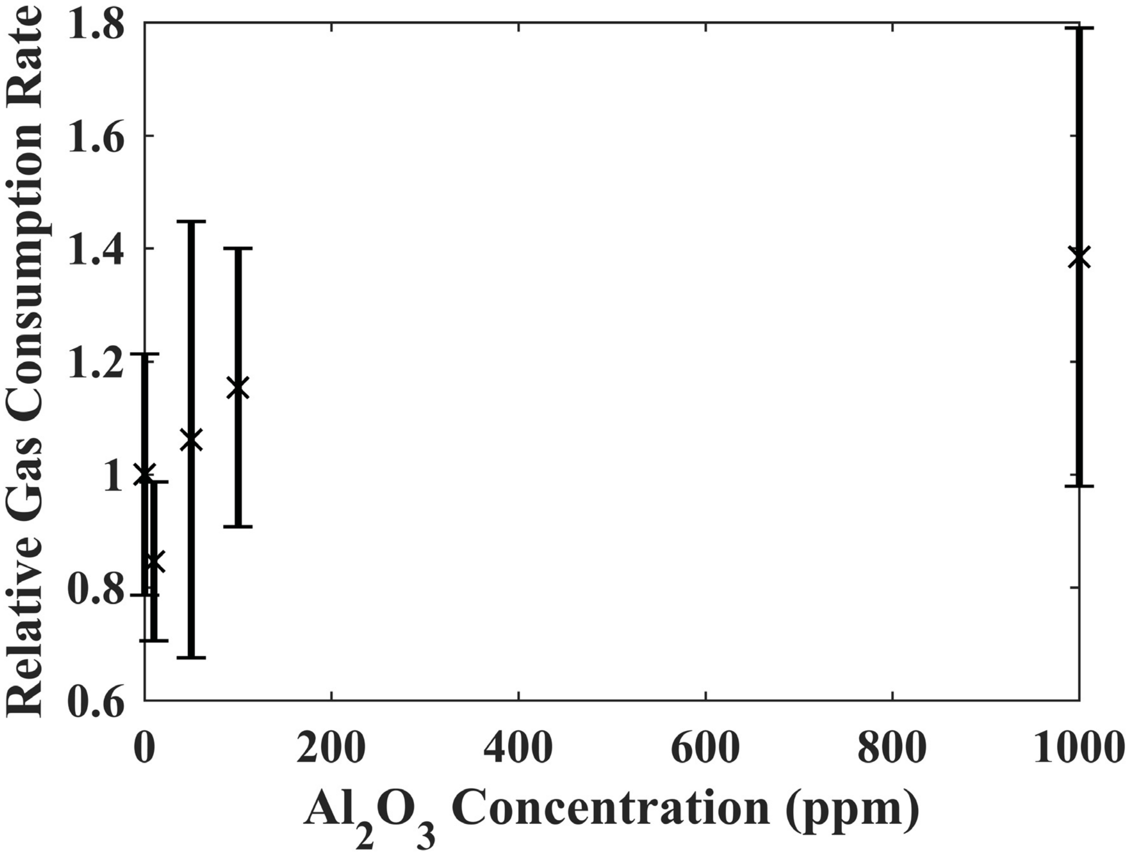

Figure 5.3: Relative methane gas consumption rate compared to 575 ppmw SDS system as a function of Al_2O_3 concentration. Vertical error bars correspond to 95 % confidence intervals.

5.6 Conclusion

The results shown in this chapter reveal that the addition of nanoparticles to a methane hydrate system with and without the presence of sodium dodecyl sulfate does not affect the gas consumption rates. Concentrations from 10 to 1000 ppmw Al_2O_3 were tested. Since this was a methane hydrate system, the induction times were long enough for dissolution to be near completion when hydrate nucleate, meaning that the effect of the nanoparticles was only observed for the hydrate growth. Statistically, no change was observed compared to pure water systems. This result agrees with the conclusion from Chapter 4 where it was shown that the addition of nanoparticles only enhanced the dissolution rates and not the growth rates, hence not affecting methane hydrate kinetics.

Chapter 6

6 Methane Gas Hydrate Kinetics with Mixtures of Sodium Dodecyl Sulfate and Tetrabutylammonium Bromide[1]

6.1 Preface

Sodium dodecyl sulfate is a kinetic promoter that has been shown to increase growth rate significantly. In this study, an investigation using the combination of SDS and TBAB in a methane hydrate system is performed. A further understanding of how these two compounds interact with each other is of relevance to hydrate promotion applications. Methane hydrates did not exhibit any trend with induction time in this study, as was the case in Chapter 3 and Chapter 5. Hence, gas consumption rates could be compared directly without having to consider the induction times. Multiple loading concentrations were examined ranging for low concentration TBAB (200 ppmw) to high concentration TBAB (200,000 ppmw) for different SDS concentrations (100 to 1500 ppmw). This allows for postulation on the mechanism of SDS-TBAB on the formed hydrates.

---

[1] Reproduced with permission from "Renault-Crispo, J.S., Servio, P. Methane Gas Hydrate Kinetics with Mixtures of Sodium Dodecyl Sulfate and Tetrabutylammonium Bromide. *Fuel*. Submitted 2017."

6.2 Abstract

The effect of combining a thermodynamic promoter, tetrabutylammonium bromide (TBAB) with a kinetic promoter, sodium dodecyl sulfate (SDS) to a methane clathrate system was investigated. Kinetic growth experiments were conducted in a semi-batch stirred tank crystallizer at driving forces of 1500 kPa using a range of 100 to 1500 ppmw SDS and 200 to 200 000 ppmw TBAB. Solutions containing low concentrations of TBAB in water reduced methane hydrate growth rates up to 55 % for 1250 ppmw TBAB compared to pure water. Solutions containing 900 ppmw SDS in water enhanced the growth rate by 880 % compared to pure water. Solutions were then tested combining both promoters. The gradual addition of SDS from concentrations between 100 to 1250 ppmw to low-concentration TBAB systems between 200 to 1250 ppmw was initially found to reduce growth kinetics, but eventually increased the growth rates once a threshold SDS concentration was reached. In all cases, the promoting effect of SDS was more pronounced in the absence of the TBAB. The growth kinetics of systems containing 5 and 20 wt % TBAB also followed a similar inhibition-promotion trend with SDS concentration. An increase of 177 % in gas consumption rate was observed when 1500 ppmw SDS was added to the 20 wt % TBAB clathrate system. This work demonstrates that SDS can be added to a TBAB-water-methane system to enhance gas consumption rates, but care must be taken to ensure that the concentration of the additives places the system in a promotion regime.

6.3 Introduction

Gas hydrates are solid inclusion compounds formed from the combination of water and gas molecules at high pressures and low temperatures. The solid phase consists of a host lattice of hydrogen-bonded water molecules that encage guest gas molecules, such as methane, carbon dioxide and propane (Sloan et al., 2008). Gas hydrate formation is problematic in oil and gas transmission lines during deep-water production and recovery (Koh et al., 2011). Prevention and mitigation is essential to ensuring a continuous and safe fluid flow within pipelines and facilities. On the other hand, gas hydrates are considered a potential large-scale energy resource. They are found in enormous natural deposits in artic regions under the permafrost and in oceanic sediments along the continental margins (Collett et al., 2015). Recognizing the immense potential energy resource that natural methane hydrates offer, the Methane Hydrate Research and Development Act was enacted by the United States Congress in the year 2000 to evaluate the feasibility of their extraction and use (National Research Council, 2004). Correspondingly, Japan (Yamamoto et al., 2014) has recently launched a research program for a methane hydrate exploratory drilling project, and India and China have invested into methane hydrate research and development programs for the possible recovery of natural deposits (Letcher, 2014).

More recently, gas hydrates have also been studied for other technological applications that include storage and transportation of natural gas and hydrogen (Gudmundsson et al., 1995; Sugahara et al., 2009). The use of gas hydrate pellets could be viable for remote natural gas recovery projects where production is too expensive for a pipeline and installing a liquefied natural gas plant is not economically viable (Gudmundsson et al., 2000). The gas hydrate pellet application is near commercialization, with current reports now focusing on optimization of production efficiency, as can be seen in the pilot-scale project in Japan (Watanabe et al., 2008). Another relevant application is the use of gas hydrates in separation processes such as flue gases, where carbon dioxide can be preferentially captured while excluding nitrogen and other benign molecules (Kang et al., 2000b; Chatti et al., 2005; Eslamimanesh et al., 2012; Babu et al., 2015; Ma et al., 2016). Collectively, each of these applications is made possible by the high storage capacity of gas hydrates. For instance, one cubic meter of methane hydrate can release up to 160 cubic meters of methane gas (at STP) (Taylor et al., 2003). At the present time, the relatively severe conditions required for formation, the slow hydrate growth kinetics and the lack of scalability studies stand as the most significant barriers to the large-scale development of the described technologies (Yin et al., 2016).

One method to facilitate the formation conditions of gas hydrates involves the use of thermodynamic promoters. These additives shift the phase equilibrium to more energetically favourable conditions, such as lower pressures and higher temperatures. One class of molecules that are effective thermodynamic promoters are quaternary ammonium salts. These molecules form a semi-clathrate structure with water by incorporating themselves into the water lattice, helping to stabilize the crystal structure and thereby significantly lowering the thermodynamic conditions required for formation. Quaternary ammonium salts usually have their cationic group occupying the interior of the cages as guest molecules, and their anionic group participating in the cage skeleton alongside water. The tetrabutylammonium bromide (TBAB) salt is the most common semi-clathrate-forming thermodynamic promoter, mainly due to its commercial availability and that it can form a hydrate phase at temperatures of up to 12.4 °C and at atmospheric pressure (Aladko et al., 2002; Shimada et al., 2005). Research in the field of semi-clathrates has generally focused on the thermodynamics of TBAB hydrates, specifically the equilibrium temperatures, pressures and TBAB liquid concentrations with single and multiple guest gases (Arjmandi et al., 2007; Sun et al., 2010; Bouchemoua et al., 2011; Verrett et al., 2015). Li et al. (Li et al., 2010) investigated the use of gas hydrates for separation of carbon dioxide from flue gases using TBAB hydrates. They demonstrated the capability of removing CO_2, and that TBAB accelerated gas hydrate growth rates and diminished induction time. Another study showed that a 40-45 wt % TBAB solution may be a promising cold storage material for air conditioning systems due to its high phase change temperature and its improved overall conversion of liquid to gas hydrate (Mahmoudi et al., 2016). A study that sparked interest for this report was completed by Nguyen et al. (Nguyen et al., 2016) where looked at the influence of a range of TBAB concentrations (0.025 to 3 wt %) on gas uptake during the formation of CO_2 gas hydrates. They noticed that low concentrations of TBAB inhibited growth kinetics, where a minimum growth rate was observed at 0.125 wt % TBAB. Considering that TBAB is meant to facilitate gas hydrate formation, this peculiar result demonstrates that while gas hydrates may be easier to form in the presence of a thermodynamic promoter, the ensuing growth kinetics may be reduced. Using Sum Frequency Generated vibrational spectroscopy, Attenuated Total Reflectance Fourier Transform Infrared and molecular dynamic simulations, Nguyen et al. concluded that the surface adsorption of TBAB at the gas-water interface gave rise to the unexpected decrease in growth rates observed at dilute TBAB concentrations, making it more difficult for the gas to enter the liquid phase.

Slow hydrate growth kinetics can be overcome using kinetic promoter molecules. Surfactants were discovered to enhance hydrate growth in 1993 by Kalogerakis (Kalogerakis et al., 1993). It was shown that the use of 242 ppmw of the surfactant sodium dodecyl sulfate (SDS) increased hydrate growth rates up to 700 times compared to pure water in a quiescent system (Zhong et al., 2000). SDS and other types of surfactants also increased gas storage capacity by converting more of the available water into solid hydrate (Sun et al., 2003). In stirred systems, SDS promoted growth rate by a factor of nearly 5 compared to a pure water system (Verrett et al., 2012a). An increasing sigmoidal trend was observed between SDS concentration and growth rate, with a maximum plateau reached around 575 ppmw SDS.(Verrett et al., 2012a) In a review on the use of surfactants for gas hydrate promotion, Kumar et al. (Kumar et al., 2015) reported that systems with added surfactants show reduced induction times, increased hydrate growth rates and increased conversion of water to hydrate (nearing unity). They noted that the promotion mechanism may not be directly linked to micelle formation, as the concentrations used are well below the critical micelle concentration (CMC) of 2278 ppmw (Mata et al., 2004; Di Profio et al., 2005). Rather, they offered that the presence of surfactants reduces the vapour-liquid surface tension. This enhances the mass transfer across the vapour-liquid interface and also changes hydrate morphology, both of which increases the surface area for gas-water interaction.

Finally, the idea of combining thermodynamic and kinetic additives has sparked renewed interest for gas hydrate promotion (and inhibition) in hopes of improving efficiencies through synergistic effects. Kakati et al. (Kakati et al., 2016c) investigated the effect of adding L-tyrosine (a thermodynamic inhibitor) and NaCl (a thermodynamic inhibitor) to Polyvinylpryvolidone (PVP) (a kinetic inhibitor), and the resulting impact on natural gas hydrate formation. The combination of these three compounds, two thermodynamic inhibitors and one kinetic inhibitor, resulted in an enhanced inhibition strength where a decrease in gas consumption rate of up to 27 % was observed compared to a pure water system. A synergistic effect in decreasing crystal growth rate was also seen by combining three thermodynamic inhibitors (PEG, PAM, HEC) with a kinetic inhibitor (PVP) (Jokandan et al., 2016). It was even suggested that a ternary solution was a better selection than a binary solution for inhibition purposes.

Mech et al. (Mech et al., 2016b) combined different thermodynamic promoters (THF and TBAB) with thermodynamic inhibitors (NaCl, methanol, ethylene glycol), and an unexpected promotion effect was observed. A ternary mixture of 0.5 wt % THF, 10 wt % TBAB, and 10 wt % ethylene glycol in water shifted the equilibrium line to the right (promotion) in a manner greater than a binary mixture of 0.5 wt % THF and 10 wt % TBAB in water. However, it is important to note that the difference in equilibrium temperature was only 0.19 K, which is a weak thermodynamic promoter effect.

The combination of two kinetic promoters has also been studied in the past. Ganji et al. (Ganji et al., 2007) added 300 ppmw of xanthan to a 500 ppmw SDS solution and observed a lower hydrate dissociation rate, which can be advantageous for storage and transportation applications. Another study looked at the behaviour of SDS on two different hydrate systems: cyclopentane and TBAB (Lo et al., 2008). They concluded that the headgroup of SDS, DS-, adsorbs via hydrophobic forces to the surface of the hydrate. The presence of the Br- ion in the TBAB systems may compete with DS- for the adsorption on the hydrate surface, but DS- is reported to have a stronger affinity for the hydrate surface (Lo et al., 2008). Recently, Brown et al. (Brown et al., 2016) studied the effect of combining different chemicals on the cyclopentane hydrate. They suggested that a mixture of dispersant, dodecylbenzenesulfonic acid, and kinetic hydrate inhibitor, polyvinylcaprolactam (PVCap), would make the cohesion forces between hydrate particles higher than the individual chemicals. However, a mixture of PVCap and a quaternary ammonium salt, Arquad 2HT-75, would result in a cohesive-reducing effect between hydrate particles greater than either additive on their own. This is a strong example of how two different chemical combinations may work either antagonistically or synergistically on gas hydrate growth. Another report from Kakati et al. (Kakati et al., 2016a) described that combining a thermodynamic promoter, THF, with a kinetic promoter, SDS, results in a gas consumption rate increase with increasing SDS concentration. A more favourable equilibrium was achieved by combining TBAB with cyclopentane than either of these promoters alone (Tzirakis et al., 2016). Lastly, the growth kinetics of methane hydrate systems containing either THF or TBAB along with SDS was investigated (Mech et al., 2016a). The experiments were conducted with mixtures of 5 to 10 wt % TBAB, 0.5 to 1 wt % THF, and 600 to 1000 ppmw SDS. The THF-SDS system showed a drastic increase in methane consumption rate compared to the TBAB-SDS system. Mech et al. (Mech et al., 2016a) also observed a behaviour where gas consumption decreases over time after the initial hydrate formation (2 hours). This was attributed to the possible absorption of SDS micelles around the TBAB molecules. The TBAB semi-clathrate system was optimal for promotion using 5 wt % TBAB + 600 ppmw SDS, promoting better than with more SDS (5 wt % TBAB + 1000 ppmw SDS) or with more TBAB (10 wt % TBAB + 600 ppmw SDS).

The objective of this study is to examine the kinetic effect of combining a common thermodynamic promoter, TBAB, with a common kinetic promoter, SDS, in a methane gas hydrate system. The concentration of TBAB was varied from 200 to 200 000 ppmw (0.02 to 20 wt %) while the range for SDS concentration was 100 to 1500 ppmw (0.01 to 0.15 wt %). To the best knowledge of the authors, this is the first time that these combinations of concentrations are used to study initial growth rates of methane hydrates. This study can contribute to scalability studies for the development of different gas hydrate applications that aim to enhance gas hydrate formation and provide a better understanding of the mechanisms behind these two promoters.

6.4 Materials and Methods

6.4.1 Experimental Setup

The experimental apparatus consists of a 600 mL stainless steel reactor that is submerged in a temperature-controlled 20 % by volume ethylene glycol-water bath, as displayed in Figure 6.1. Two MM-DO6 magnetic stirrers from Pressure Product Industries are used to evenly mix both the reactor and the temperature-controlled bath. The reservoir gas tank is used to keep the reactor pressure constant during experiments by feeding gas through a Baumann 51000 control valve. The valve receives a signal based on the difference in pressure between the reactor bias gas tank and the reactor. This signal increases when gas is consumed in the reactor and the control valve delivers gas to the reactor in response to this signal in order to maintain constant pressure. Pressures are monitored at three different locations using Rosemount pressure transducers configured to a span of 0 to 14 000 kPa for absolute pressure measurements and 0 to 2000 kPa for differential pressure measurements, with an accuracy of 0.065 % of the given span. Temperatures are recorded with RTD probes from Omega for the reactor liquid, reactor gas, and reservoir tank. Methane obtained from MEGS Inc. has a purity of 99.999 %. The water used is treated by a reverse-osmosis (RO) system with a 0.22 μm filter and has a conductivity of 10 μS and total organic content less than 10 ppmw. The 50 wt % TBAB-water mixture is obtained from Sigma Aldrich and used to prepare the different TBAB mixtures used in this study. SDS is purchased from Fisher Scientific as a solid powder and added to the liquid in measured amounts to obtain the different concentrations.

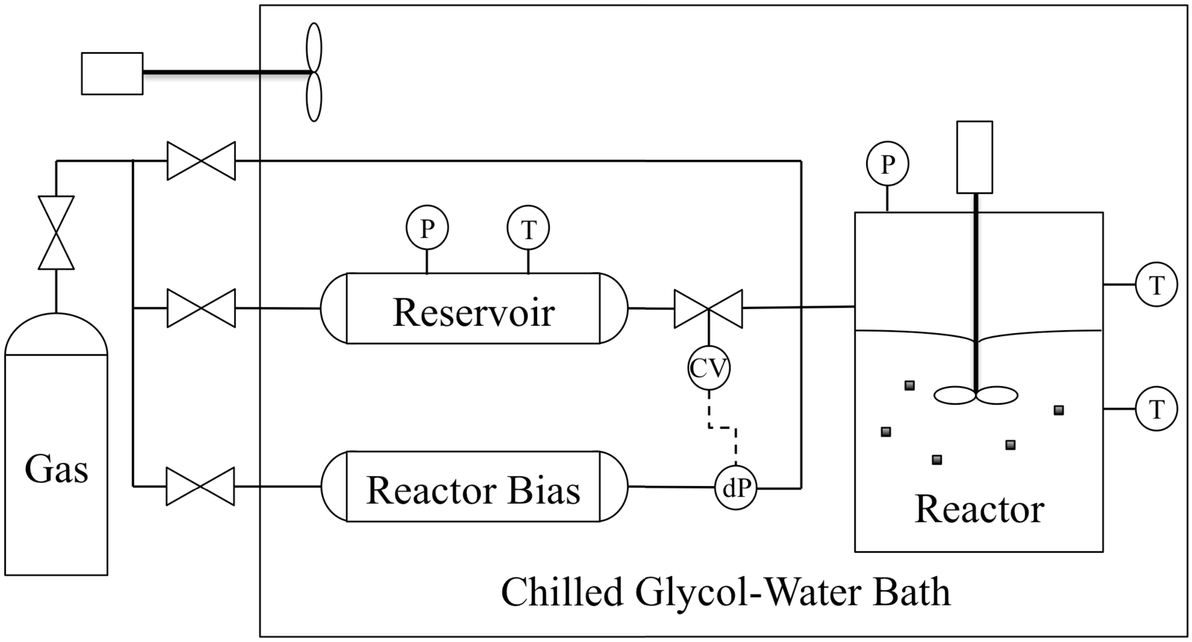

Figure 6.1: Experimental setup.

6.4.2 Experimental Procedure

Before starting experiments, the reactor was rinsed three times with 420 mL of RO water. The reactor was subsequently filled with 360 mL of the hydrate-forming liquid, which varied by experiment. The system temperature was fixed at the experimental temperature using the chiller to regulate the glycol bath. Once the liquid sample was loaded, the reactor was purged with methane gas three times by pressurizing to 1100 kPa followed by de-pressurizing to 110 kPa. The system was then pressurized to the experimental pressure based on the desired driving force. The reservoir and reactor bias gas tanks were filled with methane gas to a pressure 1000 kPa above the reactor value so as to provide a pressure differential for gas transfer during the kinetic runs. Once the reactor pressure and temperature stabilized, the data acquisition system and control valve were activated, and the magnetic stirrer inside the reactor was started. This begins the dissolution phase of a hydrate experiments that continues until the nucleation point, which is detected by a spike in bulk liquid temperature. Hydrate growth was recorded for at least 450 seconds beyond this point. After the run, the data acquisition system and control valve were turned off and the reactor pressure was brought down to 110 kPa to allow the hydrates to dissociate. At this point, the experiment was either repeated to provide replicates or the reactor liquid was changed for experiments using a different mixture. Molar gas consumption rates, or hydrate growth rates, were calculated using the reservoir pressure and temperature data over the first 450 seconds of hydrate growth and converting this data to moles using the Trebble-Bishnoi equation of state (Trebble et al., 1987; 1988).

6.5 Results and Discussion

The analysis compares gas consumption rates without taking into account the role that induction time may have on growth rate, as the results were shown not to be a function of induction time as anticipated for systems with methane gas as the hydrate former (Renault-Crispo et al., 2017). Hence the gas consumption rates of each liquid mixture can be correctly compared in the analysis. At least three runs were performed for each liquid mixture. The average value is shown in the figures with a 95 % confidence interval (based on a t-test).

6.5.1 Pure SDS

Pure SDS runs were performed as a baseline to compare with literature values. Experiments were conducted at 2 °C and 4646 kPa, equivalent to a 1500 kPa driving force. Verrett et al. (Verrett et al., 2012a) demonstrated that the methane hydrate growth rate followed a sigmoidal trend with SDS concentration, where rates start to increase at SDS concentration of 150 ppmw and reach a maximum around 575 ppmw. The results from Figure 6.2 show the relative gas consumption rate change with SDS concentration for the current methane hydrate system compared to a pure methane-water system. This data supports the literature that an increase in gas consumption rate occurs between 100 ppmw and 300 ppmw. Initially, SDS does not promote growth until a specific concentration is used (300 ppmw in this case). However, the value of gas consumption rate did not plateau as clearly as it did in the study by Verrett et al. (Verrett et al., 2012a), but seemed to continue increasing after the 575 ppmw mark. At 900 ppmw, the growth rate enhancement was 880 % compared to pure water methane hydrates, while at 575 ppmw it was 593 %. The authors believe that this slight variation in results is an effect of a different experimental setup, experimental procedure, and mixing speed. Furthermore, the complexity of hydrate growth in the presence of SDS could also contribute to different hydrodynamics. With the added surfactant, the liquid is seen to foam significantly and initial hydrate growth typically occurs along the walls of the reactor. The use of a metal stirring shaft that traverses the gas-liquid interface in Verrett at al. may also provide an extra surface for hydrates to grow. In this study, a magnetic stir bar situated at the bottom of the liquid was used to mix the system, possibly allowing for greater promotion. All these effects make it difficult to compare results between two different experimental setups in absolute terms, however the relative results are quite consistent.

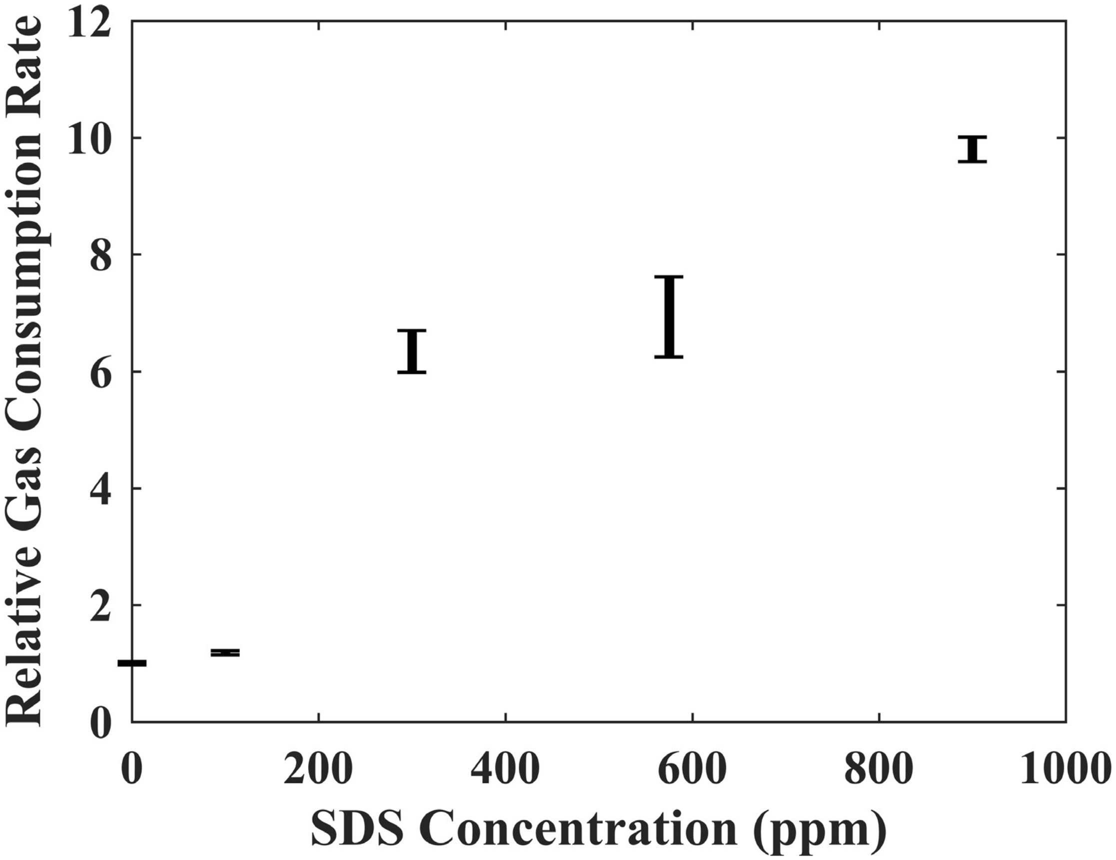

Figure 6.2: Relative methane gas consumption rate compared to pure water as a function of SDS concentration. Vertical error bars correspond to 95 % confidence intervals.

6.5.2 Pure TBAB at Low Concentrations

This section presents the results of low concentration TBAB (80 to 1250 ppmw) and to the best knowledge of the authors, it is the first time this has been reported for a methane gas hydrate system. Once again, experiments were conducted at 2 °C and 4646 kPa, equivalent to a 1500 kPa driving force. Equilibrium condition measurements were performed at the 1250 ppmw TBAB concentration. It is important to note that the equilibrium pressure was found to be 77 kPa higher than pure water, corresponding to an unexpected small degree of thermodynamic inhibition. This means that the driving force for this concentration is approximately 5 % lower than the other concentrations (1423 kPa versus 1500 kPa). The equilibrium pressure for the other TBAB concentrations (80 to 575 ppmw) were not found to be statistically different than pure water. Figure 6.3 displays the results for methane hydrate gas consumption rate with different concentrations of TBAB. It can be seen that gas consumption rates decrease with increasing TBAB concentrations. A 22 % decrease was observed for 575 ppmw TBAB, and a 55 % reduction was seen for 1250 ppmw TBAB. At 1250 ppmw, the 5 % decrease in driving force cannot completely account for the 55 % inhibition detected since the other concentrations also decrease gas consumption rate but with no noticeable equilibrium change. At these low TBAB concentrations, TBAB acts as a kinetic inhibitor, in that it reduces the observed growth rates. However, the literature suggests that the advantage of using TBAB lies in its ability to be a thermodynamic promoter, which is not yet noticeable at these low concentrations. Nguyen et al. (Nguyen et al., 2016) also reported a decreasing trend with increasing TBAB concentration, similar to the one presented here, but in carbon dioxide gas hydrate systems. They indicated that gas uptake is at a minimum at 1250 ppmw TBAB, and gas uptake will increase with either increasing or decreasing TBAB concentration from this point. It is important to note that they used the same pressure driving force for concentrations higher than 1250 ppmw. At these levels of TBAB, the shift in equilibrium conditions becomes more significant, which makes it difficult to meaningfully compare growth rate results across TBAB concentrations. For instance, the equilibrium conditions at 5 wt % TBAB is significantly different than at 0.1250 wt % (1250 ppmw) (Verrett et al., 2015). It is for this reason that the results for higher concentrations of TBAB (> 1250 ppmw) are addressed in a separate section and are not compared to the low concentration results in this article. This interesting promotion-inhibition effect from a same compound has also been observed for a well-known kinetic inhibitor, PVP. Ke at al. (Ke et al., 2016) showed that PVP at 50 and 100 ppmw can have a promotive effect on nucleation rate at certain subcoolings, yet an inhibitory effect at other subcoolings. This illustrates the possibility of the opposing effects that a single additive may have on different aspects of a gas hydrate system.

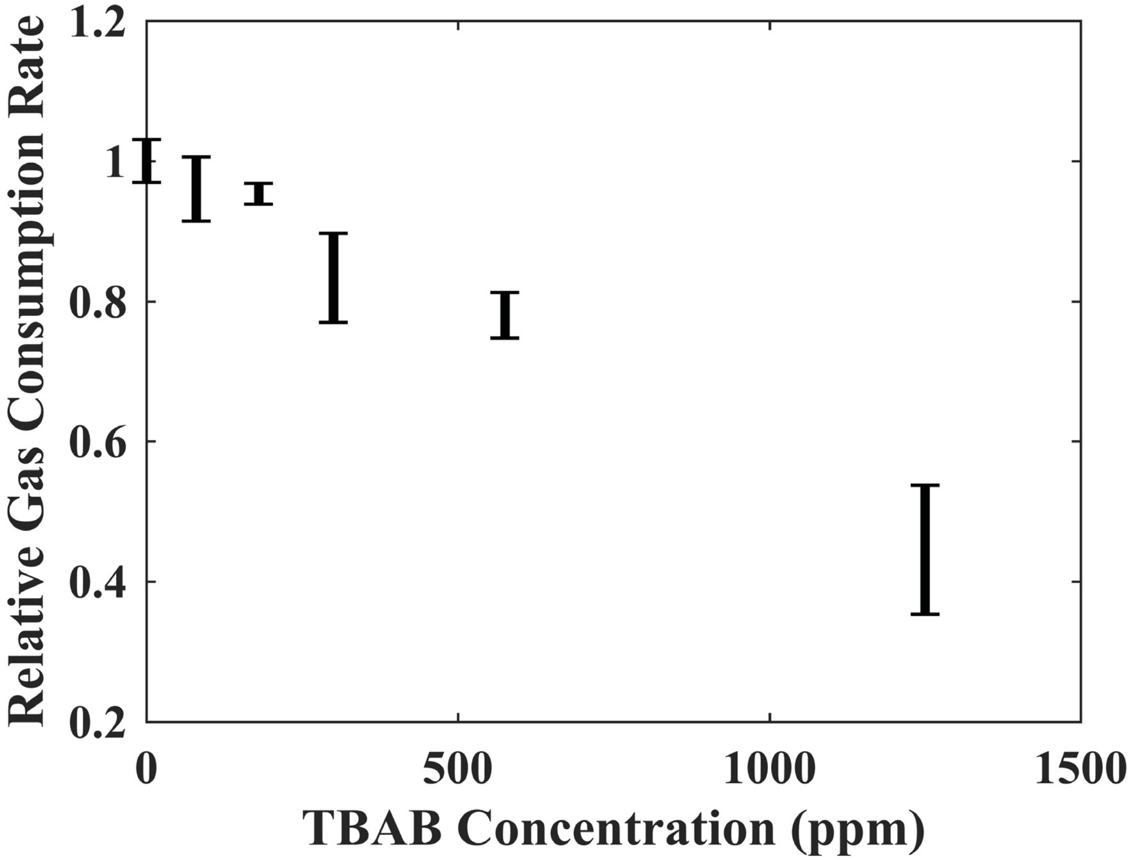

Figure 6.3: Relative methane gas consumption rate compared to pure water as a function of TBAB concentration. Vertical error bars correspond to 95 % confidence intervals.

6.5.3 Low Concentration TBAB with SDS

After noticing the decreasing trend in hydrate growth rate with TBAB concentrations up to 1250 ppmw in the previous section, an investigation was conducted to examine whether the combination of the kinetic promoter SDS with the seemingly-inhibiting TBAB could improve the hydrate growth rate. Figure 6.4 shows the relative gas consumption rates (compared to pure water) of systems containing increasing SDS concentrations (100 to 1250 ppmw) and three different concentrations of TBAB (200, 500, and 1250 ppmw). Since the results are all normalized based on the pure water run, the different TBAB concentrations have a different growth rate at 0 ppmw SDS, corresponding to the results of Figure 6.3. The absolute values of gas consumption rate are provided in Table 6.1. These experiments were also conducted at 2 °C and 4646 kPa, equivalent to a 1500 kPa driving force. At all TBAB concentrations (red, green and blue lines in Figure 6.4), a decrease in gas consumption rate compared to the baseline is observed at low SDS concentrations (lower than 400 ppmw SDS). This means that when SDS is added in a small amount to a low concentration TBAB solution, an inhibition effect greater than the low concentration TBAB solution itself is detected. At 200 ppmw TBAB, this inhibition occurs up to 200 ppmw SDS, while at 500 and 1250 ppmw TBAB, it is present up to 400 ppmw SDS. A 64 % inhibition compared to the 500 ppmw TBAB system (69 % inhibition compared to pure water) is observed when a solution of 500 ppmw TBAB with 400 ppmw SDS is used. Similarly, at 1250 ppmw TBAB, a 43 % inhibition is seen when only 100 ppmw of SDS is added. After this initial inhibition, the continued addition of SDS will eventually promote the gas consumption rate above its baseline of 0 ppmw SDS. This transition happens earlier at lower TBAB concentrations, meaning that TBAB has an antagonistic effect on the promotion of SDS of methane hydrate growth. In the case where growth rate promotion is the main goal, the best solution would be one that does not contain TBAB as shown in Figure 6.4 where the black line (no TBAB) has the greatest values of gas consumption rate and does not change the thermodynamic equilibrium significantly.

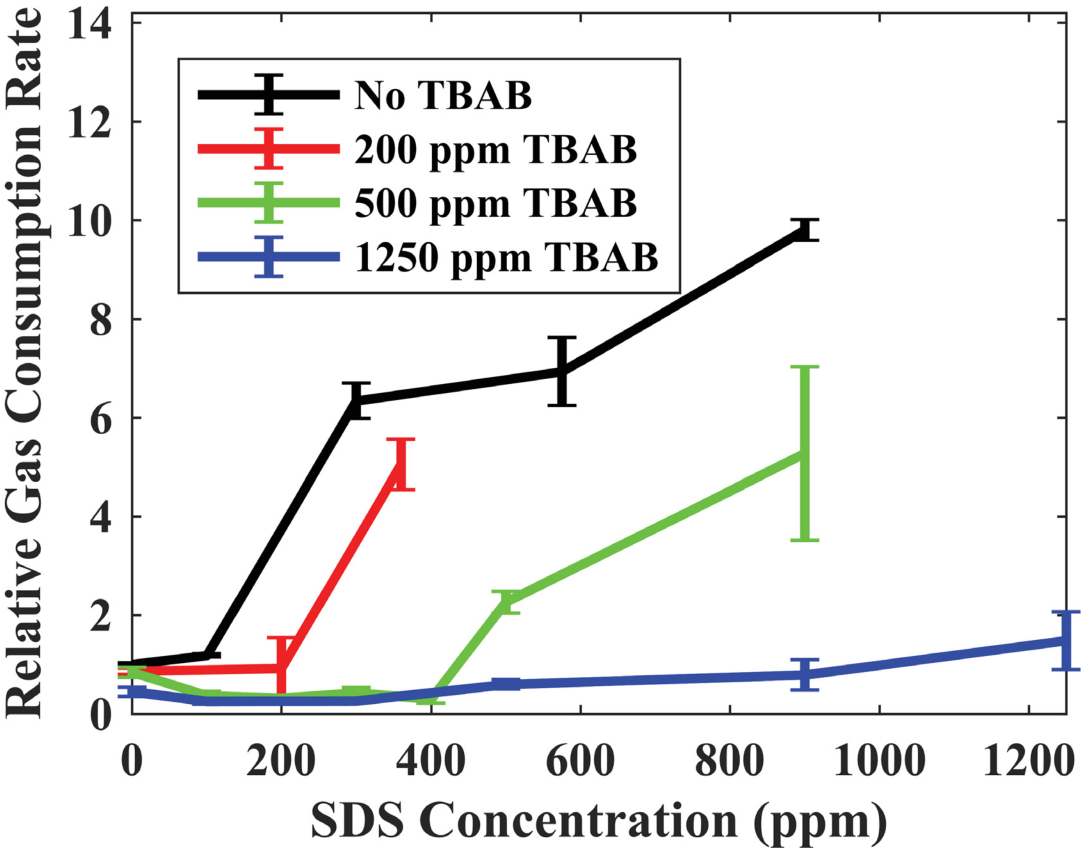

Figure 6.4: Relative methane gas consumption rate compared to pure water as a function of SDS concentration and four TBAB concentrations. Vertical error bars correspond to 95 % confidence intervals.

Table 6.1: Absolute methane gas consumption rate values for all mixtures of low concentration TBAB and SDS. Confidence intervals are omitted for clarity but can be found in Figure 6.4.

SDS Concentration (ppmw)	TBAB concentration (ppmw)	Average gas consumption rate * 1e6 (mol/s)	Relative to pure water
0	0	15.0	1
0	200	12.9	0.86
200	200	13.8	0.92
360	200	75.8	5.06
0	500	12.6	0.84
100	500	5.5	0.36
200	500	4.7	0.31
300	500	6.3	0.42
400	500	4.6	0.30
500	500	33.9	2.26
900	500	79.1	5.28
0	1250	6.7	0.45
100	1250	3.8	0.26
300	1250	3.9	0.26
500	1250	8.9	0.60
900	1250	11.8	0.79
1250	1250	22.2	1.48

Different hypotheses can be made with regards to why TBAB is inhibiting the effect of SDS on gas hydrate growth promotion. The presence of TBAB alter the critical micelle concentration (CMC) of SDS (2278 ppmw) (Mata et al., 2004), possibly causing a change in the mechanism of hydrate growth promotion. It was shown by Mata et al. (Mata et al., 2004) that SDS exhibited a decrease in CMC with the addition of TBAB at 25 °C. About a tenfold decrease of CMC from 2278 ppmw SDS at 0 ppmw TBAB to 270 ppmw SDS at 322 ppmw TBAB was observed. Micelles may prevent SDS from kinetically promoting hydrate formation and thus the need for more SDS to do the same promotion effect. Additionally, other than the change in CMC, they report that the mixture of these compounds showed enhanced solubilisation properties and a remarkable decrease in surface tension due to the increased interaction forces and thus binding ability of bulky tetrabutylammonium ion on NaDS. These concentration values are within the range at which the values of gas consumption rate start increasing in Figure 6.4, hinting that micelle formation could be essential to understanding how these two additives change the growth process. It is important to note that the reported CMC values were at 25 °C and that CMC is usually a complex function of temperature for surfactants. Mohajeri et al. have shown that below 40 °C, another surfactant, polysorbate, had its CMC increase with decreasing temperature, a trend that was inversed at temperatures above 40 °C (Mohajeri et al., 2012). Morphology studies and CMC determination at hydrate conditions would bring valuable information on the effect of TBAB and SDS on the hydrate growth mechanism.

While lower concentration TBAB solution are less likely to be used because of the adverse effects shown, higher concentration TBAB solutions are still viable additives for their thermodynamic promotion ability, and promotion effects with the kinetic promoter SDS are still viable.

6.5.4 High Concentration TBAB with SDS

Kinetic results for 5 and 20 wt % TBAB with different SDS concentration can be found in Figure 6.5. Actual values for gas consumption rates can be found in Table 6.2. The gas consumption rates have been normalized to the 0 ppmw SDS run in both the 5 and 20 wt % TBAB cases. Experiments for 5 wt % were completed at 10.2 °C and 3917 kPa, and 14.1 °C and 2935 kPa for the 20 wt %, both corresponding to a 1500 kPa driving force (Verrett et al., 2015). Both concentrations exhibit a decline in methane gas consumption rate at small concentrations of SDS (100 to 500 ppmw). At concentrations above 500 ppmw SDS, the systems start benefitting from the presence of higher concentration SDS and ultimately promote gas consumption rates relative to the 0 ppmw SDS baseline. An increase of 177 % was observed for 1500 ppmw SDS in a 20 wt % TBAB semi-clathrate system compared to 20 wt % TBAB alone. The transition of inhibition to promotion is found at a higher SDS concentration when 5 and 20 wt % TBAB is used compared to the lower TBAB concentrations in the previous section. The threshold concentration where the system transitions from inhibiting to promoting increases with increasing TBAB concentration in all cases. From Figure 6.4, 200 ppmw TBAB only needed 360 ppmw SDS to promote the methane gas consumption rate to 405 % while at 5 wt % TBAB and 500 ppmw SDS, an inhibition of 34 % is still detected. The collective results at low and high concentrations of TBAB, with and without SDS, show that opposite effects can be observed with respect to hydrate growth rates, depending on the combination and concentration of the additives used. In the design of industrial applications where the TBAB-SDS semi-clathrate hydrate system is being considered, it is vital to be aware of the existence of this dual inhibition-promotion effect so that the desired effect is achieved.

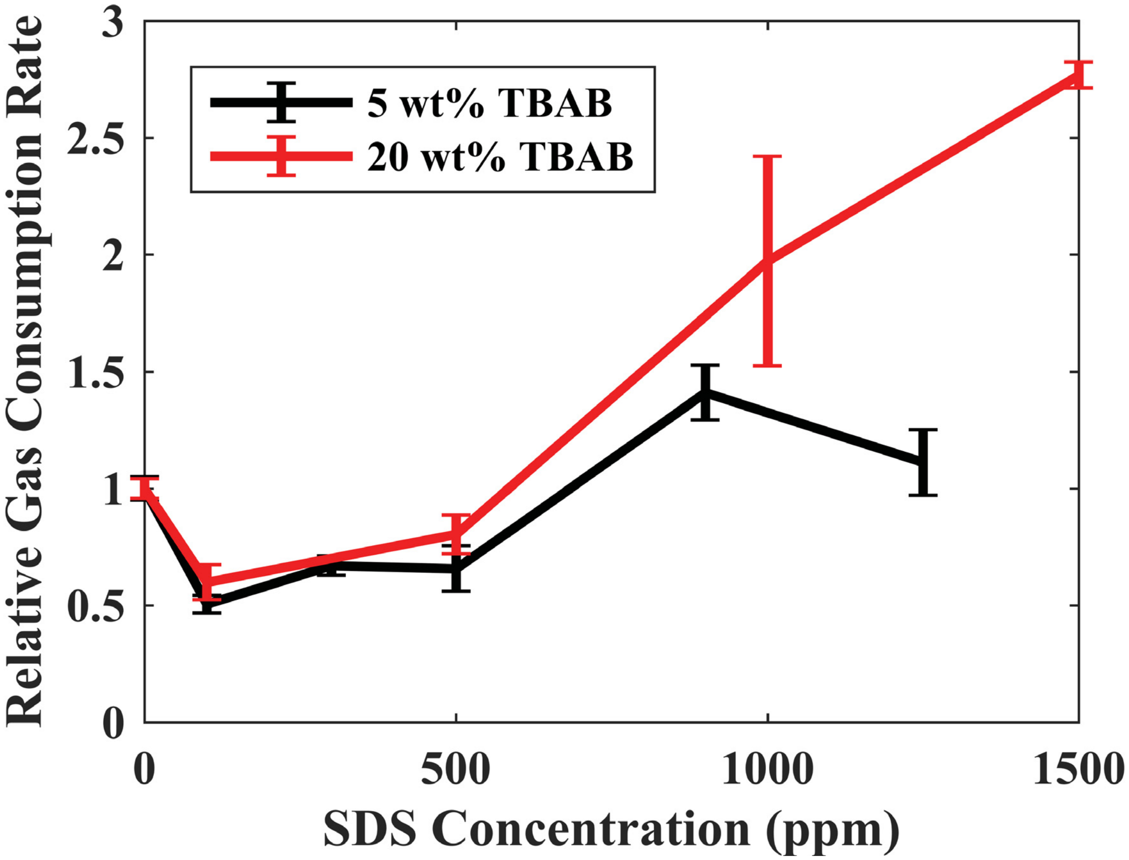

Figure 6.5: Relative methane gas consumption rate compared to 0 ppmw SDS (pure TBAB) as a function of SDS concentration. Vertical error bars correspond to 95 % confidence intervals.

Table 6.2: Absolute methane gas consumption rate values for all mixtures of high concentration TBAB and SDS. Confidence intervals are omitted for clarity but can be found in Figure 6.5.

SDS Concentration (ppmw)	TBAB concentration (wt %)	Average gas consumption rate * 1e6 (mol/s)	Relative to 0 ppmw SDS
0	5	5.6	1.00
100	5	2.8	0.51
300	5	3.7	0.67
500	5	3.7	0.66
900	5	7.9	1.41
1250	5	6.2	1.11
0	20	4.8	1.00
100	20	2.9	0.60
500	20	3.9	0.80
1000	20	9.5	1.97
1500	20	13.4	2.76

6.6 Conclusion

An investigation into the addition of the kinetic promoter SDS to a TBAB-methane semi-clathrate system was undertaken over a range of 100 to 1500 ppmw SDS and 200 to 200 000 ppmw TBAB (0.02 to 20 wt %). The growth rates of methane hydrate systems containing only SDS were found to begin to increase at similar threshold values as reported in literature, but surpassed reported plateau values without tailing off. A growth rate enhancement of 880 % compared to pure water was observed at the highest concentration of SDS used (900 ppmw). In methane hydrate systems containing low concentrations of the thermodynamic promoter TBAB (200 to 1250 ppmw), hydrate growth was found to decrease monotonically as a function of TBAB concentration, reaching 55 % inhibition at 1250 ppmw TBAB. The addition of 100 to 1250 ppmw SDS to these 200 to 1250 ppmw TBAB systems initially slowed hydrate growth to an even larger extent than just TBAB, but eventually promoted the growth rates once a threshold SDS concentration was reached. However, the promotion effect was more pronounced without the presence of TBAB. The formation kinetics of 5 and 20 wt % TBAB systems also followed a similar inhibition-promotion trend with increasing SDS concentration. An increase of 177 % in the gas consumption rate was recorded when 1500 ppmw SDS was added to the 20 wt % TBAB clathrate system. In sum, SDS can be added to a TBAB-water-methane system to enhance gas consumption rates, but care must be taking to be above the threshold concentration of the inhibition-promotion effect.

6.7 Acknowledgments

The authors are grateful to the Natural Sciences and Engineering Research Council of Canada (NSERC), les Fonds de recherche du Québec – Nature et technologies (FRQNT), the McGill Engineering Doctoral Award (MEDA) program, and the Department of Chemical Engineering of McGill University for financial support.

Chapter 7

7 Growth Kinetics of Carbon Dioxide Gas Hydrates with Tetrabutylammonium Bromide and Sodium Dodecyl Sulfate

7.1 Preface

This final study builds on results from Chapter 6 by investigating the effect of mixtures of TBAB and SDS on carbon dioxide hydrate systems. SDS is already known to inhibit CO_2 gas hydrate growth rates and an investigation on its effect when TBAB is present was performed here. The experiments were conducted with 40 wt % TBAB in this case since this is the stoichiometric hydrate concentration and equilibrium values were available at this concentration for carbon dioxide. SDS concentration was varied from 100 to 3000 ppmw.

7.2 Abstract

Carbon dioxide kinetic experiments were undertaken using different concentrations of sodium dodecyl sulfate in a 40 wt % TBAB system. SDS concentrations were varied from 100 to 3000 ppmw. Results showed that the gas consumption rates were inhibited at some SDS concentrations (100, 300 and 900 ppmw) and unchanged at other SDS concentrations (500, 1500, 3000 ppmw). To strengthen this conclusion, the gas consumption rates were also plotted with induction time of hydrate formation and the results showed a linear trend that made rates from different concentrations impossible to differentiate from a 40 wt % TBAB system.

7.3 Introduction

Gas hydrates, or clathrate hydrates, are non-stoichiometric crystalline compounds that arise when a gas or volatile liquid is encapsulated by water molecules. Suitable guest molecules are mostly determined by size and stabilize the crystal lattice of hydrogen-bonded water molecules via weak van der Waals forces (Sloan et al., 2008). Gas hydrates usually form at moderate temperatures and high pressures. There are over 180 different molecules that form hydrates, with the most notable being methane, ethane and carbon dioxide (Englezos, 1993). Clathrates hydrates were first document in 1810 by Sir Humphrey Davy and remained mainly of academic interest until industrial research was spurred by the discovery of hydrates blocking natural gas transmission lines in the 1930s (Hammerschmidt, 1934). The next turning point in the hydrate field was the discovery of *in situ* natural gas hydrates in the Siberian permafrost (Makogon, 1965). Current conservative estimates propose that the amount of energy stored in natural gas hydrate deposits is double the amount of all other fossil fuels combined (Max, 2000). Recently, various applications using hydrates have been proposed such as gas transportation, storage and separation (Thomas, 2003; Eslamimanesh et al., 2012). Carbon dioxide sequestration in hydrate form has been studied as a means to mitigate global warming (Chatti et al., 2005). Slow and unpredictable formation kinetics and the lack of scalability studies have prevented larger scale development of these proposed technologies (Eslamimanesh et al., 2012; Ma et al., 2016). This study examines the kinetic behaviour of carbon dioxide gas with a 40 wt % TBAB system and different concentrations of SDS.

7.4 Materials and Methods

7.4.1 Experimental Setup

The experimental apparatus consists of a 600 mL stainless steel reactor that is submerged in a temperature-controlled 20 % by volume ethylene glycol-water bath, as displayed in Figure 6.1. Two MM-DO6 magnetic stirrers from Pressure Product Industries are used to evenly mix both the reactor and the temperature-controlled bath. The reservoir gas tank is used to keep the reactor pressure constant during experiments by feeding gas through a Baumann 51000 control valve. The valve receives a signal based on the difference in pressure between the reactor bias gas tank and the reactor. This signal increases when gas is consumed in the reactor and the control valve delivers gas to the reactor in response to this signal in order to maintain constant pressure. Pressures are monitored at three different locations using Rosemount pressure transducers configured to a span of 0 to 14 000 kPa for absolute pressure measurements and 0 to 2000 kPa for differential pressure measurements, with an accuracy of 0.065 % of the given span. Temperatures are recorded with RTD probes from Omega for the reactor liquid, reactor gas, and reservoir tank. Carbon dioxide obtained from MEGS Inc. has a purity of 99.995 %. The water used is treated by a reverse-osmosis (RO) system with a 0.22 μm filter and has a conductivity of 10 μS and total organic content less than 10 ppmw. The 50 wt % TBAB-water mixture is obtained from Sigma Aldrich and used to prepare the 40 wt % TBAB mixtures used in this study. SDS is purchased from Fisher Scientific as a solid powder and added to the solution in measured amounts to obtain different concentrations.

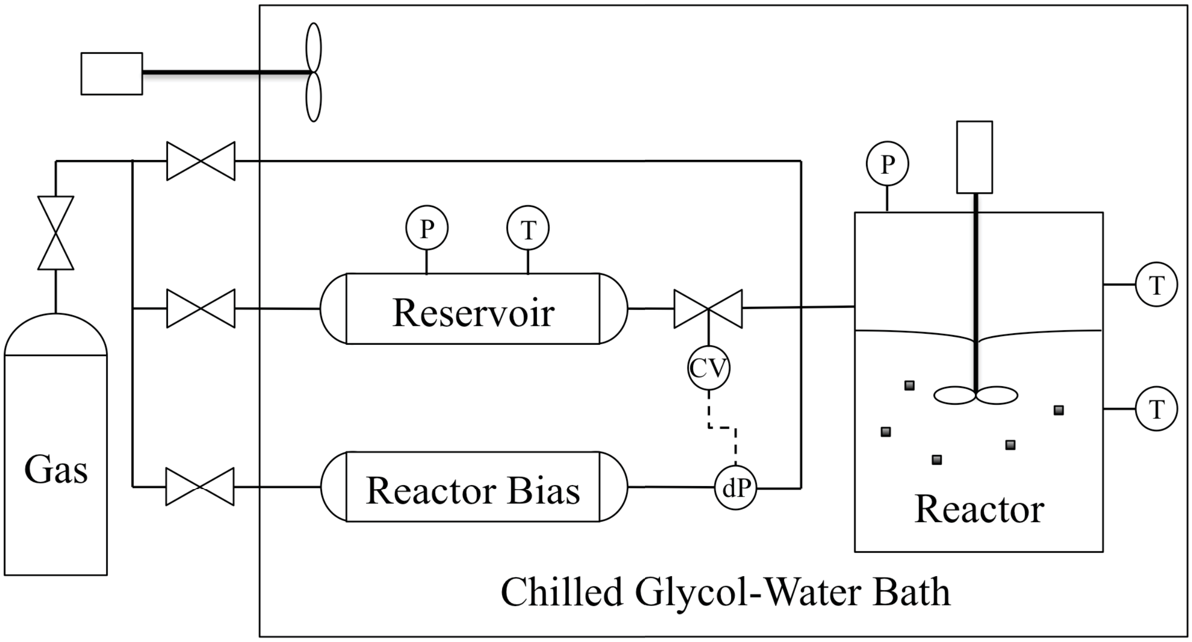

Figure 7.1: Experimental setup.

7.4.2 Experimental Procedure

Before starting experiments, the reactor was rinsed three times with 420 mL of RO water. The reactor was subsequently filled with 360 mL of the hydrate-forming solution. The system temperature was fixed at 14 °C using the chiller to regulate the glycol bath. Once the liquid sample was loaded, the reactor was purged with carbon dioxide gas three times by pressurizing to 1100 kPa followed by de-pressurizing to 110 kPa. The system was then pressurized to 2521 kPa based on the desired driving force of 1500 kPa. The reservoir and reactor bias gas tanks were filled with carbon dioxide gas to a pressure 1000 kPa above the reactor value so as to provide a pressure differential for gas transfer during the kinetic runs. Once the reactor pressure and temperature stabilized, the data acquisition system and control valve were activated, and the magnetic stirrer inside the reactor was started. This begins the dissolution phase of a hydrate experiments that continues until the nucleation point, which is detected by a spike in bulk liquid temperature. Hydrate growth was recorded for at least 450 seconds beyond this point. After the run, the data acquisition system and control valve were turned off and the reactor pressure was brought down to 110 kPa to allow the hydrates to dissociate. At this point, the experiment was either repeated to provide replicates or the reactor liquid was changed for experiments using a different mixture. Molar gas consumption rates were calculated using the reservoir pressure and temperature data over the first 450 seconds of hydrate growth and converting this data to moles using the Trebble-Bishnoi equation of state (Trebble et al., 1987; 1988).

7.5 Results and Discussion

Experiments were conducted at 14 °C and 2521 kPa based on a 1500 kPa driving force from the equilibrium value (Verrett et al., 2015). Carbon dioxide gas consumption rate results are shown in Figure 7.2 at SDS concentrations varying from 100 to 3000 ppmw. An inhibition is present at most of the SDS concentrations (100, 300 and 900 ppmw). All concentrations have their average consumption rates lower than the pure systems, however, the SDS concentrations of 500, 1500 and 3000 ppmw are not statistically different in term of growth rate from the baseline 40 wt % TBAB. This result shows that the presence of TBAB does not prevent SDS from inhibiting or at the very least nullifying carbon dioxide gas hydrate formation rates.

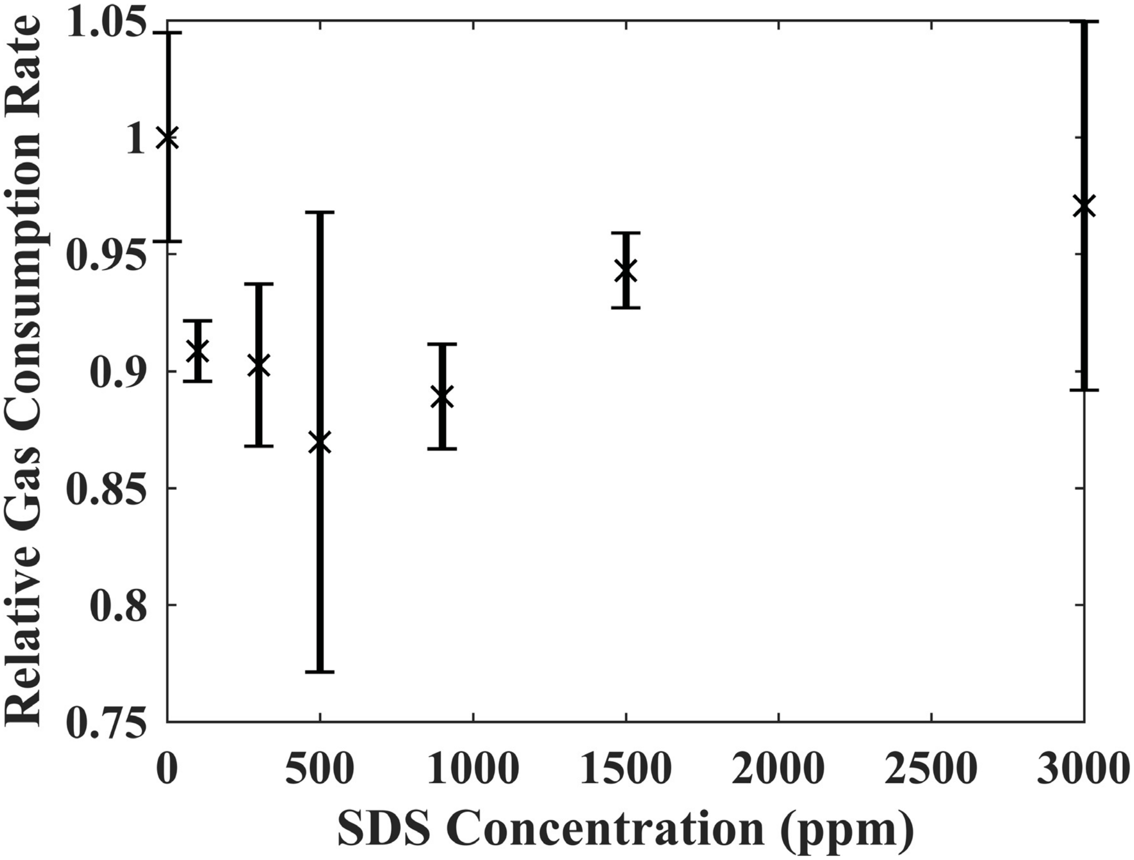

Figure 7.2: Relative carbon dioxide gas consumption rate compared to 40 wt % TBAB as a function of SDS concentration. Vertical error bars correspond to 95 % confidence intervals.

Another approach to observing these results comes from Chapter 3 and 4. It was shown that carbon dioxide systems can be studied by looking at the trend between induction time and gas consumption rate. This was plotted for all experiments of the present system in Figure 7.3. All experiments, regardless of SDS concentration, follow the same linear decreasing line between gas consumption rate and induction time. This also achieves the same conclusion that the added SDS does not statistically change the growth rate in a carbon dioxide system.

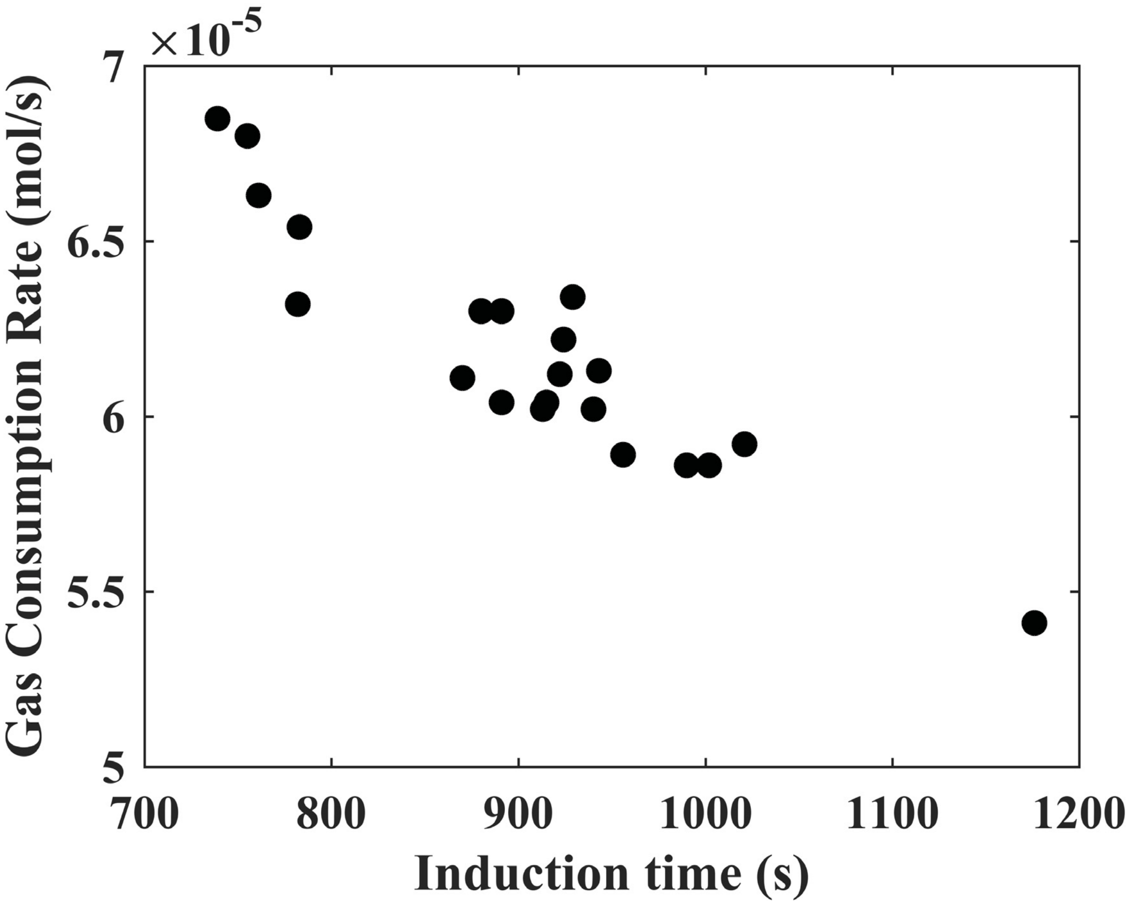

Figure 7.3: Carbon dioxide gas consumption rate against induction time for all SDS concentration in a 40 wt % TBAB system.

7.6 Conclusion

The results shown in this chapter indicate that adding sodium dodecyl sulfate to a 40 wt % TBAB carbon dioxide system does not help promote the growth kinetics. This is very different than with a methane system as reported in Chapter 6. However, it is on par with results that show that SDS slightly inhibits carbon dioxide hydrate systems. Since we are dealing with a carbon dioxide hydrate system, it was important to look at the effect of induction time on the gas consumption rates. The different concentrations of SDS in the 40 wt% TBAB system did not show statistically different results for the gas consumption rates with induction time. It was even observed that SDS concentrations between 100 and 3000 ppmw averaged a lower growth rate than a pure TBAB system.

Chapter 8

8 Conclusion and Future Recommendations

8.1 Comprehensive Conclusion

The current work investigated the kinetics of gas hydrate growth with different combination of known promoters. Chapter 3 presented a novel method to analyze gas hydrate kinetics at all induction times. A high variability in gas consumption rate was discovered at a same experimental condition for pure carbon dioxide gas hydrates. It was concluded that carbon dioxide gas consumption rate decreased with increasing induction time following a first-order response. An increasing monotonic relationship was also found in between induction time and bulk liquid temperature increase at hydrate nucleation. Methane hydrates did not exhibit the same behaviour as carbon dioxide with respect to gas consumption rate variability and the trends with induction time. Values for methane gas consumption rates were reproducible at the conditions tested and hence, these could be used directly to compare kinetics. Chapter 4 used the analysis tool established in Chapter 3 to analyze the formation kinetics of a carbon dioxide semi-clathrate hydrate system composed of 40 wt % TBAB and 9.5 ppmw MWCNTs. The addition of the kinetic promoter MWCNT to the thermodynamic promoter TBAB increased gas consumption rates during growth for induction times less than one hour but did not affect it at longer induction times. The maximum gas consumption enhancement from the added MWCNTs was 15 %. Dissolution runs were also completed and indicated that the presence of MWCNTs improved the dissolution rate by lowering the time constant by 5 %. In Chapter 5, a system composing of two hydrate kinetic promoters, SDS and Al_2O_3 nanoparticles, was studied for its effect on methane hydrate growth. Concentrations of aluminum oxide nanoparticles were varied from 10 to 1000 ppmw in a 575 ppmw SDS solution. It was shown that the added nanoparticles did not modify gas consumption rates with and without the presence of SDS. Chapter 6 followed with a study on the effect of combining the common thermodynamic promoter, TBAB, with the powerful kinetic promoter, SDS, to a methane hydrate system. Solutions containing low concentrations of TBAB in water reduced hydrate growth rates up to 55 % at 1250 ppmw TBAB compared to pure water. The addition of 100 to 1250 ppmw SDS to system with 200 to 1250 ppmw TBAB initially slowed hydrate growth to a larger extent than solely TBAB, but eventually promoted the growth rates when a threshold SDS concentration was reached. A similar trend with SDS concentration was also observed in 5 and 20 wt % TBAB systems. The last study was a continuation of the results from Chapter 6 by observing a carbon dioxide hydrate system with the same combination of chemicals. It was shown that SDS did not promote gas consumption rates at all SDS concentrations in a 40 wt % TBAB system as expected since SDS was known to inhibit pure carbon dioxide-water hydrates.

8.2 Recommendations for Future Works

The following opportunities could be pursued to provide a deeper understanding into the formation kinetics of semi-clathrate promoters and also the underlying mechanism of different combinations of hydrate promoters:

- Investigating why CO_2 hydrates are inhibited by SDS using mole fraction measurements.

- Investigating tetrabutylammonium chloride (TBAC) kinetics and comparing them to TBAB kinetics.

- Further establishing a method to systematically compare the growth kinetics of systems with different hydrate thermodynamic equilibrium.

- Determining the critical micelle concentration of different mixtures of SDS-TBAB at hydrate growth conditions.

- Performing morphology studies on the SDS-TBAB semi-clathrate system to better understand the mechanism behind the promoting-inhibiting effect.

- Analyzing stability and characteristics of MWCNTs at all moments of a hydrate kinetic run.

8.3 Other Significant Contributions

In addition to the work presented in this thesis, the author has also contributed to the following peer-reviewed publications:

- Renault-Crispo, J.-S., Lang, F. and Servio, P. "The importance of liquid phase compositions in gas hydrate modeling: Carbon dioxide–methane–water case study." *The Journal of Chemical Thermodynamics* 68(0): 153-160. 2014.

- Verrett, J., Renault-Crispo, J.-S. and Servio, P. "Phase equilibria, solubility and modeling study of CO2/CH4 + tetra-n-butylammonium bromide aqueous semi-clathrate systems." *Fluid Phase Equilibria* 388(0): 160-168. 2015.

- Ivall, J., Renault-Crispo, J.-S., Coulombe, S. and Servio, P. "Ice-dependent liquid-phase convective cells during the melting of frozen sessile droplets containing water and multiwall carbon nanotubes." *International Journal of Heat and Mass Transfer* 101: 27-37. 2016.

- Ling, E. J. Y., Uong, V., Renault-Crispo, J.-S., Kietzig, A.-M. and Servio, P. "Reducing Ice Adhesion on Nonsmooth Metallic Surfaces: Wettability and Topography Effects." *ACS Applied Materials & Interfaces*. 2016.

Chapter 9

9 Notation

A = interfacial surface area, m^2

k = mass transfer coefficient, m/s

k_r= intrinsic reaction rate constant, m/s

MW_w = molecular weight, g/mol

n = moles, mol

$n_s = n_{liq}$ = moles at saturation, mol

P = pressure, MPa

ρ_w = density of water, g/m^3

t = time, s

T = temperature, K

τ = time constant, s

μ_2= second moment of particle size distribution, m^2

V = volume, m^3

V_L = liquid volume, m^3

$x_i^L = x^L$ = liquid mole fraction

x_i^{HL} = hydrate-liquid equilibrium liquid mole fraction

x^{HLV} = hydrate-vapour-liquid equilibrium liquid mole fraction

Chapter 10

10 Bibliography

"Adoption of the Paris Agreement." 21st Conference of the Parties. Paris, United Nations. United Nations Framework Convention on Climate Change. 2015.

Aladko, L. S., Dyadin, Y. A., Rodionova, T. V. and Terekhova, I. S. "Clathrate Hydrates of Tetrabutylammonium and Tetraisoamylammonium Halides." *Journal of Structural Chemistry Journal of Structural Chemistry* 43(6): 990-994. 2002. DOI: http://dx.doi.org/10.1023/A:1023698728342

Aliabadi, M., Rasoolzadeh, A., Esmaeilzadeh, F. and Alamdari, A. "Experimental study of using CuO nanoparticles as a methane hydrate promoter." *Journal of Natural Gas Science and Engineering* 27, Part 3: 1518-1522. 2015. DOI: http://dx.doi.org/10.1016/j.jngse.2015.10.017

Arjang, S., Manteghian, M. and Mohammadi, A. "Effect of synthesized silver nanoparticles in promoting methane hydrate formation at 4.7 MPa and 5.7 MPa." *Chemical Engineering Research and Design* 91(6): 1050-1054. 2013. DOI: http://dx.doi.org/10.1016/j.cherd.2012.12.001

Arjmandi, M., Chapoy, A. and Tohidi, B. "Equilibrium Data of Hydrogen, Methane, Nitrogen, Carbon Dioxide, and Natural Gas in Semi-Clathrate Hydrates of Tetrabutyl Ammonium Bromide." *Journal of Chemical & Engineering Data* 52(6): 2153-2158. 2007. DOI: http://dx.doi.org/10.1021/je700144p

Atkins, P. W. and De Paula, J. "Elements of physical chemistry." Oxford; New York, Oxford University Press. 2009.

Babu, P., Kumar, R. and Linga, P. "Pre-combustion capture of carbon dioxide in a fixed bed reactor using the clathrate hydrate process." *Energy* 50: 364-373. 2013. DOI: http://dx.doi.org/10.1016/j.energy.2012.10.046

Babu, P., Datta, S., Kumar, R. and Linga, P. "Impact of experimental pressure and temperature on semiclathrate hydrate formation for pre-combustion capture of CO2 using tetra-n-butyl ammonium nitrate." *Energy* 78: 458-464. 2014a. DOI: http://dx.doi.org/10.1016/j.energy.2014.10.033

Babu, P., Chin, W. I., Kumar, R. and Linga, P. "Systematic Evaluation of Tetra-n-butyl Ammonium Bromide (TBAB) for Carbon Dioxide Capture Employing the Clathrate Process." *Industrial & Engineering Chemistry Research* 53(12): 4878-4887. 2014b. DOI: http://dx.doi.org/10.1021/ie4043714

Babu, P., Yao, M., Datta, S., Kumar, R. and Linga, P. "Thermodynamic and Kinetic Verification of Tetra-n-butyl Ammonium Nitrate (TBANO3) as a Promoter for the Clathrate Process Applicable to Precombustion Carbon Dioxide Capture." *Environmental Science & Technology* 48(6): 3550-3558. 2014c. DOI: http://dx.doi.org/10.1021/es4044819

Babu, P., Linga, P., Kumar, R. and Englezos, P. "A review of the hydrate based gas separation (HBGS) process for carbon dioxide pre-combustion capture." *Energy* 85: 261-279. 2015. DOI: http://dx.doi.org/10.1016/j.energy.2015.03.103

Baddour, C. E., Fadlallah, F., Nasuhoglu, D., Mitra, R., Vandsburger, L. and Meunier, J.-L. "A simple thermal CVD method for carbon nanotube synthesis on stainless steel 304 without the addition of an external catalyst." *Carbon* 47(1): 313-318. 2009. DOI: http://dx.doi.org/10.1016/j.carbon.2008.10.038

Bergeron, S. and Servio, P. "Reaction rate constant of CO2 hydrate formation and verification of old premises pertaining to hydrate growth kinetics." *AIChE Journal* 54(11): 2964-2970. 2008a. DOI: http://dx.doi.org/10.1002/aic.11601

Bergeron, S. and Servio, P. "Reaction rate constant of propane hydrate formation." *Fluid Phase Equilibria* 265(1–2): 30-36. 2008b. DOI: http://dx.doi.org/10.1016/j.fluid.2007.12.001

Bergeron, S. and Servio, P. "CO2 and CH4 mole fraction measurements during hydrate growth in a semi-batch stirred tank reactor and its significance to kinetic modeling." *Fluid Phase Equilibria* 276(2): 150-155. 2009. DOI: http://dx.doi.org/10.1016/j.fluid.2008.10.021

Bergeron, S., Beltrán, J. G. and Servio, P. "Reaction rate constant of methane clathrate formation." *Fuel* 89(2): 294-301. 2010. DOI: http://dx.doi.org/10.1016/j.fuel.2009.06.019

Bishnoi, P. R. and Natarajan, V. "Formation and decomposition of gas hydrates." *Fluid Phase Equilibria* 117(1): 168-177. 1996. DOI: http://dx.doi.org/10.1016/0378-3812(95)02950-8

Bouchemoua, A., Brantuas, P. and Herri, J.-M. "Equilibrium data of CO2-based semi-clathrates from quaternary ammonium solutions." 7th International Conference on Gas Hydrates (ICGH 2011), Edimbourg, United Kingdom. 2011.

Brown, E. P. and Koh, C. A. "Competitive Interfacial Effects of Surfactant Chemicals on Clathrate Hydrate Particle Cohesion." *Energy & Fuels* 30(10): 8065-8071. 2016. DOI: http://dx.doi.org/10.1021/acs.energyfuels.6b00145

Bruusgaard, H., Beltrán, J. G. and Servio, P. "Solubility measurements for the CH4 + CO2 + H2O system under hydrate–liquid–vapor equilibrium." *Fluid Phase Equilibria* 296(2): 106-109. 2010. DOI: http://dx.doi.org/10.1016/j.fluid.2010.02.042

Callister, W. D. and Rethwisch, D. G. "Materials science and engineering : an introduction. 2010.

CBCNews. (2010). "BP hits snag with containment dome." Retrieved July 12, 2016, from http://www.cbc.ca/news/world/bp-hits-snag-with-containment-dome-1.972603.

Chapman, W. G., Gubbins, K. E., Jackson, G. and Radosz, M. "SAFT: Equation-of-state solution model for associating fluids." *Fluid Phase Equilibria* 52: 31-38. 1989. DOI: http://dx.doi.org/10.1016/0378-3812(89)80308-5

Chatti, I., Delahaye, A., Fournaison, L. and Petitet, J.-P. "Benefits and drawbacks of clathrate hydrates: a review of their areas of interest." *Energy Conversion and Management* 46(9–10): 1333-1343. 2005. DOI: http://dx.doi.org/10.1016/j.enconman.2004.06.032

Choi, J. W., Chung, J. T. and Kang, Y. T. "CO2 hydrate formation at atmospheric pressure using high efficiency absorbent and surfactants." *Energy* 78(0): 869-876. 2014. DOI: http://dx.doi.org/10.1016/j.energy.2014.10.081

Choi, S. U. S. and Eastman, J. A. "Enhancing thermal conductivity of fluids with nanoparticles." International mechanical engineering congress and exhibition, San Fransisco, United States. 1995.

CNN. (2017). "China makes 'flammable ice' breakthrough in South China Sea." Retrieved May 24, 2017, from http://money.cnn.com/2017/05/19/news/china-flammable-ice-sea/index.html?iid=ob_article_organicsidebar_expansion.

Collett, T., Bahk, J.-J., Baker, R., Boswell, R., Divins, D., Frye, M., Goldberg, D., Husebø, J., Koh, C., Malone, M., Morell, M., Myers, G., Shipp, C. and Torres, M. "Methane Hydrates in Nature—Current Knowledge and Challenges." *Journal of Chemical & Engineering Data* 60(2): 319-329. 2015. DOI: http://dx.doi.org/10.1021/je500604h

Dallimore, S. R. and Collett, T. S. "Gas Hydrates Associated with Deep Permafrost in the Mackenzie Delat, N.W.T., Canada: Regional Overview." Permafrost, Yellowknife (Canada), Collection Nordicana. 1998.

Daniel-David, D., Guerton, F., Dicharry, C., Torré, J.-P. and Broseta, D. "Hydrate growth at the interface between water and pure or mixed CO2/CH4 gases: Influence of pressure, temperature, gas composition and water-soluble surfactants." *Chemical Engineering Science* 132: 118-127. 2015. DOI: http://dx.doi.org/10.1016/j.ces.2015.04.015

Dashti, H., Zhehao Yew, L. and Lou, X. "Recent advances in gas hydrate-based CO2 capture." *Journal of Natural Gas Science and Engineering* 23: 195-207. 2015. DOI: http://dx.doi.org/10.1016/j.jngse.2015.01.033

Davies, S. R., Sloan, E. D., Sum, A. K. and Koh, C. A. "In Situ Studies of the Mass Transfer Mechanism across a Methane Hydrate Film Using High-Resolution Confocal Raman Spectroscopy." *The Journal of Physical Chemistry C* 114(2): 1173-1180. 2010. DOI: http://dx.doi.org/10.1021/jp909416y

Deschamps, J. and Dalmazzone, D. "Dissociation enthalpies and phase equilibrium for TBAB semi-clathrate hydrates of N2, CO2, N2 + CO2 and CH4 + CO2." *Journal of Thermal Analysis and Calorimetry* 98(1): 113-118. 2009. DOI: http://dx.doi.org/10.1007/s10973-009-0399-3

Di Profio, P., Arca, S., Germani, R. and Savelli, G. "Surfactant promoting effects on clathrate hydrate formation: Are micelles really involved?" *Chemical Engineering Science* 60(15): 4141-4145. 2005. DOI: http://dx.doi.org/10.1016/j.ces.2005.02.051

Dresselhaus, M. S., Dresselhaus, G. and Avouris, P. "Carbon nanotubes : synthesis, structure, properties, and applications." Berlin; New York, Springer. 2001.

Duc, N. H., Chauvy, F. and Herri, J.-M. "CO2 capture by hydrate crystallization – A potential solution for gas emission of steelmaking industry." *Energy Conversion and Management* 48(4): 1313-1322. 2007. DOI: http://dx.doi.org/10.1016/j.enconman.2006.09.024

Elwell, L. C. and Grant, W. S. (2006) "Technology options for capturing CO2." Power 150, 60-65.

Englezos, P., Kalogerakis, N., Dholabhai, P. D. and Bishnoi, P. R. "Kinetics of formation of methane and ethane gas hydrates." *Chemical Engineering Science* 42(11): 2647-2658. 1987. DOI: http://dx.doi.org/10.1016/0009-2509(87)87015-X

Englezos, P. and Bishnoi, P. R. "Gibbs free energy analysis for the supersaturation limits of methane in liquid water and the hydrate-gas-liquid water phase behavior." *Fluid Phase Equilibria* 42: 129-140. 1988. DOI: http://dx.doi.org/10.1016/0378-3812(88)80054-2

Englezos, P. "Clathrate hydrates." *Industrial & Engineering Chemistry Research* 32(7): 1251-1274. 1993. DOI: http://dx.doi.org/10.1021/ie00019a001

Eslamimanesh, A., Mohammadi, A. H., Richon, D., Naidoo, P. and Ramjugernath, D. "Application of gas hydrate formation in separation processes: A review of experimental studies." *The Journal of Chemical Thermodynamics* 46: 62-71. 2012. DOI: http://dx.doi.org/10.1016/j.jct.2011.10.006

Gabitto, J. F. and Tsouris, C. "Physical Properties of Gas Hydrates: A Review." *Journal of Thermodynamics* 2010: 12. 2010. DOI: http://dx.doi.org/10.1155/2010/271291

Ganji, H., Manteghian, M. and Rahimi Mofrad, H. "Effect of mixed compounds on methane hydrate formation and dissociation rates and storage capacity." *Fuel Processing Technology* 88(9): 891-895. 2007. DOI: http://dx.doi.org/10.1016/j.fuproc.2007.04.010

Gaudette, J. and Servio, P. "Measurement of Dissolved Propane in Water in the Presence of Gas Hydrate." *Journal of Chemical & Engineering Data* 52(4): 1449-1451. 2007. DOI: http://dx.doi.org/10.1021/je7001286

Glew, D. N. and Haggett, M. L. "Kinetics of formation of ethylene oxide hydrate. Part I. Experimental method and congruent solutions." *Canadian Journal of Chemistry* 46(24): 3857-3865. 1968a. DOI: http://dx.doi.org/10.1139/v68-639

Glew, D. N. and Haggett, M. L. "Kinetics of formation of ethylene oxide hydrate. Part II. Incongruent solutions and discussion." *Canadian Journal of Chemistry* 46(24): 3867-3877. 1968b. DOI: http://dx.doi.org/10.1139/v68-640

Gudmundsson, J. S., Hveding, F. and Børrehaug, A. "Transport Or Natural Gas As Frozen Hydrate, International Society of Offshore and Polar Engineers. 1995.

Gudmundsson, J. S., Andersson, V., Levik, O. I. and Mork, M. "Hydrate Technology for Capturing Stranded Gas." *Annals of the New York Academy of Sciences* 912(1): 403-410. 2000. DOI: http://dx.doi.org/10.1111/j.1749-6632.2000.tb06794.x

Hammerschmidt, E. G. "Formation of Gas Hydrates in Natural Gas Transmission Lines." *Industrial & Engineering Chemistry* 26(8): 851-855. 1934. DOI: http://dx.doi.org/10.1021/ie50296a010

Hashemi, S., Macchi, A., Bergeron, S. and Servio, P. "Prediction of methane and carbon dioxide solubility in water in the presence of hydrate." *Fluid Phase Equilibria* 246(1-2): 131-136. 2006. DOI: http://dx.doi.org/10.1016/j.fluid.2006.05.010

Hashemi, S., Macchi, A. and Servio, P. "Dynamic Simulation of Gas Hydrate Formation in a Three-Phase Slurry Reactor." *Industrial & Engineering Chemistry Research* 48(15): 6983-6991. 2009. DOI: http://dx.doi.org/10.1021/ie801674e

Herri, J. M., Pic, J. S., Gruy, F. and Cournil, M. "Methane hydrate crystallization mechanism from in-situ particle sizing." *AIChE Journal* 45(3): 590-602. 1999. DOI: http://dx.doi.org/10.1002/aic.690450316

Hordy, N., Mendoza-Gonzalez, N.-Y., Coulombe, S. and Meunier, J.-L. "The effect of carbon input on the morphology and attachment of carbon nanotubes grown directly from stainless steel." *Carbon* 63: 348-357. 2013a. DOI: http://dx.doi.org/10.1016/j.carbon.2013.06.089

Hordy, N., Coulombe, S. and Meunier, J.-L. "Plasma Functionalization of Carbon Nanotubes for the Synthesis of Stable Aqueous Nanofluids and Poly(vinyl alcohol) Nanocomposites." *Plasma Processes and Polymers* 10(2): 110-118. 2013b. DOI: http://dx.doi.org/10.1002/ppap.201200075

Hordy, N., Rabilloud, D., Meunier, J.-L. and Coulombe, S. "High temperature and long-term stability of carbon nanotube nanofluids for direct absorption solar thermal collectors." *Solar Energy* 105: 82-90. 2014. DOI: http://dx.doi.org/10.1016/j.solener.2014.03.013

Hosseini, M., Ghozatloo, A. and Shariaty-Niassar, M. "Effect of CVD graphene on hydrate formation of natural gas." *J Nanostruct Chem Journal of Nanostructure in Chemistry* 5(2): 219-226. 2015. DOI: http://dx.doi.org/10.1007/s40097-015-0153-2

Jeffrey, G. A. "Hydrate inclusion compounds." *Journal of Inclusion Phenomena Journal of inclusion phenomena* 1(3): 211-222. 1984. DOI: http://dx.doi.org/10.1007/BF00656757

Jokandan, E. F., Naeiji, P. and Varaminian, F. "The synergism of the binary and ternary solutions of polyethylene glycol, polyacrylamide and Hydroxyethyl cellulose to methane hydrate kinetic inhibitor." *Journal of Natural Gas Science and Engineering* 29: 15-20. 2016. DOI: http://dx.doi.org/10.1016/j.jngse.2015.12.016

Jorge, L., Girard-Lauriault, P.-L. and Coulombe, S. "pH-reversible destabilization-dispersion of MWCNTs coated with functional plasma polymer films in water." *Plasma Processes and Polymers*: 1700026-n/a. 2017. DOI: http://dx.doi.org/10.1002/ppap.201700026

Kakati, H., Mandal, A. and Laik, S. "Effect of SDS/THF on thermodynamic and kinetic properties of formation of hydrate from a mixture of gases (CH 4+ C 2 H 6+ C 3 H 8) for storing gas as hydrate." *Journal of Energy Chemistry* 25(3): 409-417. 2016a. DOI: http://dx.doi.org/10.1016/j.jechem.2016.01.018

Kakati, H., Mandal, A. and Laik, S. "Promoting effect of Al2O3/ZnO-based nanofluids stabilized by SDS surfactant on CH4+C2H6+C3H8 hydrate formation." *Journal of Industrial and Engineering Chemistry* 35: 357-368. 2016b. DOI: http://dx.doi.org/10.1016/j.jiec.2016.01.014

Kakati, H., Mandal, A. and Laik, S. "Synergistic effect of Polyvinylpyrrolidone (PVP) and L-tyrosine on kinetic inhibition of CH4+ C2H4+ C3H8 hydrate formation." *Journal of Natural Gas Science and Engineering* 34: 1361-1368. 2016c. DOI: http://dx.doi.org/10.1016/j.jngse.2016.08.027

Kalogerakis, N., Jamaluddin, A. K. M., Dholabhai, P. D. and Bishnoi, P. R. "Effect of Surfactants on Hydrate Formation Kinetics, Society of Petroleum Engineers. 1993.

Kang, S.-P. and Lee, H. "Recovery of CO2 from Flue Gas Using Gas Hydrate: Thermodynamic Verification through Phase Equilibrium Measurements." *Environmental Science & Technology* 34(20): 4397-4400. 2000a. DOI: http://dx.doi.org/10.1021/es001148l

Kang, S.-P. and Lee, H. "Recovery of CO2 from flue gas using gas hydrate: thermodynamic verification through phase equilibrium measurements." *Environmental science & technology* 34(20): 4397-4400. 2000b. DOI: http://dx.doi.org/10.1021/es001148l

Kashchiev, D. "Nucleation : basic theory with applications." Oxford; Boston, Butterworth Heinemann. 2000.

Ke, W., Svartaas, T. M., Kvaløy, J. T. and Kosberg, B. R. "Inhibition–Promotion: Dual Effects of Polyvinylpyrrolidone (PVP) on Structure-II Hydrate Nucleation." *Energy & Fuels* 30(9): 7646-7655. 2016. DOI: http://dx.doi.org/10.1021/acs.energyfuels.6b01321

Khan, M. U., Reddy, K. R., Snguanwongchai, T., Haque, E. and Gomes, V. G. "Polymer brush synthesis on surface modified carbon nanotubes via in situ emulsion polymerization." *Colloid and Polymer Science* 294(10): 1599-1610. 2016. DOI: http://dx.doi.org/10.1007/s00396-016-3922-7

Koh, C. A., Sloan, E. D., Sum, A. K. and Wu, D. T. "Fundamentals and Applications of Gas Hydrates." *Annual Review of Chemical and Biomolecular Engineering* 2: 237-257. 2011. DOI: http://dx.doi.org/10.1146/annurev-chembioeng-061010-114152

Kumar, A., Sakpal, T., Linga, P. and Kumar, R. "Influence of contact medium and surfactants on carbon dioxide clathrate hydrate kinetics." *Fuel* 105(0): 664-671. 2013. DOI: http://dx.doi.org/10.1016/j.fuel.2012.10.031

Kumar, A., Bhattacharjee, G., Kulkarni, B. D. and Kumar, R. "Role of Surfactants in Promoting Gas Hydrate Formation." *Industrial & Engineering Chemistry Research* 54(49): 12217-12232. 2015. DOI: http://dx.doi.org/10.1021/acs.iecr.5b03476

Lederhos, J. P., Long, J. P., Sum, A., Christiansen, R. L. and Sloan Jr, E. D. "Effective kinetic inhibitors for natural gas hydrates." *Chemical Engineering Science* 51(8): 1221-1229. 1996. DOI: http://dx.doi.org/10.1016/0009-2509(95)00370-3

Letcher, T. M. "Future Energy: Improved, Sustainable and Clean Options for our Planet. 2014.

Li, J., Qi, X., Wu, J., Liang, D., Guo, K. and Wang, R. Z. (2006a) "Experimental study on the formation process of gas hydrate in nanofluids." Journal of Xi'an Jiaotong University 40.

Li, J. P., Liang, D. Q., Guo, K. H., Wang, R. Z. and Fan, S. S. "Formation and dissociation of HFC134a gas hydrate in nano-copper suspension." *Energy Conversion and Management* 47(2): 201-210. 2006b. DOI: http://dx.doi.org/10.1016/j.enconman.2005.03.018

Li, X.-S., Xia, Z.-M., Chen, Z.-Y., Yan, K.-F., Li, G. and Wu, H.-J. "Gas Hydrate Formation Process for Capture of Carbon Dioxide from Fuel Gas Mixture." *Industrial & Engineering Chemistry Research* 49(22): 11614-11619. 2010. DOI: http://dx.doi.org/10.1021/ie100851u

Lim, S.-H., Riffat, S. B., Park, S.-S., Oh, S.-J., Chun, W. and Kim, N.-J. "Enhancement of methane hydrate formation using a mixture of tetrahydrofuran and oxidized multi-wall carbon nanotubes." *International Journal of Energy Research* 38(3): 374-379. 2014. DOI: http://dx.doi.org/10.1002/er.3051

Linga, P., Kumar, R. and Englezos, P. "The clathrate hydrate process for post and pre-combustion capture of carbon dioxide." *Journal of Hazardous Materials* 149(3): 625-629. 2007. DOI: http://dx.doi.org/10.1016/j.jhazmat.2007.06.086

Linga, P. and Clarke, M. A. "A Review of Reactor Designs and Materials Employed for Increasing the Rate of Gas Hydrate Formation." *Energy & Fuels* 31(1): 1-13. 2017. DOI: http://dx.doi.org/10.1021/acs.energyfuels.6b02304

Lirio, C. F. d. S., Pessoa, F. L. P. and Uller, A. M. C. "Storage capacity of carbon dioxide hydrates in the presence of sodium dodecyl sulfate (SDS) and tetrahydrofuran (THF)."

Chemical Engineering Science 96(0): 118-123. 2013. DOI: http://dx.doi.org/10.1016/j.ces.2012.10.022

Lo, C., Zhang, J. S., Somasundaran, P., Lu, S., Couzis, A. and Lee, J. W. "Adsorption of Surfactants on Two Different Hydrates." *Langmuir* 24(22): 12723-12726. 2008. DOI: http://dx.doi.org/10.1021/la802362m

Ma, Z. W., Zhang, P., Bao, H. S. and Deng, S. "Review of fundamental properties of CO2 hydrates and CO2 capture and separation using hydration method." *Renewable and Sustainable Energy Reviews* 53: 1273-1302. 2016. DOI: http://dx.doi.org/10.1016/j.rser.2015.09.076

Mahmoudi, B., Naeiji, P. and Varaminian, F. "Study of tetra-n-butylammonium bromide and tetrahydrofuran hydrate formation kinetics as a cold storage material for air conditioning system." *Journal of Molecular Liquids Journal of Molecular Liquids* 214: 96-100. 2016. DOI: http://dx.doi.org/10.1016/j.molliq.2015.11.048

Mak, T. C. W. and McMullan, R. K. "Polyhedral Clathrate Hydrates. X. Structure of the Double Hydrate of Tetrahydrofuran and Hydrogen Sulfide." *The Journal of Chemical Physics* 42(8): 2732-2737. 1965. DOI: http://dx.doi.org/10.1063/1.1703229

Makogon, Y. F. (1965) "Hydrate Formation in the Gas-Bearing Layer in Permafrost Conditions." Gazovaya Promyshlennost (Gas Industry) 5.

Mata, J., Varade, D., Ghosh, G. and Bahadur, P. "Effect of tetrabutylammonium bromide on the micelles of sodium dodecyl sulfate." *Colloids and Surfaces A: Physicochemical and Engineering Aspects* 245(1–3): 69-73. 2004. DOI: http://dx.doi.org/10.1016/j.colsurfa.2004.07.009

Max, M. D. "Natural gas hydrate : in oceanic and permafrost environments." Dordrecht; Boston, Kluwer Academic Publishers. 2000.

Mayoufi, N., Dalmazzone, D., Fürst, W., Delahaye, A. and Fournaison, L. "CO2 Enclathration in Hydrates of Peralkyl-(Ammonium/Phosphonium) Salts: Stability Conditions and Dissociation Enthalpies." *Journal of Chemical & Engineering Data* 55(3): 1271-1275. 2010. DOI: http://dx.doi.org/10.1021/je9006212

Mech, D., Gupta, P. and Sangwai, J. S. "Kinetics of methane hydrate formation in an aqueous solution of thermodynamic promoters (THF and TBAB) with and without kinetic promoter (SDS)." *Journal of Natural Gas Science and Engineering* 35, Part B: 1519-1534. 2016a. DOI: http://dx.doi.org/10.1016/j.jngse.2016.06.013

Mech, D. and Sangwai, J. S. "Phase Equilibrium of the Methane Hydrate System in the Presence of Mixed Promoters (THF+ TBAB) and the Effect of Inhibitors (NaCl, Methanol, and Ethylene Glycol)." *Journal of Chemical & Engineering Data* 61(10): 3607-3617. 2016b. DOI: http://dx.doi.org/10.1021/acs.jced.6b00518

Mohajeri, E. and Noudeh, G. D. "Effect of Temperature on the Critical Micelle Concentration and Micellization Thermodynamic of Nonionic Surfactants: Polyoxyethylene Sorbitan Fatty Acid Esters." *E-Journal of Chemistry* 9(4). 2012. DOI: http://dx.doi.org/10.1155/2012/961739

Mohammadi, A., Manteghian, M., Hoseini-Nasab, S. M. and Safavi, S. M. M. "The Effect of Multi-walled Carbon Nanotubes on Solubility of Methane in Water." *Petroleum Science and Technology* 31(11): 1206-1213. 2013a. DOI: http://dx.doi.org/10.1080/10916466.2011.576370

Mohammadi, A., Manteghian, M. and Mousavi Safavi, S. M. "Solubility of Methane in Water at the Presence of β-Cyclodextrin, SDS, and Multi Wall Carbon Nanotubes at Low Temperatures." *Pet. Sci. Technol.* 31(10): 1085-1091. 2013b. DOI: http://dx.doi.org/10.1080/10916466.2011.588643

Mohammadi, A., Manteghian, M., Haghtalab, A., Mohammadi, A. H. and Rahmati-Abkenar, M. "Kinetic study of carbon dioxide hydrate formation in presence of silver nanoparticles and SDS." *Chemical Engineering Journal* 237: 387-395. 2014. DOI: http://dx.doi.org/10.1016/j.cej.2013.09.026

Moraveji, M. K., Golkaram, M. and Davarnejad, R. "Effect of CuO nanoparticle on dissolution of methane in water." *Journal of Molecular Liquids* 180: 45-50. 2013. DOI: http://dx.doi.org/10.1016/j.molliq.2012.12.014

Mullin, J. W. "Crystallization." Oxford; Boston, Butterworth-Heinemann. 2001.

Najibi, H., Mirzaee Shayegan, M. and Heidary, H. "Experimental investigation of methane hydrate formation in the presence of copper oxide nanoparticles and SDS." *Journal of Natural Gas Science and Engineering* 23(0): 315-323. 2015. DOI: http://dx.doi.org/10.1016/j.jngse.2015.02.009

Natarajan, V., Bishnoi, P. R. and Kalogerakis, N. "Induction phenomena in gas hydrate nucleation." *Chemical Engineering Science* 49(13): 2075. 1994. DOI: http://dx.doi.org/10.1016/0009-2509(94)E0026-M

National Research Council. "Charting the future of methane hydrate research in the United States. Washington, D.C., National Academies Press. 2004.

Nesterov, A. N., Reshetnikov, A. M., Manakov, A. Y., Rodionova, T. V., Paukshtis, E. A., Asanov, I. P., Bardakhanov, S. P. and Bulavchenko, A. I. "Promotion and inhibition of gas hydrate formation by oxide powders." *Journal of Molecular Liquids* 204(0): 118-125. 2015. DOI: http://dx.doi.org/10.1016/j.molliq.2015.01.037

Nguyen, N. N., Nguyen, A. V., Nguyen, K. T., Rintoul, L. and Dang, L. X. "Unexpected inhibition of CO2 gas hydrate formation in dilute TBAB solutions and the critical role of interfacial water structure." *Fuel* 185: 517-523. 2016. DOI: http://dx.doi.org/10.1016/j.fuel.2016.08.006

Park, S.-S., Lee, S.-B. and Kim, N.-J. "Effect of multi-walled carbon nanotubes on methane hydrate formation." *Journal of Industrial and Engineering Chemistry* 16(4): 551-555. 2010. DOI: http://dx.doi.org/10.1016/j.jiec.2010.03.023

Park, S.-S., An, E.-J., Lee, S.-B., Chun, W.-g. and Kim, N.-J. "Characteristics of methane hydrate formation in carbon nanofluids." *Journal of Industrial and Engineering Chemistry* 18(1): 443-448. 2012. DOI: http://dx.doi.org/10.1016/j.jiec.2011.11.045

Parrish, W. R. and Prausnitz, J. M. "Dissociation Pressures of Gas Hydrates Formed by Gas Mixtures." *Industrial & Engineering Chemistry Process Design and Development* 11(1): 26-35. 1972. DOI: http://dx.doi.org/10.1021/i260041a006

Pasieka, J., Coulombe, S. and Servio, P. "Investigating the effects of hydrophobic and hydrophilic multi-wall carbon nanotubes on methane hydrate growth kinetics." *Chemical Engineering Science* 104: 998-1002. 2013a. DOI: http://dx.doi.org/10.1016/j.ces.2013.10.037

Pasieka, J., Hordy, N., Coulombe, S. and Servio, P. "Measuring the effect of multi-wall carbon nanotubes on tetrahydrofuran- water hydrate front velocities using thermal imaging." *Crystal Growth and Design* 13(9): 4017-4024. 2013b. DOI: http://dx.doi.org/10.1021/cg400767u

Pasieka, J., Coulombe, S. and Servio, P. "The Effect of Hydrophilic and Hydrophobic Multi-Wall Carbon Nanotubes on Methane Dissolution Rates in Water at Three Phase Equilibrium (V-Lw-H) Conditions." *Industrial & Engineering Chemistry Research* 53(37): 14519-14525. 2014. DOI: http://dx.doi.org/10.1021/ie502457c

Pasieka, J., Servio, P., Jorge, L. and Coulombe, S. "Effects of As-Produced and Amine-Functionalized Multi-Wall Carbon Nanotubes on Carbon Dioxide Hydrate Formation." *Energy & Fuels* 29(8): 5259-5266. 2015. DOI: http://dx.doi.org/10.1021/i260041a006

Pellenbarg, R. E. and Max, M. D. Introduction, Physical Properties, and Natural Occurrences of Hydrate. Natural Gas Hydrate in Oceanic and Permaforst Environments. Dordrecht, Kluwer Academic Publishers: 1-8. 2000.

Peng, D.-Y. and Robinson, D. B. "A New Two-Constant Equation of State." *Industrial & Engineering Chemistry Fundamentals* 15(1): 59-64. 1976. DOI: http://dx.doi.org/10.1021/i160057a011

Reddy, K. R., Sin, B. C., Yoo, C. H., Park, W., Ryu, K. S., Lee, J.-S., Sohn, D. and Lee, Y. "A new one-step synthesis method for coating multi-walled carbon nanotubes with cuprous oxide nanoparticles." *Scripta Materialia* 58(11): 1010-1013. 2008. DOI: http://dx.doi.org/10.1016/j.scriptamat.2008.01.047

Reddy, K. R., Sin, B. C., Yoo, C. H., Sohn, D. and Lee, Y. "Coating of multiwalled carbon nanotubes with polymer nanospheres through microemulsion polymerization." *Journal of Colloid and Interface Science* 340(2): 160-165. 2009. DOI: http://dx.doi.org/10.1016/j.jcis.2009.08.044

Reddy, K. R., Jeong, H. M., Lee, Y. and Raghu, A. V. "Synthesis of MWCNTs-core/thiophene polymer-sheath composite nanocables by a cationic surfactant-assisted chemical oxidative polymerization and their structural properties." *Journal of Polymer Science Part A: Polymer Chemistry* 48(7): 1477-1484. 2010. DOI: http://dx.doi.org/10.1002/pola.23883

Renault-Crispo, J.-S., Lang, F. and Servio, P. "The importance of liquid phase compositions in gas hydrate modeling: Carbon dioxide–methane–water case study." *The Journal of Chemical Thermodynamics* 68(0): 153-160. 2014. DOI: http://dx.doi.org/10.1016/j.jct.2013.09.011

Renault-Crispo, J.-S. and Servio, P. "Role of induction time on carbon dioxide and methane gas hydrate kinetics." *Journal of Natural Gas Science and Engineering* 43: 81-89. 2017. DOI: http://dx.doi.org/10.1016/j.jngse.2017.03.030

Renon, H. and Prausnitz, J. M. "Local compositions in thermodynamic excess functions for liquid mixtures." *AIChE Journal* 14(1): 135-144. 1968. DOI: http://dx.doi.org/10.1002/aic.690140124

Ricaurte, M., Dicharry, C., Broseta, D., Renaud, X. and Torré, J.-P. "CO2 Removal from a CO2–CH4 Gas Mixture by Clathrate Hydrate Formation Using THF and SDS as Water-Soluble Hydrate Promoters." *Industrial & Engineering Chemistry Research* 52(2): 899-910. 2012. DOI: http://dx.doi.org/10.1021/ie3025888

Ripmeester, J. A., Tse, J. S., Ratcliffe, C. I. and Powell, B. M. "A new clathrate hydrate structure." *Nature* 325(6100): 135-136. 1987. DOI: http://dx.doi.org/10.1038/325135a0

Servio, P. and Englezos, P. "Measurement of Dissolved Methane in Water in Equilibrium with Its Hydrate." *Journal of Chemical & Engineering Data* 47(1): 87-90. 2002. DOI: http://dx.doi.org/10.1021/je0102255

Shimada, W., Shiro, M., Kondo, H., Takeya, S., Oyama, H., Ebinuma, T. and Narita, H. "Tetra-n-butylammonium bromide-water (1/38)." *Acta Crystallographica Section C* 61(2): o65-o66. 2005. DOI: http://dx.doi.org/10.1107/S0108270104032743

Skovborg, P. and Rasmussen, P. "A mass transport limited model for the growth of methane and ethane gas hydrates." *Chemical Engineering Science* 49(8): 1131-1143. 1994. DOI: http://dx.doi.org/10.1016/0009-2509(94)85085-2

Sloan, E. D., Subramanian, S., Matthews, P. N., Lederhos, J. P. and Khokhar, A. A. "Quantifying Hydrate Formation and Kinetic Inhibition." *Industrial & Engineering Chemistry Research* 37(8): 3124-3132. 1998. DOI: http://dx.doi.org/10.1021/ie970902h

Sloan, E. D. and Koh, C. A. "Clathrate hydrates of natural gases." Boca Raton, FL, CRC Press. 2008.

Smith, J. M., Van Ness, H. C. and Abbott, M. M. "Introduction to chemical engineering thermodynamics." Boston, McGraw-Hill. 2005.

Söhnel, O. and Mullin, J. W. "Interpretation of crystallization induction periods." *Journal of Colloid and Interface Science* 123(1): 43-50. 1988. DOI: http://dx.doi.org/10.1016/0021-9797(88)90219-6

Suess, E., Bohrmann, G., Greinert, J. and Lausch, E. (1999) "Flammable Ice." Sci Am Scientific American 281, 76-83.

Sugahara, T., Haag, J. C., Prasad, P. S., Warntjes, A. A., Sloan, E. D., Sum, A. K. and Koh, C. A. "Increasing hydrogen storage capacity using tetrahydrofuran." *Journal of the American Chemical Society* 131(41): 14616-14617. 2009. DOI: http://dx.doi.org/10.1021/ja905819z

Sun, Z., Wang, R., Ma, R., Guo, K. and Fan, S. "Effect of surfactants and liquid hydrocarbons on gas hydrate formation rate and storage capacity." *International Journal of Energy Research* 27(8): 747-756. 2003. DOI: http://dx.doi.org/10.1002/er.909

Sun, Z.-G. and Sun, L. "Equilibrium Conditions of Semi-Clathrate Hydrate Dissociation for Methane + Tetra-n-butyl Ammonium Bromide." *Journal of Chemical & Engineering Data* 55(9): 3538-3541. 2010. DOI: http://dx.doi.org/10.1021/je100183s

Tabuchi, H. "An Energy Coup for Japan: 'Flammable Ice'." The New York Times. New York, The New York Times Company. 2013.

Taylor, C. J., Miller, K. T., Koh, C. A. and Sloan Jr, E. D. "Macroscopic investigation of hydrate film growth at the hydrocarbon/water interface." *Chemical Engineering Science* 62(23): 6524-6533. 2007. DOI: http://dx.doi.org/10.1016/j.ces.2007.07.038

Taylor, M., Dawe, R. A. and Thomas, S. "Fire and Ice: Gas Hydrate Transportation - A Possibility for the Caribbean Region." SPE Latin American and Caribbean Petroleum Engineering Conference. Port-of-Spain, Trinidad and Tobago, Society of Petroleum Engineers. 2003.

Thomas, S. "Review of ways to transport natural gas energy from countries which do not need the gas for domestic use." *Energy* 28(14): 1461-1477. 2003. DOI: http://dx.doi.org/10.1016/S0360-5442(03)00124-5

Torré, J.-P., Ricaurte, M., Dicharry, C. and Broseta, D. "CO2 enclathration in the presence of water-soluble hydrate promoters: Hydrate phase equilibria and kinetic studies in quiescent conditions." *Chemical Engineering Science* 82(0): 1-13. 2012. DOI: http://dx.doi.org/10.1016/j.ces.2012.07.025

Trebble, M. A. and Bishnoi, P. R. "Development of a new four-parameter cubic equation of state." *Fluid Phase Equilibria* 35(1-3): 1-18. 1987. DOI: http://dx.doi.org/10.1016/0378-3812(87)80001-8

Trebble, M. A. and Bishnoi, P. R. "Extension of the Trebble-Bishnoi equation of state to fluid mixtures." *Fluid Phase Equilibria* 40(1): 1-21. 1988. DOI: http://dx.doi.org/10.1016/0378-3812(88)80020-7

Tzirakis, F., Stringari, P., von Solms, N., Coquelet, C. and Kontogeorgis, G. "Hydrate equilibrium data for the CO2 + N2 system with the use of tetra-nbutylammonium bromide (TBAB), cyclopentane (CP) and their mixture." *Fluid Phase Equilibria* 408(24): 0e247. 2016. DOI: http://dx.doi.org/10.1016/j.fluid.2015.09.021

van der Waals, J. H. and Platteeuw, J. C. "Clathrate Solutions." *Advances in Chemical Physics* 2: 1-57. 1959. DOI: http://dx.doi.org/10.1002/9780470143483.ch1

Vandsburger, L., Swanson, E., Tavares, J., Meunier, J.-L. and Coulombe, S. "Stabilized aqueous dispersion of multi-walled carbon nanotubes obtained by RF glow-discharge treatment." *Journal of Nanoparticle Research* 11(7): 1817-1822. 2009. DOI: http://dx.doi.org/10.1007/s11051-009-9656-4

Verrett, J. and Servio, P. "Evaluating Surfactants and Their Effect on Methane Mole Fraction during Hydrate Growth." *Industrial & Engineering Chemistry Research* 51(40): 13144-13149. 2012a. DOI: http://dx.doi.org/10.1021/ie301931m

Verrett, J., Posteraro, D. and Servio, P. "Surfactant effects on methane solubility and mole fraction during hydrate growth." *Chemical Engineering Science* 84(0): 80-84. 2012b. DOI: http://dx.doi.org/10.1016/j.ces.2012.08.009

Verrett, J., Renault-Crispo, J.-S. and Servio, P. "Phase equilibria, solubility and modeling study of CO2/CH4 + tetra-n-butylammonium bromide aqueous semi-clathrate systems." *Fluid Phase Equilibria* 388(0): 160-168. 2015. DOI: http://dx.doi.org/10.1016/j.fluid.2014.12.045

Verrett, J. and Servio, P. "Reaction rate constant of CO2—Tetra-n-butylammounium bromide semi-clathrate formation." *The Canadian Journal of Chemical Engineering*. 2016. DOI: http://dx.doi.org/10.1002/cjce.22612

Vysniauskas, A. and Bishnoi, P. R. "A kinetic study of methane hydrate formation." *Chemical Engineering Science* 38(7): 1061-1072. 1983. DOI: http://dx.doi.org/10.1016/0009-2509(83)80027-X

Vysniauskas, A. and Bishnoi, P. R. "Kinetics of ethane hydrate formation." *Chemical Engineering Science Chemical Engineering Science* 40(2): 299-303. 1985. DOI: http://dx.doi.org/10.1016/0009-2509(85)80070-1

Watanabe, S., Takahashi, S., Mizubayashi, H., Murata, S. and Murakami, H. "A demonstration project of NGH land transportation system." Proceedings of the 6th international conference on gas hydrates. 2008.

Xia, Z.-M., Li, X.-S., Chen, Z.-Y., Li, G., Yan, K.-F., Xu, C.-G., Lv, Q.-N. and Cai, J. "Hydrate-based CO2 capture and CH4 purification from simulated biogas with synergic additives based on gas solvent." *Applied Energy* 162: 1153-1159. 2016. DOI: http://dx.doi.org/10.1016/j.apenergy.2015.02.016

Yamamoto, K., Terao, Y., Fujii, T., Ikawa, T., Seki, M., Matsuzawa, M. and Kanno, T. "Operational overview of the first offshore production test of methane hydrates in the Eastern Nankai Trough, Offshore Technology Conference. 2014.

Yin, Z., Chong, Z. R., Tan, H. K. and Linga, P. "Review of gas hydrate dissociation kinetic models for energy recovery." *Journal of Natural Gas Science and Engineering*. 2016. DOI: http://dx.doi.org/10.1016/j.jngse.2016.04.050

Young, R. J. and Lovell, P. A. "Introduction to polymers." Boca Raton, CRC Press. 2011.

Yulong, W., Fei, W., Guohua, L., Guoqing, N. and Mingde, Y. "Methane storage in multi-walled carbon nanotubes at the quantity of 80 g." *Materials Research Bulletin* 43(6): 1431-1439. 2008. DOI: http://dx.doi.org/10.1016/j.materresbull.2007.06.046

ZareNezhad, B. and Montazeri, V. "Nanofluid-assisted gas to hydrate (GTH) energy conversion for promoting CO2 recovery and sequestration processes in the petroleum industry." *Petroleum Science and Technology* 34(1): 37-43. 2016. DOI: http://dx.doi.org/10.1080/10916466.2015.1115872

Zheng, J., Lee, Y. K., Babu, P., Zhang, P. and Linga, P. "Impact of fixed bed reactor orientation, liquid saturation, bed volume and temperature on the clathrate hydrate process for pre-combustion carbon capture." *Journal of Natural Gas Science and Engineering*. 2016a. DOI: http://dx.doi.org/10.1016/j.jngse.2016.03.100

Zheng, J., Zhang, P. and Linga, P. "Semiclathrate hydrate process for pre-combustion capture of CO2 at near ambient temperatures." *Applied Energy*. 2016b. DOI: http://dx.doi.org/10.1016/j.apenergy.2016.10.118

Zhong, D.-L., Ding, K., Yan, J., Yang, C. and Sun, D.-J. "Influence of Cyclopentane and SDS on Methane Separation from Coal Mine Gas by Hydrate Crystallization." *Energy & Fuels*: 131120070125006. 2013. DOI: http://dx.doi.org/10.1021/ef401491e

Zhong, Y. and Rogers, R. E. "Surfactant effects on gas hydrate formation." *Chemical Engineering Science* 55(19): 4175-4187. 2000. DOI: http://dx.doi.org/10.1016/S0009-2509(00)00072-5

Zhou, S.-d., Yu, Y.-s., Zhao, M.-m., Wang, S.-l. and Zhang, G.-Z. "Effect of Graphite Nanoparticles on Promoting CO2 Hydrate Formation." *Energy & Fuels* 28(7): 4694-4698. 2014. DOI: http://dx.doi.org/10.1021/ef5000886

Zhu, H., Shanks, B. H. and Heindel, T. J. "Enhancing CO–Water Mass Transfer by Functionalized MCM41 Nanoparticles." *Industrial & Engineering Chemistry Research* 47(20): 7881-7887. 2008. DOI: http://dx.doi.org/10.1021/ie800238w